

Bombesin Receptor-Targeted Liposomes for Enhanced Delivery to Lung Cancer Cells



SCHOOL OF PHARMACY

Mohammad Jamal A Akbar

University of East Anglia

School of Pharmacy

Thesis Submitted for the Degree of Doctor of
Philosophy (Ph.D.) in Pharmacy

October, 2021

Dedication



FOR
MY PARENTS
MY WIFE
MY CHILDREN
MY BROTHER
MY SISTERS



Declaration of authorship

I declare that the work in this thesis submitted by me for the degree of Doctor of Philosophy is my work and it is original, to the best of my knowledge, except where stated, referenced and acknowledged.

Mohammad. J. A. Akbar

Table of Contents

ABSTRACT	VI
ACKNOWLEDGEMENT	VII
LIST OF FIGURES	VIII
LIST OF TABLES	X
LIST OF ABBREVIATIONS	XI
PUBLICATIONS ASSOCIATED WITH THIS WORK	XIV
CHAPTER 1 : GENERAL INTRODUCTION	1
1.1 SMALL CELL LUNG CANCER (SCLC)	2
1.1.1 CLINICAL PRESENTATION.....	3
1.1.2 HISTOLOGY OF SCLC	3
1.1.3 STAGING OF SCLC.....	4
1.1.4 TREATMENT	5
1.2 GASTRIN RELEASING PEPTIDE (GRP) AND SCLC.....	6
1.2.1 GASTRIN RELEASING PEPTIDE AND ITS RECEPTOR	6
1.2.2 PHYSIOLOGICAL ROLE OF GRP	7
1.2.3 GRP-R DISTRIBUTION IN NORMAL TISSUE.....	7
1.2.4 GRP-R DISTRIBUTION IN TUMOURS	8
1.2.5 GRP RECEPTOR SIGNALLING AND INTERNALIZATION	9
1.3 CANCER TARGETING	11
1.4 GRP-R AS A TARGET IN SCLC	13
1.5 LIPOSOMES AS DRUG DELIVERY PLATFORMS.....	15
1.5.1 DEFINITION AND BACKGROUND	15
1.5.2 LIPOSOMES FOR TARGETING	16
1.5.3 LIPOSOME ROLE IN ENHANCING THE PHARMACOLOGY OF THE DRUG	17
1.5.4 LIPOSOME CLASSIFICATION.....	18
1.5.5 FACTORS AFFECTING THE EFFICACY OF LIPOSOMAL DRUG DELIVERY SYSTEMS	19
1.6 AIMS AND OBJECTIVES OF THIS THESIS:	20
CHAPTER 2 : MATERIALS AND METHODS	21
2.1 MATERIALS AND METHODS.....	22
2.1.1 MATERIALS	22
2.1.2 CELL CULTURE.....	22
2.1.3 TECHNIQUES USED TO STUDY GRP-R EXPRESSION, FUNCTIONALITY AND MITOGENICITY	23
2.1.4 GENETIC MANIPULATIONS OF GRP-R EXPRESSION	29
2.1.5 TECHNIQUES USED TO GENERATE AND STUDY GRP-R TARGETED FORMULATIONS	39
2.1.6 STATISTICAL ANALYSES.....	44
CHAPTER 3 : GRPR EXPRESSION IN HUMAN SCLC CELL MODELS	45
3.1 INTRODUCTION.....	46
3.2 RESULTS.....	47
3.2.1 SCLC CELL LINES CHARACTERIZATION.....	47

3.2.2 GRP-R EXPRESSION.....	48
3.2.3 GRP-R EXPRESSION BY FLOW CYTOMETRY.....	52
3.2.4 GRP-R LOCALIZATION BY IMMUNOFLUORESCENT IMAGING.....	54
3.2.5 INTRACELLULAR CA ²⁺ RELEASE ASSAY.....	55
3.2.6 MTS ASSAY.....	58
3.2.7 CLONOGENIC ASSAY.....	60
3.3 DISCUSSION.....	61
3.4 CONCLUSION.....	66

CHAPTER 4 : MANIPULATING BOMBESIN RECEPTOR EXPRESSION LEVELS IN SCLC **67**

4.1 INTRODUCTION.....	68
4.2 RESULTS.....	69
4.2.1 GRP-R KNOCKDOWN EFFICIENCY BY QRT-PCR.....	69
4.2.2 CONFIRMATION OF GRP-R KD AFTER PUROMYCIN SELECTION OF STABLE TRANSFECTANTS	70
4.2.3 INTRACELLULAR CALCIUM RESPONSE IN SCLC AFTER GRP-R KD.....	74
4.2.4 SIGNALLING PATHWAY ACTIVATION IN THE GRP-R KD SCLC.....	75
4.2.5 GRP-R KNOCKDOWN EFFICIENCY BY QRT-PCR IN A549.....	77
4.2.6 GRP-R KD CONFIRMATION AFTER PUROMYCIN SELECTION BY WESTERN BLOT IN A549.....	78
4.2.7 GRP-R OVEREXPRESSION IN A549.....	79
4.2.8 HA-GRP-R EXPRESSION BY IMMUNOFLUORESCENT IMAGING.....	80
4.3 DISCUSSION.....	81
4.4 CONCLUSION.....	84

CHAPTER 5 : TARGETED LIPOSOMAL FORMULATION UPTAKE IN A GRP-R OVEREXPRESSING CELL LINE **85**

5.1 INTRODUCTION.....	86
5.2 RESULTS.....	87
5.2.1 CHARACTERISATION OF PEPTIDES, CONJUGATE AND LIPOSOMES.....	87
5.2.2 LIPOSOME COLLOIDAL STABILITY STUDY.....	90
5.2.3 CELL UPTAKE OF GRP-R-TARGETED LIPOSOMES BY FLOW CYTOMETER.....	91
5.2.4 CELL UPTAKE OF GRP-R-TARGETED LIPOSOMES BY FLUORESCENCE MICROSCOPY.....	97
5.2.5 INSIGHT INTO THE MECHANISM OF INTRACELLULAR UPTAKE OF GRP-R-TARGETED LIPOSOMES BY LIVE CELL FLUORESCENCE IMAGING.....	98
5.3 DISCUSSION.....	102
5.4 CONCLUSION.....	108

CHAPTER 6 : GENERAL DISCUSSION AND CONCLUSION **109**

6.1 GENERAL DISCUSSION.....	110
6.2 GENERAL CONCLUSION.....	114
6.3 FUTURE WORK.....	114

BIBLIOGRAPHY **115**

CHAPTER A : APPENDIX **127**

Abstract

Targeted nanotherapeutics have been used in cancer to overcome the limitations of conventional chemotherapeutics. Liposomes are versatile carriers which can be tuned for targeting specific type of cancer. Small cell lung cancer (SCLC) represents about 15% of all lung cancers and is characterized by rapid proliferation, metastasis, recurrence and poor prognosis. It is strongly associated with tobacco smoking and patients usually present with metastatic disease. It is also categorized as a neuroendocrine type of cancer. This means that it produces neuropeptides such as GRP. GRP act as a mitogen and highly express its receptor (GRP-R) which creates autocrine loop. This loop of GRP/GRP-R drives the SCLC growth which makes the system appealing for targeting therapy. There are almost no novel treatments have been approved or introduced into the standard SCLC regimen in the last few decades. Therefore, this study offers an insight into utilizing GRP/GRP-R growth loop to target SCLC using targeted liposomes that features antagonistic peptide to enhance safe delivery, accumulation, and internalization into GRP-R overexpressing SCLC via receptor-mediated approach.

The aim of this project was to synthesize targeted liposomes for SCLC that enhances accumulation to GRP-R overexpressing cells. This was performed by functionalizing pegylated liposomes with a GRP-R antagonist peptide. To achieve this aim, we studied GRP-R expression and functionality in a number of selected SCLC cell lines (H510, H345, H209, H82 and N417). In addition to that, we manipulated GRP-R expression in selected SCLC cell lines (H510 and H345) as well as A549 in order to develop an in vitro cell line model to test the capability of the targeting formulation. an N-terminally cysteine modified GRP-R antagonist (termed cystabn) was synthesised and shown to inhibit cell growth in vitro. Cystabn was used to prepare a targeted DSPE-PEG₂₀₀₀ lipid conjugate that was formulated into liposomes. The liposomes were colloiddally stable with favourable properties in terms of size and surface charge and good stability under storage conditions. Flow cytometric and microscopic studies showed that fluorescently labelled cystabn-functionalized liposomes are preferentially internalised by receptor-mediated approach into GRP-R overexpressing cells more extensively than plain pegylated liposomes that contained no cystabn targeting motif. In conclusion, the finding of this work offer promising targeted liposomal delivery system, which can be delivered safely (without triggering receptor-mediated growth signalling), in a targeted manner, and actively via receptor mediated approach, into SCLC or any other GRP-R overexpressing cancer using small antagonistic ligand formulated into the liposomes.

Access Condition and Agreement

Each deposit in UEA Digital Repository is protected by copyright and other intellectual property rights, and duplication or sale of all or part of any of the Data Collections is not permitted, except that material may be duplicated by you for your research use or for educational purposes in electronic or print form. You must obtain permission from the copyright holder, usually the author, for any other use. Exceptions only apply where a deposit may be explicitly provided under a stated licence, such as a Creative Commons licence or Open Government licence.

Electronic or print copies may not be offered, whether for sale or otherwise to anyone, unless explicitly stated under a Creative Commons or Open Government license. Unauthorised reproduction, editing or reformatting for resale purposes is explicitly prohibited (except where approved by the copyright holder themselves) and UEA reserves the right to take immediate 'take down' action on behalf of the copyright and/or rights holder if this Access condition of the UEA Digital Repository is breached. Any material in this database has been supplied on the understanding that it is copyright material and that no quotation from the material may be published without proper acknowledgement.

Acknowledgement

I would like to thank both my supervisors Dr. Chris Morris and Dr. Leanne Stokes for all their support, advice, guidance, and encouragement during my PhD. Both my supervisors have been extremely supportive and understanding throughout the time of my PhD. There are not enough words to put in here to appreciate their help and support in this journey. I would especially like to thank and sincerely appreciate Dr. Chris Morris my mentor who has helped me through both professional and personal challenges and for his support, patience, motivation, advice, immense knowledge, and for challenging me to be a better scientist has with no doubt helped me to develop as a researcher. His guidance helped me in all the time of research and writing of this thesis.

I would also like to extend my sincere thanks to Dr. Morris group for being supportive, for the stimulating discussions, for the sleepless nights we were working together, and for all the fun we have had in this journey. I would also like to extend my sincere thanks to the other groups in the School of Pharmacy and the BMRC for their help and support. Especially, Dr. Stokes group, Dr. Wafa Al-Jamal and her team, Dr. Stephen Robinson and his team, Prof. Stuart Rushworth and his team, Prof. Tom Wileman and his team, Prof. Penny Powell and her team for their invaluable help and support. I would also like to thank Mr. Matthew Jefferson, Dr. Abdullah Alghamdi and Dr. Sophia Wang for their invaluable help and stimulating discussions. Thanks also to the members of the School of Pharmacy and BMRC who gave me access to their laboratory and research facilities. I would also like to extend my sincere thanks to the Imam Abdulrahman Bin Faisal University through Saudi Arabia Cultural Bureau in London for granting me this opportunity and for their financial support.

I would like to thank my friends who supported me intellectually and spiritually throughout this journey Mr. Fahad Alqahtani and Dr. Abdullah Alghamdi. Last but not the least, I would like to give my special thanks to my wife and parents for their invaluable support and for their patience. Thanks to my wife, my parents and to my brother and sisters for supporting me spiritually throughout this journey and throughout writing this thesis and my life in general.

List of Figures

FIGURE 1.1: SCHEMATIC FOR LUNG CANCER TYPES AND THEIR CORRESPONDING SUBTYPES. ...	2
FIGURE 1.2: HUMAN LUNG CANCER CELLS BY LIGHT MICROSCOPY.....	4
FIGURE 1.3: AMINO ACID SEQUENCES OF TWO PEPTIDES- BOMBESIN(1-14) (TOP) AND GRP(14-27) (BOTTOM).	7
FIGURE 1.4: GPCRS SIGNALLING PATHWAY WITH GRP AS AN EXAMPLE.....	10
FIGURE 1.5: INTERNALIZATION MECHANISM OF GPCR.....	11
FIGURE 1.6: SCHEMATIC REPRESENTATION OF THE ENHANCED PERMEABILITY AND RETENTION (EPR) EFFECT.	13
FIGURE 1.7: SCHEMATIC REPRESENTATION OF LIPOSOMES AND THEIR COMPONENT PHOSPHOLIPIDS.....	16
FIGURE 1.8: PLASMA PHARMACOKINETICS OF FREE DOXORUBICIN COMPARED TO LIPOSOMAL DOXORUBICIN (DOXIL [®]).....	17
FIGURE 2.1: SCHEMATIC ILLUSTRATION SHOWING THE WORKFLOW OF THE GENERATION OF THE STABLE KNOCKDOWN GRP-R EXPRESSION FROM BACTERIAL STOCK.....	30
FIGURE 2.2: SCHEMATIC ILLUSTRATION SHOWING THE WORKFLOW OF THE GENERATION OF THE STABLE OVEREXPRESSION OF GRP-R FROM PURIFIED PLASMID DNA.....	37
FIGURE 3.1: SCLC CELL LINES MORPHOLOGICAL MICROGRAPHS.	47
FIGURE 3.2: GRPR EXPRESSION COMPARISONS USING THREE DIFFERENT ANTIBODIES IN A PANEL OF SCLC CELL LINES.....	49
FIGURE 3.3: GRPR EXPRESSION IN A PANEL OF SCLC CELL LINES USING SANTA CRUZ ANTIBODY.....	50
FIGURE 3.4: GRP EXPRESSION IN A PANEL OF SCLC CELL LINES USING ABCAM ANTIBODY.	51
FIGURE 3.5: TITRATION MATRIX OF GRP-R ANTIBODY IN PC-3 CELL LINE.....	52
FIGURE 3.6: GRP-R EXPRESSION IN A PANEL OF SCLC CELL LINES BY FLOW CYTOMETRY...	53
FIGURE 3.7: GRP-R EXPRESSION IN SCLC CELL LINES BY IMMUNOFLUORESCENCE.....	54
FIGURE 3.8: CALCIUM RESPONSE INDUCED BY GRP-R LIGAND IN SCLC CELL LINE.	56
FIGURE 3.9: CALCIUM RESPONSE INDUCED BY NMB IN SCLC CELL LINE.	57
FIGURE 3.10: SCLC CELL LINES GROWTH MODULATION BY GRP-R AGENTS.....	59
FIGURE 3.11: GROWTH MODULATION BY GRP-R LIGAND USING CLONOGENIC ASSAY.	60
FIGURE 4.1: GRP-R KNOCKDOWN EFFICIENCY CONFIRMATION BY QRT-PCR IN SCLC.....	69
FIGURE 4.2: GRP-R KNOCKDOWN EFFICIENCY CONFIRMATION BY WESTERN BLOT IN H345.	71

FIGURE 4.3: GRP-R KNOCKDOWN EFFICIENCY CONFIRMATION BY WESTERN BLOT IN H510.	72
FIGURE 4.4: GRP-R KNOCKDOWN EFFICIENCY CONFIRMATION BY FCM IN SCLC.	73
FIGURE 4.5: CALCIUM RESPONSE INDUCED BY GRP-R LIGAND IN GRP-R KD SCLC CELL LINE.	74
FIGURE 4.6: EFFECT OF GRP-R KNOCKDOWN ON ERK1/2 DOWNSTREAM SIGNALLING PATHWAY BY WESTERN BLOT IN H345.	75
FIGURE 4.7: EFFECT OF GRP-R KNOCKDOWN ON ERK1/2 DOWNSTREAM SIGNALLING PATHWAY BY WESTERN BLOT IN H510.	76
FIGURE 4.8: GRP-R KNOCKDOWN EFFICIENCY CONFIRMATION BY QRT-PCR IN A549.....	77
FIGURE 4.9: GRP-R KNOCKDOWN EFFICIENCY CONFIRMATION BY WESTERN BLOT IN A549.	78
FIGURE 4.10: VALIDATION OF A549 TRANSFECTION WITH HA-GRPR pDNA BY WESTERN BLOT.	79
FIGURE 4.11: HA-GRP-R EXPRESSION IN A549-GRPR CELL LINE BY IMMUNOFLUORESCENCE.....	80
FIGURE 5.1: SYNTHESIS OF TARGETED AND CONTROL LIPOSOMES.	88
FIGURE 5.2: COLLOIDAL STABILITY OF LIPOSOMES.....	91
FIGURE 5.3: UPTAKE OF THE TARGETED LIPOSOMAL FORMULATION USING 1MOLE% PEPTIDE- PEG-LIPID.	92
FIGURE 5.4: UPTAKE OF THE TARGETED LIPOSOMAL FORMULATION OVER TIME.	93
FIGURE 5.5: UPTAKE OF THE TARGETED LIPOSOMAL FORMULATION USING DIFFERENT CONCENTRATIONS.....	94
FIGURE 5.6: UPTAKE OF THE TARGETED LIPOSOMAL FORMULATION OVER EXPANDED TIME PERIOD.	95
FIGURE 5.7: QUANTIFICATION OF GRP-R TARGETING WITH CYSTABN DECORATED LIPOSOMES.	96
FIGURE 5.8: GRP-R TARGETING WITH CYSTABN INCREASES CELL ACCUMULATION OF LIPOSOMES.	97
FIGURE 5.9: PEPTIDES COLOCALIZATION WITH TRANSFERRIN (TFN) AND LYSOTRACKER GREEN.....	99
FIGURE 5.10: LYSOSOMES COLOCALIZATION WITH TRANSFERRIN (TFN) AND LYSOGREEN.	101

List of Tables

TABLE 2.1: BUFFER RECIPES USED IN WESTERN BLOT.....	24
TABLE 2.2: ANTIBODIES USED IN WESTERN BLOT.	25
TABLE 2.3: SIGMA MISSION shRNAs USED TO KNOCKDOWN OF GRP-R GENE (Xp22.2)...	31
TABLE 2.4: FORMULATION COMPONENTS OF LIPOSOMES REPORTED IN THIS STUDY	42
TABLE 3.1: OPTIMIZATION OF LYSIS CONDITIONS.....	48
TABLE 5.1: HPLC DATA SUMMARY FOR CYSTABN.....	87
TABLE 5.2: MALDI TOF MS DATA SUMMARY FOR CYSTABN	87
TABLE 5.3: COLLOIDAL PROPERTIES OF CONTROL AND TARGET-LIPO FORMULATIONS	89

List of Abbreviations

Ab	Antibody
AJCC	American joint committee on cancer
AUC	The area under the curve
BB	Bombesin receptor
BLPs	Bombesin-like peptides
BN	Bombesin
BRS-3	Bombesin receptor subtype 3
BSA	Bovine serum albumin
Caelyx[®]	Pegylated liposomal doxorubicin
Chol	Cholesterol
CNS	The central nervous system
Ctrl	Control
Cystabn	Cys-D-Phe-Gln-Trp-Ala-Val-Gly-His-Sta-Leu-NH ₂
DCM	Dichloromethane
DFs	Dilution factors
DHPE-Fluorescein	<i>N</i> -(Fluorescein-5-Thiocarbamoyl)-1,2-Dihexadecanoyl- <i>sn</i> -Glycero-3-Phosphoethanolamine
DIPEA	<i>N,N</i> -Diisopropylethylamine
DLS	Dynamic light scattering
DMEM	Dulbecco's modified eagle medium
DMF	Dimethylformamide
DMSO	Dimethyl sulfoxide
DOPC	1,2-dioleoyl- <i>sn</i> -glycero-3-phosphocholine
DOPE-PEG2000	
DOTA	1,4,7,10 tetraazacyclododecane-1,4,7,10-tetraacetic acid
Doxil[®]	A liposomal doxorubicin
DSPE-PEG₂₀₀₀-maleimide	1,2-distearoyl- <i>sn</i> -glycero-3-phosphoethanolamine- <i>N</i> -[maleimide(polyethylene glycol)-2000]
DTT	Dithiothreitol
EDT	Ethylmethyl sulfide
EDTA	Ethylenediaminetetraacetic acid
EPR	Enhanced permeability and retention
ERK	Extracellular signal-regulated kinase
FBS	Fetal bovine serum
FMOC	Fluorenylmethyloxycarbonyl
FS	Forward light scatter
G protein	Guanine nucleotide binding protein
GDP	Guanosine diphosphate
GPCRs	G protein coupled receptors
GRKs	GPCR kinases

GRP	Gastrin releasing peptide
GRP-R or GRPR	Gastrin releasing peptide receptor
GTP	Guanosine-5'-triphosphate
HA	Hemagglutinin
HBSS	Hank's Balanced Salt Solution
HER2	Human epidermal growth factor receptor 2
HPLC	High performance liquid chromatography
HRP	Horseradish peroxidase
IASLC	International association for the study of lung cancer
IC₅₀	Half maximal inhibitory concentration
IV	Intravenous
JMV594 or RM2	DPhe-Gln-Trp-Ala-Val-Gly-His-Sta-LeuNH ₂
KD	Dissociation constant
K_D	Apparent binding constant
K_i	Inhibition constant
LB	Lysogeny Broth
LC	Liquid chromatography
Lipo	Liposomes
Lipoplatin®	Liposomal cisplatin
LUV	Large unilamellar vesicles
LVs	Lentiviral vectors
m/z	Mass-to-charge ratio
MALDI-Tof	Matrix-assisted laser desorption/ionization – time of flight
MAPK	Mitogen-activated protein kinase
MBHA	4-methylbenzhydramine hydrochloride
MFI	Median fluorescence intensity
MLV	Multilamellar vesicles
MPS	Mononuclear phagocyte system
MS	Mass spectrometry
MTS	3-(4,5-dimethylthiazol-2-yl)-5-(3-carboxymethoxyphenyl)-2-(4-sulfophenyl)-2H-tetrazolium
MTT	3-(4,5-dimethylthiazolyl)-2,5-diphenyltetrazolium
MW	molecular weight
MWCO	Molecular weight cut off
NHBE	Normal human bronchial epithelial
NICE	National institute for health and care excellence
NMB	Neuromedin B
NMB-R	Neuromedin B receptor
NSCLC	Non-small cell lung cancer
p-44/42	Mitogen-activated protein kinases (p42/p44 MAPK, also called Erk2 and Erk1)
PBS	Phosphate buffered saline

PCC	Pearson correlation coefficient
PCR	Polymerase chain reaction
PDI	Polydispersity index
PEG	Polyethylene glycol
Perm	Permeabilized
PF	Plain liposomes or control liposomes
PFA	Paraformaldehyde
PKC	Protein kinase C
PLC	Phospholipase C
PMT	Photomultiplier tubes
RES	Reticuloendothelial system
ROI	Region of interest
RPM	Revolutions per minute
RPMI	Roswell Park Memorial Institute medium
Rt	Retention time
RT	Room temperature
RT-PCR	Reverse transcription polymerase chain reaction
SCLC	Small cell lung cancer
SD	Standard deviation
SDS	Sodium dodecyl sulphate
SDS-PAGE	Sodium dodecyl sulphate polyacrylamide gel electrophoresis
SEM	The standard error of the mean
SFM	Serum-free media
SIT	Selenium-Insulin-Transferrin
SOC Medium	Super optimal culture
SPPS	Solid phase peptide synthesis
SS	Side light scatter
SUV	Small unilamellar vesicles
TB	Terrific Broth
TF	Targeted formulation
TFA	Trifluoroacetic acid
TFn	Transferrin
TNM	Tumour, node and metastasis
TRC #	The RNAi consortium number
Tx	No treatment
ULV	Unilamellar vesicles
UV	Ultraviolet
VALG	Veterans administration lung study group
WT	Wild type

Publications Associated With This Work

Akbar MJ, Lukasewicz Ferreira PC, Giorgetti M, Stokes L, Morris CJ. Bombesin receptor-targeted liposomes for enhanced delivery to lung cancer cells. *Beilstein J Nanotechnol.* 2019 Dec 19;10:2553-2562. doi: 10.3762/bjnano.10.246. PMID: 31921534; PMCID: PMC6941431.

GENERAL INTRODUCTION

Chapter 1

1.1 Small cell lung cancer (SCLC)

Lung cancer is one of the most common cancer types, preceded only by prostate and breast cancer in men and woman, respectively, in the UK [1, 2]. Lung cancer is the leading cause of death by cancer [3]. There are two types of lung cancer including small cell lung cancer (SCLC) and non-small cell lung cancer (NSCLC). SCLC has a unique clinical presentation, histological features, and treatment response. Therefore, SCLC is classified as a separate type of lung cancer. The other lung cancer types are collectively classified as NSCLC. SCLC and NSCLC are further subdivided into subtypes as shown in Figure 1.1.

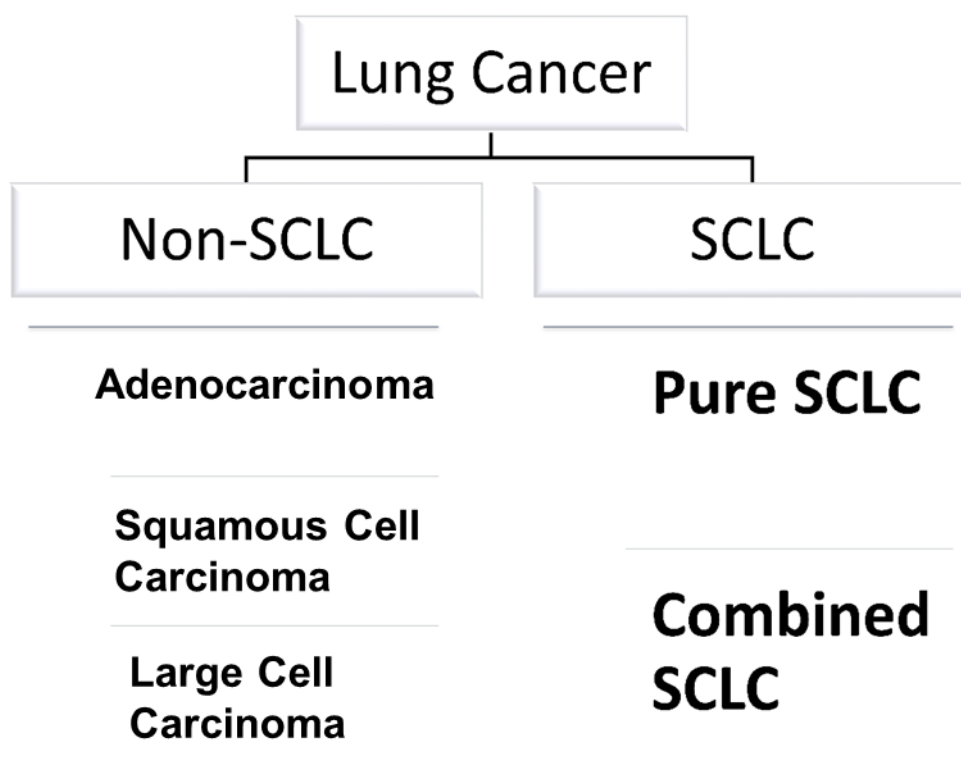


Figure 1.1: schematic for lung cancer types and their corresponding subtypes.

SCLC accounts for about 11% of all diagnosed lung cancer cases in England and Wales and is considered the most aggressive type of lung cancer [4]. The 5-year survival rate from SCLC is in the range of 1% to 40% depending on the clinical stage, using the tumour, node and metastasis (TNM) staging system [5]. Most SCLC patients develop resistance to chemotherapy regardless of their stage at the time of diagnosis or response to therapy [6]. SCLC has a strong association with tobacco smoking with < 3% of SCLC patients having no history of tobacco smoking [7].

The standard first-line therapy for SCLC is cisplatin or carboplatin plus etoposide for both stages of the disease (limited stage and extensive stage) [8-10]. This standard treatment for SCLC has not changed for 30 years. There have been limited advances made in the treatment and understanding of the pathology of SCLC compared to NSCLC. Other than the standard treatment, there is no targeted or any other types of novel therapy approved for treatment of SCLC [11, 12]. However, the use of immunotherapy is emerging and increased survival rate in other types of cancers such as NSCLC and still under evaluation in the treatment of SCLC [13]. In order to approach SCLC, it is imperative to draw efforts to further our understanding of the pathology as well as diagnosis and development of effective treatment for SCLC.

1.1.1 Clinical presentation

SCLC presentation is diverse ranging from no symptoms to relatively mild symptoms or tumour spread to other parts in the body. These relatively mild symptoms include cough and dyspnoea. However, patients with metastasized SCLC have more serious symptoms. Most SCLC patients (80%) have metastasized SCLC at the time of diagnosis [14, 15].

SCLC is a neuroendocrine type of cancer, which produces several hormone-like substances and growth factors. The neuroendocrine nature of SCLC often causes a number of syndromes collectively called paraneoplastic syndromes such as inadequate antidiuretic hormone homeostasis [16]. Generally, these syndromes are groups of symptoms, which manifest themselves at distant locations to that of the causative malignancy in the body. These symptoms result from substances produced by the tumour itself or as consequence to the body's immune response against tumour [14, 16-18].

1.1.2 Histology of SCLC

SCLC is a neuroendocrine lung tumour of small, monomorphic, poorly differentiated epithelial cells with a small amount of cytoplasm [19]. As high proliferating type of cancer, SCLC cells form a confluent cell population with granular nuclear chromatin, frequent mitoses and with undistinguishable nucleoli in addition to scarce cytoplasm. The cells of origin for SCLC are not yet fully characterised but it is believed that the cancer originates from pulmonary neuroendocrine cells [20, 21].

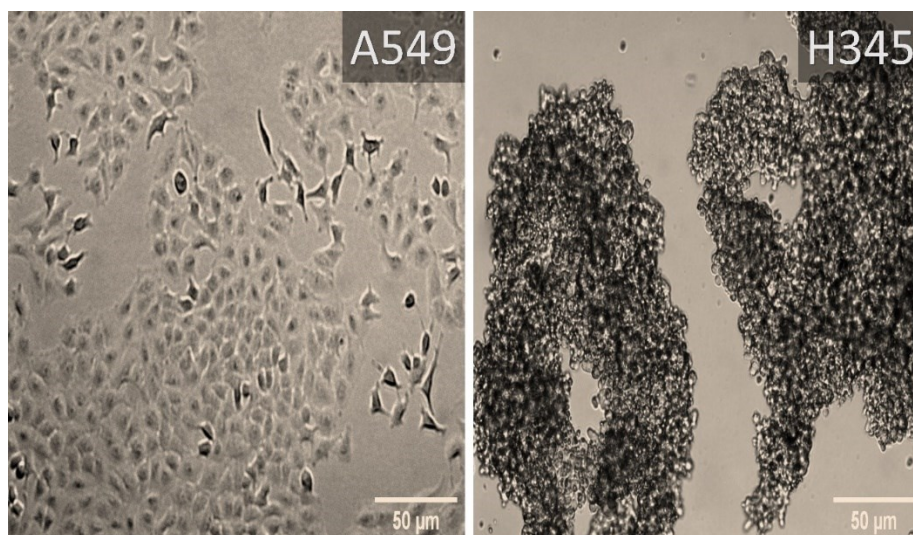


Figure 1.2: Human lung cancer cells by light microscopy. Non-SCLC represented by A549 cell line and SCLC by H345 cell line.

Most cases of SCLC are diagnosed reliably under the light microscope. For some cases however, immunohistochemistry is used to aid the diagnosis [19]. Figure 1.2 shows the SCLC tumour cell line sample under the light microscope. When comparing the sample to NSCLC cell line, it shows frequent mitoses, undistinguishable nucleoli and scarce cytoplasm. Anchorage independent growth in vitro is the most noteworthy difference. This means that the SCLC has the ability to grow in the absence of anchorage to the extracellular matrix in vitro. This is correlated with tumorigenicity in vivo [22].

An accurate pathological diagnosis of SCLC is crucial for treatment guidance and disease prognoses. For example, limited stage SCLC is treated mostly with chemotherapy and radiation. For metastatic disease, treatment with the same chemotherapy protocol without the radiation [9].

1.1.3 Staging of SCLC

The importance of cancer staging is to identify the magnitude of cancer cell localization in the body. Therefore, it is one of the most important factors in making successful cancer treatment decisions and, also it helps physicians predict the likely course of the cancer. A simple two-stage system for SCLC was introduced by the Veterans Administration Lung Study Group (VALG) in 1957 [23]. This system divides SCLC into limited stage and extensive stage. This system helps to determine treatments options for patients. For example, chemotherapy combined with radiation for limited stage or chemotherapy alone for extensive stage [9, 24].

The system modified by International Association for the Study of Lung Cancer (IASLC) and redefined the limited stage disease [23]. Limited stage disease is generally defined as a case where the tumour(s) are confined to one half of the thorax, with ipsilateral pleural effusion and with ipsilateral and contralateral regional lymph node metastasis. Metastasis to regional lymph nodes includes the hilar node, nodes in the supraclavicular area of the body, and nodes in the mediastinal area of the body, which can be treated with one tolerable radiotherapy session. Extensive stage disease is any presentation of the disease not labelled as limited stage [25]. Most (65%) patients present with extensive stage disease and the median survival and 5 years survival for this stage are 6–12 months and 2% of the initial diagnosed patients, respectively. For the limited stage disease, 16–24 months' median survival and 14% survive 5 years after the initial diagnosis [14, 19].

There is another well-established staging system in non-small cell lung cancer (NSCLC) as well as in other solid tumours called tumour-node-metastasis (TNM). TNM staging system includes the size of the tumour (T), whether or not the cancer cells have metastasised to local lymph nodes (N) and whether the tumour has metastasised distally (M). More recently, the international association for the study of lung cancer (IASLC) developed a modified TNM staging for lung cancer. This modified system included in the 7th edition of cancer staging manual issued by American Joint Committee on Cancer (AJCC). In the UK, the National Institute for Health and Care Excellence (NICE) uses this system for SCLC staging. This system can be used to stage both NSCLC and SCLC. The TNM staging system provide more detailed classification of SCLC, give more survival insight and more precise nodal staging. This makes the limited stage SCLC equivalent to T1–4, N0–3, and M0 tumours, Based on the TNM system. It is also equivalent to stage I-III, based on the number staging system [18, 23, 25-29].

1.1.4 Treatment

Combination chemotherapy is the standard treatment for both limited and extensive stages of SCLC. Etoposide and cisplatin plus chest radiotherapy are used as first choice of therapy for patients with good performance status and limited-stage disease (broadly corresponding to T1–4, N0–3, M0). Good performance status is determined by using a scale for assessing cancer progression and its effects on the daily activities of the patient [30].

In general, this treatment approach for limited stage has complete initial treatment response rate of 80% or higher, increased median survival period, and increased 5-year cancer-free survival before tumour re-establishment. In contrast, patients with extensive stage disease (broadly T1–4, N0–3, M1a/b) show only 20% response rate and the median survival extends to 6-12 months with a the 5-year cancer-free survival of 2%. Surgical resection of very early-stage SCLC (T1–2a, N0, M0) can extend the 5-year survival to 35–40%, if followed by chemotherapy, chest radiotherapy or both. These statistics highlight the need to improve treatment using novel strategies for early diagnosis and treatment [9, 14, 19, 31-33].

1.2 Gastrin Releasing Peptide (GRP) and SCLC

As previously mentioned, SCLC is neuroendocrine in nature and produces several hormone-like substances and growth factors. For instance, SCLC tumours produce GRP, which stimulates cancer growth. SCLC cell lines have been shown to not only produce GRP but express its receptor as well. This means that the cancer can stimulate its own growth in an autocrine fashion. The growth of SCLC cells has been shown to be inhibited by blocking GRP receptor (GRP-R) or by blocking GRP, indicating the importance of autocrine growth in SCLC [34-39]. This autocrine growth stimulation exerted by GRP and its receptor in SCLC can be utilised for cancer growth inhibition or for targeting therapy *in vivo*. For example, blocking peptides or antibodies against the receptor or the ligand can slow cancer growth. In addition to that, the receptor can be targeted by cancer drugs so that drugs can be actively internalized inside the cells by the receptor (well-known characteristic of G protein coupled receptors like GRPR) [40, 41].

1.2.1 Gastrin Releasing Peptide and its Receptor

GRP is a mammalian 27-amino acid peptide and belongs to a group of peptides called bombesin-like peptides (BLPs) [42]. Its amphibian relative, bombesin, was the first member of the family to be isolated from frog skin [43]. Bombesin is a 14-amino acid peptide and it bind with high affinity to most receptors in the family both in amphibians and mammals [44]. Researchers developed antisera against bombesin and used it on porcine stomach and intestine. This led to the discovery of the mammalian counterpart of bombesin, which was named GRP after its first known activity of releasing gastrin in the stomach [42]. After that, neuromedin B (NMB) was discovered in the porcine spinal cord [45]. All three peptides are related in sequence. GRP and bombesin share a highly conserved 7-amino acids C-terminal sequence (shown in Figure 1.3), which is essential for high-affinity binding to GRP-R [43].

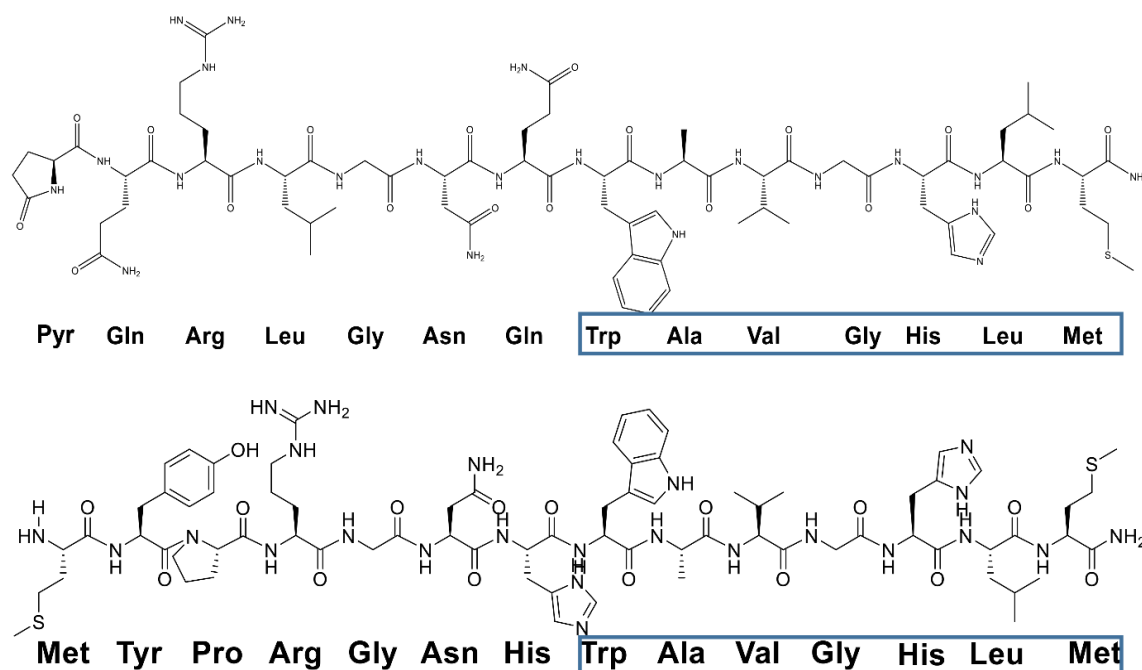


Figure 1.3: Amino acid sequences of two peptides- Bombesin(1-14) (top) and GRP(14-27) (bottom). The 7-amino acid sequence shared between the two is highlighted with blue rectangle.

1.2.2 Physiological Role of GRP

GRP-R perform numerous functions around the body including in the gastrointestinal and central nervous systems. These include release of gastrointestinal hormones, suppression of food intake, improvement of memory and stimulation of proliferation of epithelial tissue in gastrointestinal tract [46]. There is growing interest in the bombesin receptor family for a number of reasons. This family of receptors, particularly GRP-R, has been shown to be overexpressed in a wide spectrum of human cancers, as well as it found to be involved in tumour growth in various tumours [38].

1.2.3 GRP-R Distribution in Normal Tissue

There are studies which have demonstrated expression of GRP-R in fetal or adult tissues most commonly by detecting mRNA levels using RT-PCR. Human GRP-R is expressed in the pancreas [47], stomach [48], prostate [49], uterus [50] and in the CNS [51]. The receptor protein also detected in human fetal lung epithelium by detection of Bombesin-like peptide immunoreactivity using antibody. In addition to that, immunoreactivity for GRP detected by antibody in the human fetal lung which suggest auto- and paracrine growth stimulation. However, this upregulation of receptor in fetal lung was only during airway development period [52-54].

GRP immunoreactivity has been detected in many tissues in humans. These tissues include CNS [55], fetal lung [56], pregnant uterus [57], urethra [58], pancreas [59], thymus [60] and prostate [58]. GRP immunoreactivity was also detected in normal human lung but with low levels compared to fetal or neoplastic tissues [61]. So, according to literature, the overexpression of the receptor and its ligand occur in the human lung during fetal stage, lung cancer or localized in adult lung in areas that undergo growth and differentiation, 200 fold higher than the full term lung [62-64].

1.2.4 GRP-R Distribution in Tumours

GRP-R is reported to be overexpressed in numerous cancers such as lung, colon, and prostate [38]. SCLC cells express the receptors, GRP-R, NMB-R and the orphan BRS-3, and also secrete the cognate ligands, GRP and NMB [65]. The appearance of GRP-R in SCLC cells but not in normal adult lung might be due to the origin of the SCLC cells. This type of cancer originates from a type of stem cells partially differentiated toward pulmonary neuroendocrine cells [66].

The expression of GRP-R has been evaluated in a variety of human cancers such as SCLC by RT-PCR and immunoreactivity experiments. GRP-R has been shown to be expressed in 85% SCLC cell lines (Toi-Scott et al. 1996), and was found to be more than other Bombesin receptors in the cells - NMB-R expression was 55%, BRS-3 expression was 25% [65]. GRP-R was also detected by PCR technique in primary SCLC samples (2/5; 29%) in another study [67]. There is evidence of GRP-R expression in NSCLC in the literature. GRP-R was found to be expressed in 11/13 NSCLC cell lines [65]. The growth of NSCLC tumour in mice was suppressed by more than 30% using GRP-R antagonist [68].

GRP was found to be a potent mitogen in cancers such as SCLC [34], breast [69], colon [70] and prostate [35] cancers. NMB has also been found to stimulate growth in SCLC cells *in vitro* [71]. Taken together the expression data for GRP and GRP-R in SCLC offers the opportunity to target this pathway for SCLC treatment.

1.2.5 GRP Receptor Signalling and Internalization

The Bombesin receptor family belongs to the guanine nucleotide binding protein (G protein)-coupled receptor (GPCRs) superfamily. Three mammalian receptors have been identified as members of bombesin receptor family. These include GRP-R, neuromedin B receptor and an orphan bombesin receptor subtype 3 (BRS-3). The human GRP-R is a GPCR comprising 384 amino acids and seven transmembrane regions. The binding of bombesin and GRP to GRP-R triggers the activation of multiple signal transduction pathways that act in synergy to conduct the mitogenic signal to the nucleus and promote cell proliferation. For example, bombesin stimulated Ca^{2+} mobilization and activation of protein kinase C [72, 73]. After binding of bombesin or GRP to GRP-R, the heterotrimeric G protein G_q is activated. This leads to the activation of phospholipase C (PLC) which produces two second messengers, inositol 1,4,5-trisphosphate (IP_3) and 1,2 - diacylglycerol (DAG). IP_3 mobilises Ca^{2+} in the endoplasmic reticulum. DAG activates protein kinase C (PKC), which eventually leads to activation of The Ras/Raf/MAPK pathway which is also activated by PLC. This pathway transduces signals from the GRP to the cell nucleus where specific genes are activated for cell growth, division and differentiation. GRP-R activation also stimulate the small GTPase Rho, which plays important role in cancer survival and migration through the stimulation of ROCK, and it activates growth signals by the stimulation of MAPK cascades such as JNK and ERK5 which is still not fully studied and detailed mechanism. [74, 75] as shown in Figure 1.4.

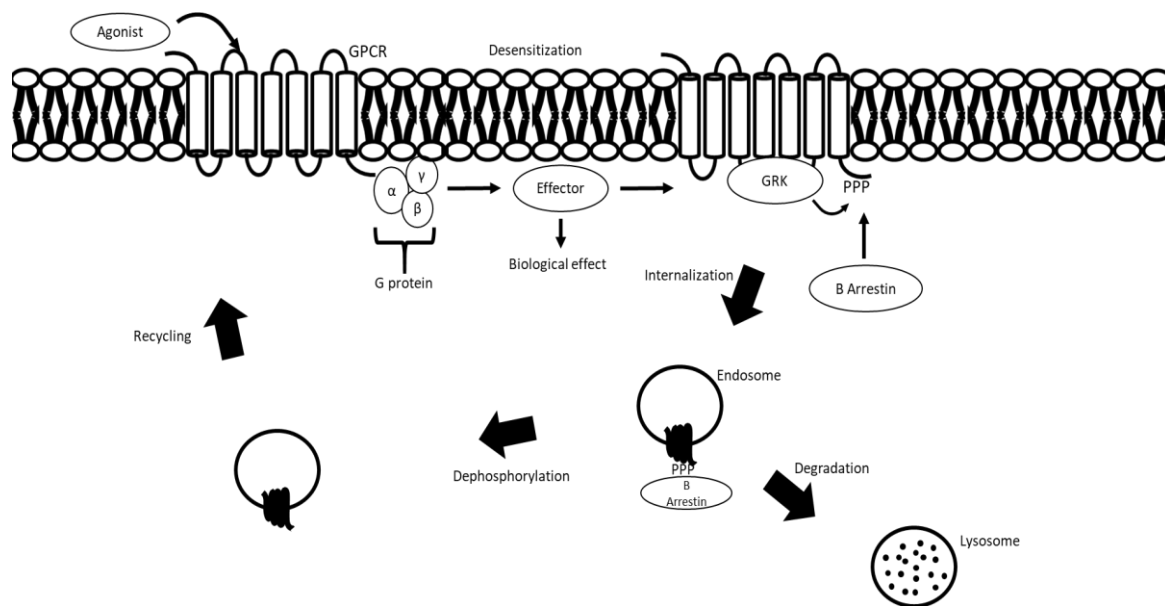


Figure 1.5: Internalization mechanism of GPCR. Binding of an agonist to a GPCR leads to the activation of heterotrimeric G proteins, which in turn stimulate or inhibit effector proteins. The activation of downstream signalling cascades ultimately produces biological effects. In the case of persistent stimulation, GPCRs are phosphorylated by GRKs and recruit β -arrestins, events responsible for fast signal desensitization. Subsequently, GPCRs are often internalized into endosomes. Internalized GPCRs are either targeted to lysosomes for degradation or dephosphorylated and recycled back to the cell surface to sustain a new cycle of activation. Figure redrawn from [76].

1.3 Cancer Targeting

The main advantage of cancer drug targeting is to enhance drug accumulation in the cancer tumour while limiting drug exposure and unwanted toxicity to healthy tissues. In general, there are two ways to target anticancer drugs to the desired site of action, which include passive and active targeting strategies. Passive targeting is achieved by utilising the enhanced permeability and retention (EPR) effect (Figure 1.6). This approach exploits the defective vascularisation of solid tumours which display increased permeability to particles in the nanometre range with cut-off size of 300 – 700 nm. This leads to enhanced penetration into the tumour mass and prolonged retention within the tumour due to inefficient permeation back into the vasculature or lymphatic drainage [78]. However, passive targeting by EPR effect alone is not enough because for the nanoparticles to utilize this effect, it needs long circulation time and size larger than the renal clearance threshold. This leads to increased nanoparticle concentration in tumour site due to increased extravasation from leaky blood vesicles.

In addition to that, some rapidly growing cancers such as pancreatic cancer have poor EPR effect due to rapid growth which rapidly change tumour microenvironment and leads to collapsed, blocked or tightly packed tumour vasculature. This means EPR effect alone is not enough to enhance nanoparticle delivery to tumour site and other strategies such as active targeting, direct delivery to cancer site, and the use of pharmacological and physical co-treatments needs to be considered [79-82]. Active targeting of cancer tissue can be used to increase efficiency and specific targeting of cancer cells. This can be achieved by directing drug delivery platforms toward receptors in the tumour cells that are overexpressed on their surface. Optimal active targeting requires the presence of a highly specific tumour receptor that is not expressed or highly under-expressed in non-target (healthy) tissue. Any expression of target receptor in other tissues could result in off-target effects and significant toxicity. It is difficult to find the ideal target that shows significantly increased cell surface expression on cancer tissue.

Many studies showed that small molecules such as folic acid, epidermal growth factor (EGF) and transferrin can be used to actively target their specific receptors on cancer cell surface. Those targeting moieties can bind to their receptor on the cancer cell surface which increase the drug concentration in the tumour area and improve cellular uptake of drug loaded nanoparticles and leads to improved therapeutic outcomes. For example, folate-targeted pegylated liposomes shown to have enhanced accumulation into tumours in vivo compared to non-targeted nanoparticles [83]. Furthermore, EGF-R ligand conjugated liposomes shown to have enhanced binding and internalization to EGF-R expressing cells in vitro and in vivo [84]. Targeted gold multifunctional nanoparticles loaded with doxorubicin functionalized with transferrin and pH sensitive linker shown to have enhanced anticancer properties in lung cancer [85]. The targeted delivery of nanomaterials can overcome many difficulties encountered with free drugs, including poor solubility, rapid clearance, degradation, lack of selectivity and nonspecific toxicity as well as reducing the drug dosage [86-90].

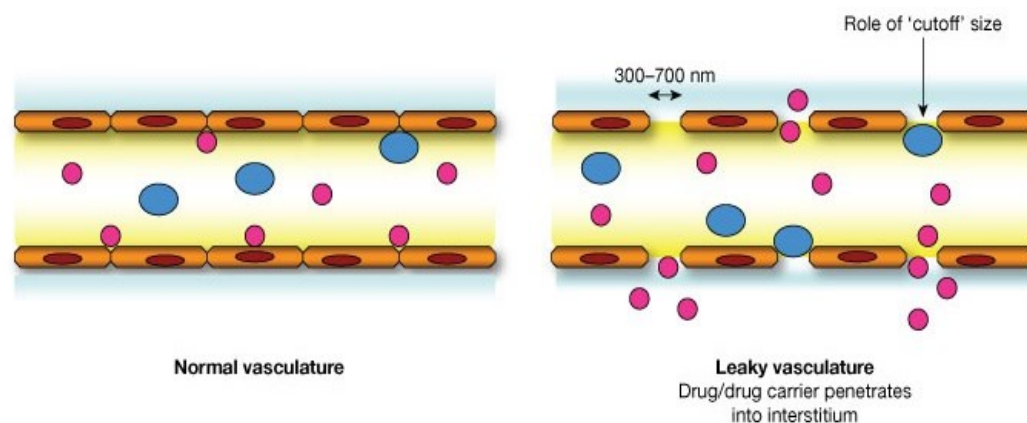


Figure 1.6: Schematic representation of the enhanced permeability and retention (EPR) effect. Passive targeting is achieved by using EPR. Leaky tumour vascular with impaired lymphatic drainage, increase permeability to nanoparticulates. This image adapted from [91].

1.4 GRP-R as a target in SCLC

GRP-R has been identified as a therapeutic target in cancer by many studies. A number of groups have developed peptide ligands and antibodies targeting GRP and GRP-R. Cuttitta et al. [34] showed in 1985 that an antibody raised against GRP could block GRP binding to its receptor and subsequently blocked clonal growth of SCLC cells in vitro and xenograft growth in vivo. This antibody (named 2A11) was later confirmed by Avis et al. to bind to the peptide with high affinity and was taken forward into a number of pre-clinical [92] and later clinical trials, reaching Phase II [93]. However, the Phase II trial showed that there is clinical antitumor activity only in small number of patients with relapsed tumour. This might be due to the cancer high tendency to develop drug resistance. It also could be due to targeting of GRP only which is the ligand of the GRP-R which may leave the cancer to relay on other growth promoting receptors expressed by the cells to survive. On the other hand, the receptor can be targeted to deliver chemotherapeutic drugs inside the cells which can be more effective approach [94-97].

In a complementary approach, other labs have developed antagonistic peptides that bind the GRP-R, thus blocking ligand binding and autocrine growth stimulation. For example, one unnatural peptide sequence termed RC-3095 is a potent antagonist to the GRP-R receptor which decreased by 50–70% the tumour volume of xenografts in nude mice following subcutaneous administration for 5 weeks [98].

A third approach to the treatment of GRP-R positive tumours involves the conjugation of a cytotoxic drug (doxorubicin) to a bombesin-derived peptide antagonist (RC-3094) [99]. This approach, which has the benefit of smaller molecular weight and lower immunogenicity was also reported to inhibit growth of H69 SCLC xenografts in vitro and in vivo [100].

There are some synthetic antagonists which bind with high affinity to GRP-R. A study used two GRP-R antagonistic peptides ([d-Cpa1- β -Leu8-des-Met9]litorin and [d-Phe6, Leu13-CH₂NH-Cpa14]bombesin(6–14)) showed inhibition in growth both in vitro and in vivo using GRP-R positive SCLC cell lines, SCLC 41M and SCLC 75 [101]. The first GRP-R antagonist used in the study was developed from litorin (pGlu-Gln-Trp-Ala-Val-Gly-His-Phe-Met-NH₂), which is an amphibian Bombesin-like peptide. Another study showed that a number of GRP-R antagonist peptides caused inhibition in the growth of the NCI-H345 SCLC cell line as well as in mice [102]. Llinares et al. synthesised GRP-R antagonist (JMV594) (H-D-Phe-Gln-Trp-Ala-Val-Gly-His-Sta-NH₂) by solution phase peptide synthesis. The peptide was tested on rat pancreatic acini and Swiss 3T3 cells. The antagonist recognized the GRP-R receptor on pancreatic acini (binding 34 ± 14 nM) and antagonized GRP stimulated amylase secretion ($IC_{50} = 190.0 \pm 57$ nM) and was also able to recognize the GRP receptor in 3T3 cells (binding $K_i 18.9 \pm 8.1$ nM) [103]. In another study, the selectivity of the JMV94 for GRP-R ($IC_{50} = 2.2 \pm 0.1$ nM) was demonstrated over the NMB-R ($IC_{50} = >10,000$ nM) by using competitive cell binding assay on Balb/c 3T3 cells transfected with other receptors [104]. Marsouvanidis et al., developed the JMV594 peptide further by coupling the chelator DOTA (1,4,7,10 tetraazacyclododecane-1,4,7,10-tetraacetic acid) to the N-terminal end of the peptide by using (β Ala)₂ as linker and labelled it with ¹¹¹In. The ¹¹¹In-DOTA-(β Ala)₂-JMV594 showed internalized to some extent in PC-3 prostate cell line at 37 °C. More than 60% of the radiopeptide remained intact for 5 min after entering the bloodstream of healthy mice. The radiopeptide also showed high tumour uptake and rapid background clearance via the kidneys [105]. From these findings, it is clear that GRP-R can be targeted in SCLC using antagonist peptides. In order to treat SCLC effectively, the drug could be encapsulated into a carrier and the carrier functionalized with the targeting peptide. This increases the concentration of the drug in the cancer site more than normal tissues.

1.5 Liposomes as drug delivery platforms

Nanoparticles are colloidal carriers of drugs in the nano-size scale. Liposomes in the nano-range are nanoparticles that can be used to address some of the challenges associated with traditional chemotherapy. These challenges include a lack of specificity and high toxicity to healthy tissue. Their advantage includes their small and reproducible size, control over their composition, surface functionalization, and stability relative to free drug which can be utilized to target the tumour microenvironment. Liposomes are a well-established nano-carrier platform for drugs that is used clinically around the globe.

1.5.1 Definition and background

Alec Bangham discovered closed bilayer structures [106], which were later called liposomes by Sessa [107]. Bangham discovered that when phospholipids are dispersed in water, they form a bilayer vesicle that he termed multilamellar smectic mesophases. Since then, liposomes have gained much interest and contributed to many areas such as pharmaceuticals, cosmetics and food science such as in the treatment of cancer [108], anti-ageing creams [109] and flavour retention agent [110] respectively. At first, liposomes were used as a model membrane system in the area of biophysical research before moving to the pharmaceutical industry to be used as drug carriers after Gregoriadis' demonstration of their drug-carrying capacity [111].

Liposomes are self-assembled artificial colloidal spherical vesicles composed of one or more bilayers of amphiphilic molecules called phospholipids (Figure 1.7). Liposomes can transport hydrophilic or hydrophobic drugs, depending on the nature of the drug. Liposomes are classified according to their bilayer number into multilamellar vesicles (MLV) and unilamellar vesicles (ULV). ULV subclassified into large unilamellar vesicles (LUV) and small unilamellar vesicles (SUV). Liposomes range in size from tens of nanometres to tens of micrometres. Liposomes are commonly used as drug delivery carriers for a number of reasons. They are biocompatible, biodegradable and they have the capacity to encapsulate both hydrophilic and hydrophobic drugs.

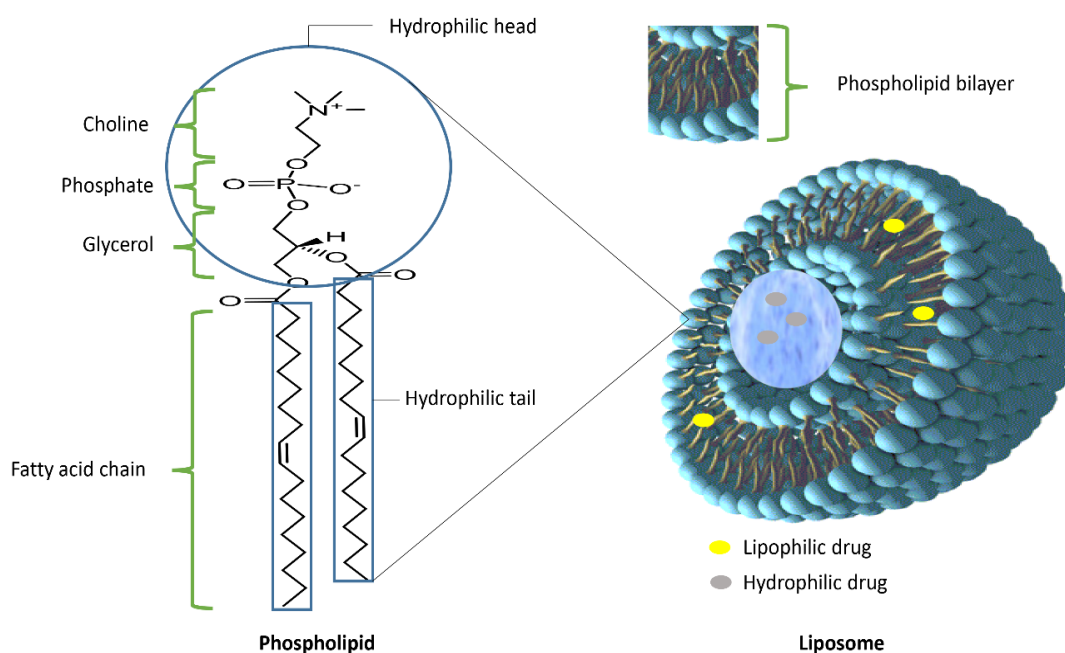


Figure 1.7: Schematic representation of liposomes and their component phospholipids. Liposome vesicles consist of an aqueous core, in which hydrophilic molecules can be encapsulated and phospholipid bilayer, in which lipophilic molecules can be encapsulated. The bilayer consists mainly of amphiphilic phospholipids. Phospholipids consist of hydrophilic head (phosphate group) and hydrophobic fatty acid chains joined together by a glycerol molecule. The phosphate molecule can be modified for instance by choline to form 1,2-dioleoyl-*sn*-glycero-3-phosphocholine (DOPC), which shown in the left of the figure. The liposome image was modified from [112].

1.5.2 Liposomes for targeting

Liposomes can be designed to target specific cell types. In cancer drug delivery, there are two types of targeting, which include passive and active targeting. This can be done by designing liposomes in a size range of 100 nm to 200 nm, which promote the accumulation in the target tumour site due to the EPR effect [113]. Smaller liposomes in the size range of 20 nm are cleared by kidney glomerulus and larger liposomes (>200 nm) tend to be recognised and cleared by the reticuloendothelial system (RES) [114]. For the active targeting, functionalization of the liposomal surface with antibodies, ligands and other biomolecules is used encourage selective liposomal interaction with the targeted cells. This can improve cellular drug accumulation by increasing the local concentration of drug in the vicinity of the target cell and thus increase passive drug uptake into the cell.

Alternatively, the liposome encapsulated drug can be delivered directly into the cell by internalisation / endocytosis. Liposomal composition and physical characteristics, such as size and surface charge, are crucial determinants to the liposome stability and application [115-117].

1.5.3 Liposome role in enhancing the pharmacology of the drug

Liposomes greatly improve the drug pharmacokinetics, pharmacodynamics and toxicity profile when compared to the free drug [118]. Non-targeted liposomal anticancer drug formulations of the appropriate size passively accumulate in tumour tissues by the EPR effect and this is associated with greater amounts of drug in tumour tissues compared to free drug. For example, Doxil[®] (a.k.a. Caelyx[®]), a pegylated liposomal doxorubicin offers unique pharmacokinetic profile compared to free drug (Figure 1.8).

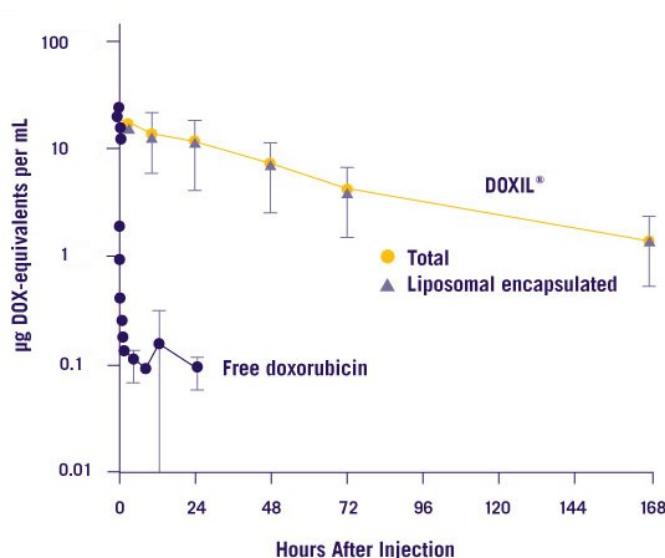


Figure 1.8: Plasma pharmacokinetics of free doxorubicin compared to liposomal doxorubicin (Doxil[®]). Figure adapted from [119].

The liposomal carrier (Doxil[®]) slowed the plasma clearance compared to the free drug from 45 L/h to 0.1 L/h in patients after IV dose of 25 mg/m² or 50 mg/m² of both free and liposomal drug. Doxil[®] also showed smaller volume of distribution compared to free drug (4 L versus 254 L respectively). The liposomal drug also enhanced the drug level in the tumour to > 4 folds [119]. Doxil is an example of a “stealth liposome” in which a hydrophilic PEG polymer shields the liposomal surface in such a way to reduce detection by the immune system and rapid clearance by the mononuclear phagocyte system (MPS) [120, 121].

1.5.4 Liposome classification

Liposomes can be classified according to their size and lamellarity into multilamellar vesicles (MLVs, $> 0.1\mu\text{m}$), large unilamellar vesicles (LUVs, $> 0.1\mu\text{m}$) and small unilamellar vesicles (SUVs, 25–100 nm) [115]. The size and lamellarity of liposomes depends on their composition and their method of preparation. MLVs are more suitable for lipophilic drug encapsulation due to their increased lamellarity which provides a larger volume into which hydrophobic drugs can partition. On the other hand, LUVs and SUVs are more suitable for parenteral administration due to their homogenous size distribution. However, the smaller the size of the vesicles the lower the amount of encapsulation of hydrophilic drugs.

The traditional method of making MLVs is the thin film hydration technique. The lipidic components are dissolved in organic solvent (e.g. chloroform) followed by the removal of the organic solvents using a rotary evaporator to produce a thin lipid film. The addition of an aqueous phase above the phase transition temperature of the lipid mixture with shaking results in the formation of the MLVs [122].

Extrusion of MLVs through polycarbonate membrane filters was an important methodological development in SUV/LUV manufacture. This method allows the production of homogenous vesicles with improved trapping efficiency. Moreover, using a reverse phase evaporation method or ethanol-based proliposome technology, oligolamellar vesicles (0.1–1 μm) have been produced. The manual extrusion system with relatively low pressure is usually used for lab scale production. For large scale production, higher pressure systems were developed. The production of SUVs with diameters less than 50 nm is only possible using sonication or homogenization. However, for a large scale production of SUVs in the 20 nm to 50 nm size range, microfluidic mixing techniques can be used [115].

Liposome can also be classified according to their compositions to four general classes of liposome for delivery of drugs. These include conventional liposomes, sterically-stabilized liposomes, ligand-targeted liposomes and stimuli-responsive liposomes. Traditionally, liposomes were formulated from phospholipids and cholesterol with neutral, cationic, or anionic phospholipids as well as cholesterol. Further developments led to the formulations of the other types of liposomes [117].

1.5.5 Factors affecting the efficacy of liposomal drug delivery systems

Factors such as lipid composition, size and surface charge are important in determining the properties of liposomes and their clearance route from the body. Adjustment of the size of the nanoparticles is crucial to take advantage of the EPR effect. *In vivo*, nanoparticles generally within the size range of 20 nm to 400 nm will diffuse through the gaps in the cancer vascular endothelium, which is not the case in normal tissue. The porous nature of the cancer vasculature varies in size depending on the cancer type, site, and the stage of the disease, but the upper size threshold is generally around 300 to 400 nm. In addition, nanoparticles must be larger than 10 nm to avoid kidney first pass elimination and smaller than 150 to 200 nm to avoid clearance by the liver and spleen [116].

Liposome opsonisation and clearance by the reticuloendothelial system (RES) are dependent on vesicle composition and size. RES is part of the immune system and its main function is to eliminate foreign materials from the blood. The RES consists of cells such as blood monocytes and macrophages found mainly in liver, the lung and the spleen. Naked phospholipid liposomes can be rapidly cleared by RES cells due to coating of liposomal surface with serum proteins called opsonins. Large liposomes (>200 nm in diameter) are rapidly opsonised and taken up by the RES. Opsonisation decreases with a reduction in liposome size. Small liposomes have a relatively larger surface area and will have a lower density of opsonins on the membrane surface which results in lower uptake by the macrophages. Liposomes with a size of 70 to 200 nm will have a greater chance to escape from RES and remain in the circulation longer and then reach the target. Due to extravasation through the fenestrated capillary walls in the liver, the small liposomes (< 70 nm in diameter) show shorter circulation time and therefore reduced drug activity [123].

On the other hand, several studies have showed the potential of pulmonary delivery of chemotherapeutics using liposomes. pulmonary delivery of drugs to lung cancer offers localized delivery to lung cancer which increase the drug concentration at the tumour site compared to systemic delivery. a study showed that liposomal Paclitaxel has a slower clearance and higher concentration in the mice lung when aerosolised into the lung compared to the IV administration. This effect could be due to the pulmonary deposition of liposome in the lung which increase the drug concentration in the tumour site. In addition to that, the pulmonary delivery of anticancer drugs using liposomes also, improve the toxicity profile and side effects. For example, liposomal cisplatin has been shown to has improved safety, efficacy and response in lung carcinoma [124-128].

1.6 Aims and Objectives of This Thesis:

- The thesis aim was to develop a targeted liposomal system that utilises the overexpression of GRP-R to offer specific, safe, and enhanced accumulation and internalization of liposomes into SCLC through the use of antagonistic peptide, which decorate the liposomes, that actively target the GRP-R and internalises via receptor mediated approach. To identify candidate SCLC cell lines based on the expression and functionality of the GRP-R
- To develop human lung cancer cell models, with varied levels of GRP-R expression.
- To synthesise cystabn-targeted liposome toward SCLC cells
- To test the GRP-R targeting liposomes in A549 overexpressing GRP-R and compare it with non-targeting (control) liposomes.

MATERIALS AND METHODS

Chapter 2

2.1 Materials and methods

2.1.1 Materials

All materials were of analytical grade and sourced from either Merck or Fisher unless mentioned otherwise. The lipids were from Avanti Polar Lipids (USA). The lipids used in this work include DOPC, Cholesterol, DOPE-PEG₂₀₀₀, and DSPE-PEG₂₀₀₀.

2.1.2 Cell Culture

All cell cultures were maintained at 37 °C, 5 % CO₂, and 95 % air in a humidified incubator and routinely passaged at 70-90% confluency. The incubator with these incubation conditions will be referred to as the cell incubator hereafter.

A panel of cell lines used in this part of the project, including SCLC lines (H510, H345, H209, H82 and N417) and the prostate cancer line (PC-3). The SCLC lines were kindly donated by Prof. Tyson Sharp (Barts Cancer Institute, UK) and the prostate cancer line was kindly given by Dr. Wafa Al-Jamal (Queen's University Belfast, UK). SCLC cell lines were grown in RPMI 1640 media supplemented with 10% FBS, 5 mM L-glutamine, 100 units/ml penicillin, and 100 µg/ml streptomycin (hereafter called complete RPMI medium). PC-3 and A549 were grown in DMEM medium with 4 mM GlutaMAX™ supplemented with 10% FBS, 100 units/ml penicillin, and 100 µg/ml streptomycin (hereafter called complete DMEM medium).

SCLC cells were passaged by centrifugation at 200 xg for 5 min. The supernatant was removed and the pellet re-suspended in fresh complete media and counted manually using haemocytometer or automatically using cell counter (TC20, Bio-Rad) before passaging it onto the required culture surface at 2×10^5 cells/mL. Adherent A549 and PC3 cells were passaged by washing with PBS (1 x 5 mL) followed by trypsinization (0.05% trypsin + 0.48 mM EDTA) for 5 minutes at 37°C. The cells were centrifuged at 200 xg for 5 min. The supernatant was removed and the pellet re-suspended in fresh media and counted before passaging it onto the required culture surface at density of 3×10^4 cells / cm².

HEK293T cells were kindly provided by Prof. Tom Wileman (University of East Anglia, Norwich, UK). The cells were maintained at 70-90% confluence and grown in antibiotic-free DMEM medium with 4 mM GlutaMAX™ supplemented with 10% FBS (hereafter called complete DMEM medium). HEK293T cells are a highly transfectable derivative of human embryonic kidney 293 cells. HEK 293T cells were passaged at a 1:4 ratio in complete culture media. The media was gently removed and the cells were washed once with phosphate buffered saline (PBS). 5 mL of pre-warmed complete culture media was added to the cells and cell scraper was gently used to detached the semi-adherent cells. The cell suspension was centrifuged at 200 xg for 5 min. The supernatant was removed and the pellet re-suspended in fresh media. The cells were re-suspended in the complete culture media and diluted 1:4 before incubation.

2.1.3 Techniques used to study GRP-R expression, functionality and mitogenicity

2.1.3.1 GRP-R expression by Western Blot

The relevant buffers recipes used in this experiment in this thesis are detailed in Table 2.1. Details of antibodies used in this thesis are detailed in Table 2.2.

Suspension cells were cultured in 75 cm² cell culture flasks. The cells were harvested at their 70-90% confluency and washed with (x3) PBS at 200 xg at 4 °C for 5 min. Cells were lysed on ice using 1 mL RIPA buffer per T75-flask followed by homogenization. Adherent cells were cultured into 75 cm² cell culture flasks. The cells were washed (x3) with PBS in their flasks at their 70-90% confluency. Cells were lysed on ice using 1 mL RIPA buffer per T75-flask followed by scraping and homogenization.

Lysates were collected into microtubes on ice and sonicated by pulsed sonication using Soniprep 150 Plus for 1 minute at 15.7 µm amplitude. The protein concentration was determined using Pierce® BCA protein assay kit. A total amount of 50 µg of proteins per lysate was diluted in the sample loading buffer with 41.6 mM dithiothreitol (DTT). The samples denatured for 5 min at 95 °C and loaded into a 12% SDS-PAGE gel.

Proteins were electrophoresed at 100 V then electrotransferred to nitrocellulose membrane at 100 V for 1 h at 4 °C. The blotted membranes were stained with Ponceau S stain to confirm protein transfer. The membrane blocked with 5% skimmed milk in washing buffer for 1 hour at RT.

The membrane was washed (x3) with washing buffer for 5 min at RT and stained with primary antibody in blocking buffer and incubated at 4 °C overnight. The membrane was washed (x3) with washing buffer for 5 min at RT and stained with horseradish peroxidase (HRP)-linked secondary antibody in blocking buffer and incubated at RT for 1 hour. The blot was washed (x3) with washing buffer for 5 min at RT and developed with Pierce™ enhanced chemiluminescence substrate. The blot was imaged with ChemiDoc™ XRS+ system using Image Lab™ software and analysed using ImageJ software.

Table 2.1: Buffer recipes used in Western Blot.

<i>Buffer</i>	<i>Recipe</i>
<i>RIPA buffer</i>	<i>25 mM Tris-HCl pH 7.6, 150 mM NaCl, 5 mM EDTA, 1% Triton X-100, 1% sodium deoxycholate, 0.1% SDS</i>
<i>Loading buffer</i>	<i>2% SDS, 10% glycerol and 0.01% Bromophenol Blue in 62.5 mM Tris-HCl, pH 7.0</i>
<i>Running buffer</i>	<i>25 mM Tris, 192 mM Glycine, 0.1% SDS and pH 8.3</i>
<i>Blotting buffer</i>	<i>25 mM Tris, 192 mM Glycine and 20% Methanol</i>
<i>Washing buffer</i>	<i>10 mM Tris (pH 7.5), 100 mM NaCl, 0.1% Tween 20 and pH to 7.5</i>
<i>Blocking buffer</i>	<i>5% skimmed milk powder in washing buffer</i>

Table 2.2: Antibodies used in Western blot.

<i>Antibodies</i>	<i>Concentration used</i>
<i>Mouse monoclonal anti-human GRP-R antibody - SC-377316, Santa Cruz Biotechnology, UK.</i>	<i>1 µg/ml</i>
<i>Rabbit polyclonal anti-human GRP-R antibody - 39883 Abcam, UK.</i>	<i>1 µg/ml</i>
<i>Rabbit polyclonal anti-human GRP antibody - 202123 Abcam, UK.</i>	<i>1 µg/ml</i>
<i>Anti-rabbit IgG HRP-linked antibody - 7074 Cell Signalling Technology, UK.</i>	<i>65 ng/ml (1:1000)</i>
<i>Mouse monoclonal anti-alpha Tubulin [DM1A] - Loading Control - ab7291 Abcam, UK.</i>	<i>1 µg/ml (1:1000)</i>
<i>Mouse monoclonal anti-GAPDH - Loading Control - ab9484 Abcam, UK.</i>	<i>1 µg/ml (1:1000)</i>
<i>Anti-mouse IgG HRP-linked antibody - 7076 Cell Signalling Technology, UK.</i>	<i>0.153 µg/ml (1:1000)</i>
<i>Mouse monoclonal Anti-HA - H9658 Sigma-Aldrich, UK.</i>	<i>0.5 µg/ml</i>
<i>Rabbit monoclonal anti-Phospho-p44/42 MAPK (Erk1/2) - 4370S Cell Signalling Technology, UK.</i>	<i>0.25 µg/ml (1:2000)</i>
<i>Rabbit monoclonal anti-p44/42 MAPK (Erk1/2) - 4695S Cell Signalling Technology, UK.</i>	<i>84 ng/ml (1:1000)</i>

2.1.3.2 GRP-R expression by flow cytometry

Cell lines were harvested and diluted to 5×10^5 cells per mL and centrifuged at 200 xg at 4 °C for 5 min. The cell pellets were washed (x3) with cold PBS and resuspended in cold blocking buffer (3% BSA and 0.2% sodium azide in PBS) for 10 min on ice as 1×10^6 cells per mL. The cells were washed (x3) with cold PBS and resuspended gently in cold fixation buffer (2% PFA in PBS) for 30 min at 4 °C on a tube roller.

The cells suspension of each cell line was washed (x3) with cold PBS then split in half. Permeabilized cells were resuspended dropwise in cold (-20 °C) 100% methanol and incubated for 5 min at 4 °C before washing with PBS (x3). The non-permeabilized cells were treated in the same way with PBS used in lieu of permeabilization buffer.

Samples were washed (PBS x3) and resuspended in the primary antibody solution, then incubated on ice for 30 minutes. Cells were washed (PBS x3) before incubation with a secondary antibody solution, on ice for 30 min. All samples were washed (PBS x3) and resuspended in PBS before acquisition.

Samples acquisitions were performed using a Beckman Coulter, CytoFlex flow cytometer with CytExpert Software. Cells were analysed based on forward light scatter (FS), side light scatter (SS) and florescent intensity. Cells were gated for singlets by width against the height for FS. Typically, fluorescence information for 10,000 singlets-gated events was collected for each sample. Median fluorescence intensity (MFI) of these events were plotted in a histogram. Fluorescence profiles or histograms shown were representative of those obtained from the number of experiments indicated.

2.1.3.3 GRP-R localization by immunofluorescence imaging

Adherent cells were seeded on uncoated 18 mm coverslips and cultured overnight. Suspension cells were washed (x3 PBS) and diluted to 1×10^4 cells/mL in PBS. Cells were spun into L-polylysine coated coverslips using Cytospin cytocentrifuge to form an adhered cell smear. Cells were washed (x3) with PBS for 5 min at RT and fixed with 4% PFA for 10 min at RT on a plate shaker. The cells washed with PBS (x3) for 5 min at RT and residual PFA was quenched by 50 mM NH_4Cl for 15 min at RT on a plate shaker. Cells were washed with PBS (x3) for 5 min at RT and permeabilized with 0.2% Triton X-100 for 10 min at RT on a plate shaker. The cells washed with PBST (x3, PBS + 0.1% Tween 20) for 5 min at RT and blocked by 10% FBS in PBST for 30 min at RT on a plate shaker. Samples were washed (PBST x3) for 5 min and resuspended in mouse monoclonal anti-human GRP-R antibody (SC-377316 Santa Cruz Biotechnology, UK, 4 $\mu\text{g}/\text{mL}$ in PBST with 1% FBS) then incubated in humidified chamber for 1 hour. Cells were washed (PBST x3) for 5 min before incubation with a secondary donkey anti-mouse with Alexa Fluor 647 (A- 31571 Thermo Fisher Scientific, UK, 2 $\mu\text{g}/\text{mL}$ in PBST with 1% FBS) then incubated in humidified chamber for 1 hour. All samples were washed (PBST x3) and counter stained with nuclear stain (Hoechst 33258, 5 $\mu\text{g}/\text{mL}$ in PBST) for 5 min in humidified chamber. The samples were washed (PBS x3) for 5 min on a plate shaker. The coverslips were dipped once in PBS and once in deionized water then dried with tissue then air-dried before mounting them on slides using 15 μL Vectashield H-1000. The cells were viewed under a widefield microscope (Zeiss AxioPlan 2ie) and images taken using Axiovision software. Images were analysed using ImageJ.

2.1.3.4 Intracellular Ca^{2+} release assay

Cells (1×10^6 cells/mL) were loaded with 2 μM Fura-2AM in Hank's Balanced Salt Solution (HBSS) loading buffer containing 250 μM sulfinpyrazone for 40-60 minutes at 37 °C protected from light. Following loading, the buffer was replaced with HBSS and allowed to warm to 37 °C in a Flexstation 3 microplate reader (Molecular Devices). Fluorescence of Fura-2 was recorded using dual excitation (340 and 380 nm) and emission 520 nm. Agonist was automatically injected using the Flexstation compound plate and tips at a specific time point (30 seconds). PMT settings were medium and 3 reads performed per well. Data is represented as F340/F380 ratio of the zero treatment-baseline for normalisation.

2.1.3.5 MTS assay

The proliferation of H345 and H82 cells in the presence or absence of Tyr⁴-Bn and Cystabn was studied in Selenium-Insulin-Transferrin (SIT) medium comprising 30 nM sodium selenite, 5 µg/mL human insulin, 10 µg /mL human transferrin and 2 mM L-glutamine in RPMI-1640 media. The cells were seeded in 96 well plates overnight at a density of 30,000 cells per well. The cells were then treated with 100 or 500 nM Tyr⁴-Bn or Cystabn and for 5 days with peptide replenishment at day 3. Cell proliferation was determined using the CellTiter 96® AQueous One assay (Promega). The reagent incubated in at 37 °C for two hours before reading the plate absorbance at 490 nm using endpoint mode. The data acquired using SpectraMax M2 microplate Reader (Molecular Devices, UK) by SoftMax® Pro Software.

2.1.3.6 Clonogenic assay

A hard agarose lower layer (0.5% sterile low melting point agarose in complete RPMI) was added as 0.5 ml/well in 12-well plates and left in the cell incubator to harden. For the soft upper layer, 0.5% sterile low melting point agarose in 2% FBS RPMI containing 2X concentration of peptide treatments (solution A) was prepared in microfuge tube (0.5 ml/tube) and kept at 42 °C. Cell lines were quickly suspended (5×10^4 cells/ml) in pre-warmed 2% FBS RPMI and mixed with an equal volume of solution A. This mixture of 0.25% sterile agarose, 2% FBS RPMI, and 1X treatment was laid carefully upon the hard agarose layer (1 mL/well). The soft layer was incubated at 37°C for 2 hours before adding 100 µl feeding layer which contain 10X concentrated treatments in 2% FBS RPMI. The feeding layer was replaced every day for the duration of the experiment. After one week, the wells treated with 100 µl of 5 mg/mL MTT reagent and kept in the cell incubator for one hour before counting the colonies manually under the light microscopy using x 10 magnification.

2.1.4 Genetic manipulations of GRP-R expression

In the second experimental chapter, GRP-R expression was manipulated genetically in vitro. GRP-R expression was knocked down by lentiviral transduction and overexpressed by plasmid transfection.

For GRP-R knockdown, MISSION® shRNA plasmids (*SHCLNG-NM_005314*, Sigma) were bought as glycerol stocks, in *E. coli* strain (*DH5alphaT1R*). The plasmid construct contains the shRNA insert with the pLKO.1-puro vector which has a total length of 7,086 bp. The insert in this study is the human GRP-R shRNA DNA, which targeted specific region of GRP-R mRNA transcript. The MISSION pLKO.1-puro Control Vector (SHC001, Sigma-Aldrich) was used as a control. The two viral packaging plasmids were the packing plasmid, psPAX2 (#12260, Addgene), and the envelope plasmid, pMD2.G (#12259, Addgene). These plasmids were kindly provided by Dr Penny Powell (UEA, Norwich, UK). Viral particles stocks were concentrated using Lenti-X™ Concentrator (631232, Takara Bio, UK). Samples of lentiviral RNA was extracted using NucleoSpin RNA Virus (740956.10 MACHEREY-NAGEL, Germany) for titration. Lentiviral titres were determined using the Lenti-X™ qRT-PCR titration kit (631235, Takara Bio, UK).

For overexpression of GRP-R, HA-tagged GRP-R DNA construct was bought (#GRPR00TN00, cDNA Resource Centre). The backbone vector is pcDNA3.1+ (Invitrogen). The plasmid was transformed in *E. coli* strain *DH5α* competent cells in the lab then propagated, purified and used for transfection. All plasmid DNA was extracted and purified using NucleoBond® Xtra kit (740410.10 MACHEREY-NAGEL, Germany) according to the manufacturer's instructions.

2.1.4.1 Knockdown of GRP-R

Cell clones with stable knockdown of the GRP-R gene were prepared as shown in Figure 2.1. Before selection of stable cell clones five GRP-R shRNA plasmid vectors (Table 2.3) were screened for knockdown efficiency. shRNA control is an empty vector confirmed to not activate the RNAi pathway, as it does not contain an shRNA insert. Briefly, shRNA plasmids were propagated from bacterial stocks then purified. After that, lentiviral vectors of those shRNAs were produced. The viral RNA was isolated and titrated before viral transduction into cells. GRP-R KD was evaluated by qPCR then selection of stable clones was performed and confirmed by Western blot or flow cytometry.

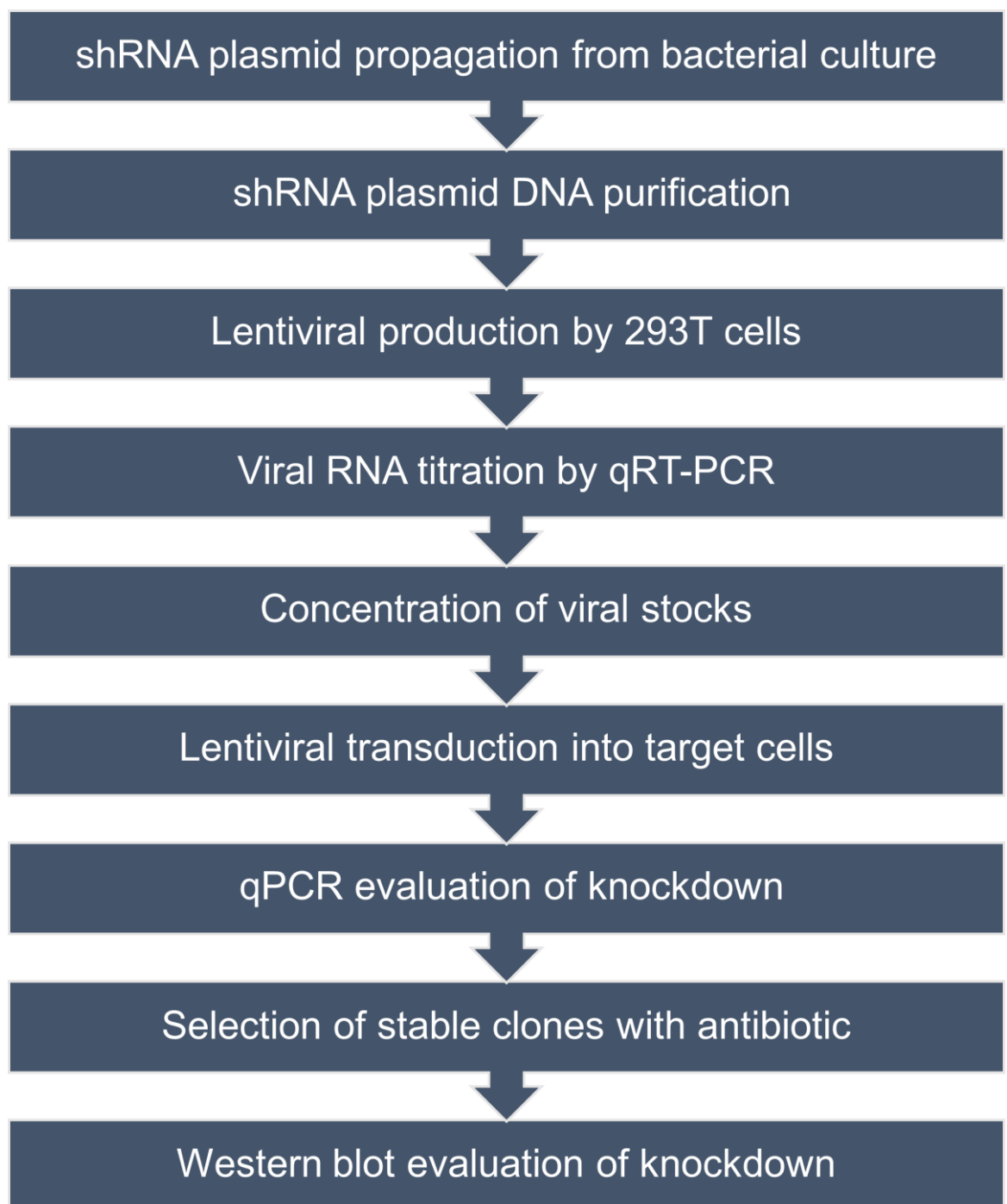


Figure 2.1: Schematic illustration showing the workflow of the generation of the stable knockdown GRP-R expression from bacterial stock.

Table 2.3: Sigma MISSION shRNAs used to knockdown of GRP-R gene (Xp22.2)

<i>Gene/re gion</i>	<i>Clone ID</i>	<i>TRC #</i>	<i>Sequence 5 ' to 3 '</i>
<i>Xp22.2 (2681 bp)/ 3UTR</i>	NM_0053 14.1- 1576s1c1	000000 9043	CCGGTGAGGGACGGTTTTGCTTTATCTCGAGATAAAGCA AAACCGTCCCTCATTTTT
<i>Xp22.2 (2681 bp)/ CDS</i>	NM_0053 14.1- 1119s1c1	000000 9044	CCGGGCTTACAATCTTCCCGTGGAACCTCGAGTTCCACGG GAAGATTGTAAGCTTTTT
<i>Xp22.2 (2681 bp)/ CDS</i>	NM_0053 14.1- 1062s1c1	000000 9045	CCGGCCACTGTCGATCATCTCTGTTCTCGAGAACAGAGA TGATCGACAGTGGTTTTT
<i>Xp22.2 (2681 bp)/ CDS</i>	NM_0053 14.1- 1503s1c1	000000 9046	CCGGGCCACCTTTAGCCTCATCAATCTCGAGATTGATGA GGCTAAAGGTGGCTTTTT
<i>Xp22.2 (2681 bp)/ CDS</i>	NM_0053 14.1- 440s1c1	000000 9047	CCGGCCATTTTCATGCACTGCAACATCTCGAGATGTTGCA GTGCATGAAATGGTTTTT

2.1.4.1.1 shRNA plasmid propagation

The shRNA plasmids were propagated by amplification of bacterial stocks. For bacterial cultures, 1.5 % agar plates were made by combining Lysogeny Broth (LB) (containing 10 g/L Tryptone, 5 g/L NaCl and 5 g/L yeast extract) with agar at 15 g/L. The LB-Agar media was sterilised and cooled to 50 °C before supplementing with ampicillin at 100 µg/ml. 10 ml aliquots were pipetted into 10 cm dishes. An ice splinter from frozen bacterial glycerol stock was removed by a sterile streaking loop and placed it into a sterile culture tube containing 0.5 ml Terrific Broth (TB) or Lennox Broth (Luria Bertani Broth, Sigma L3022) without antibiotics. The tube incubated at 37 °C with shaking for 30 minutes. Using a sterile loop, 50 µL of the incubated culture was streaked onto LB-agar plate containing 100 µg/ml ampicillin or carbenicillin, followed by incubation at 37 °C overnight. To propagate the plasmids, the plasmid-containing selected bacterial colonies were inoculated into 5 mL starter culture of LB medium with 100 µg/ml ampicillin or carbenicillin. The bacteria were cultured for 8 hours at 37 °C with shaking at 200 RPM. The starter culture was diluted 1 in 1000 in a final volume of 200 ml per plasmid. The cultures were kept overnight at 37 °C with shaking at 200 RPM. The selection of isolated colonies ensured colony homogeneity and helped to avoid picking satellite colonies that tend to grow in antibiotic depleted areas of the plate. 3 to 5 colonies were cultured per plasmid to ensure high yield of plasmid DNA.

2.1.4.1.2 Plasmid purification

The plasmid purification and precipitation kit (Macherey-Nagel, Germany) was used according to the manufacturer protocol was followed. The bacterial cultures were pelleted by centrifugation and re-suspended in 500 µL re-suspension buffer (A1), followed by the addition of 500 µL of SDS/alkaline lysis buffer (A2), and incubation at RT for 4 min. Next, 300 µL A3 buffer was added to neutralise the suspension and aid the binding of plasmid DNA onto the silica membrane of the spin columns. The contents were mixed by gentle inversion. Precipitated proteins, genomic DNA and cell debris were pelleted by centrifuging the tubes at 11000 xg for 7 minutes. The supernatant was then loaded onto the spin column. The column was washed twice at 11000 g for 1 minute using ethanolic wash buffer A4, followed by a final drying spin for 3 min. Finally, the DNA was eluted in 50 µl nuclease-free water at 70 °C. the yield was quantified by the NanoDrop spectrophotometer. The optimal concentration of plasmid DNA required for transfection of packaging cells is <180 ng/µL. In case of yield lower than the desired yield, plasmid DNA of the highest purity from different colonies was pooled together and ethanol-precipitated.

Ethanol precipitation is a well-established method for the concentration and desalting of nucleic acids. In this method, a solution of 3M sodium acetate (pH 5.2) was added at 1/10th of the volume of pooled plasmid DNA. Next the volume was completed to 1 ml with ice-cold ethanol, which precipitated the plasmid DNA. The resulting solution was then stored overnight at -20°C, or for 4-5 hours at -80°C to precipitate. After precipitation, the DNA was pelleted by centrifugation at maximum speed (14000 xg) for 15 minutes. The pellet was washed in cold 70% ethanol and centrifuged again. Ethanol was aspirated without disturbing the pellet, which was then left to dry in a culture hood. As it dried, the translucent pellet became whiter. Finally, the pellet was rehydrated in nuclease free water and stored at -20 °C. NanoDrop was used for quantification.

2.1.4.1.3 Lentiviral particle production

For transfection of the target and viral plasmids in the packaging cell, FuGENE® transfection reagent (Promega, E2691) was used. 24-48 h prior to transfection, HEK293T cells were cultured in T75 culture flasks and passaged so that the cells were ~ 80% confluent. On the day of transfection, packaging cell media was replaced with 8 ml of fresh, antibiotic free, complete culture media. The amount of the target plasmid used for each T75 flask was 3.4 µg ($\approx 45 \text{ ng/cm}^2$). DNA mix was prepared in the ratio of 1 µg of each of the viral plasmids to each 1.5 µg of the target plasmid. The DNA mix was then topped up to 15 µL TE buffer. The transfection reagent to total DNA ratio used was 2.5:1. 20 µL of transfection reagent (FuGENE®, Promega, E2691) was mixed with 200 µL of Opti-MEM (Life Technologies, USA.) reduced serum media in a separate tube. The DNA mix was then added onto the reagent-media mix, and gently mixed by pipetting, before being incubated at RT for 15 minutes. The resulting solution was added drop wise onto the flask of packaging cells. The plates were incubated in normal culture conditions and the media was changed every 24 hours, with 8 mL of fresh culture media. Culture media was collected at 48, 72 and 96 hours. The collected viral particles stocks were pooled together and Lenti-X™ Concentrator (631232, Takara Bio, UK) was used to produce a concentrated stock.

2.1.4.1.4 Lentiviral RNA isolation for titration

Viral RNA was isolated using the NucleoSpin® RNA Virus isolation kit (Macherey-Nagel). The manufacturer protocol was followed. 150 µL was taken from the viral particle stock for viral RNA extraction. 600 µL of RAV1 was added, vortexed, and incubated at RT for 5 minutes.

600 μ L of absolute ethanol was next added and the tube was vortexed for 30 seconds. 675 μ L of this solution was transferred into a spin column and centrifuged at 8,000 xg for 1 minute. The spin step was repeated with the remaining 675 μ L. Next, the column was washed once with 500 μ L of RAW buffer and then with 600 μ L of RAV3, followed by centrifugation at 8,000 xg for 1 minute. Waste was discarded after every wash step. To dry the columns, a final wash step was required, where 200 μ L of RAV3 was added to the tube and centrifuged at 11,000 xg for 5 minutes. Finally, viral RNA was eluted by adding 50 μ L of nuclease-free water (at 70 °C, as hot water aids in RNA elution), and incubating at RT for 1 - 2 minutes followed by a spin at 11,000 xg for 1 minute.

2.1.4.1.5 Lentiviral RNA titration

The Lenti-X™ qRT-PCR titration kit (631235, Takara Bio, UK) was used. The manufacturer protocol was followed. The viral RNA samples were treated with DNase I. This was done by mixing 12.5 μ L of RNA sample with 10X DNase I buffer, 4 μ L DNase I (5 units/ μ L) and 6 μ L of nuclease-free water. The 25 μ L reaction mix was incubated at 37 °C for 30 minutes followed by 5 minutes at 70 °C. After that, the treated samples were kept on ice and qRT-PCR was performed for titre determination. A Serial dilutions of Lenti-X RNA control stock of known copy number were made. In addition to that, serial dilutions of the DNase-treated viral RNA samples were made. Next, a master mix was made following the manufacture's recommendation, using the Quant- X™ One-Step qRT-PCR SYBR® kit (Clontech). The appropriate amount of control or unknown dilutions were mixed with the appropriate amount of the master reaction mix in a 96 multi-well PCR plate as per manufacturer protocol. The plate was sealed and the qRT-PCR reaction was performed using a Rotor-Gene Q (Qiagen). The copy number of the viral RNA samples, used in the qRT-PCR, were determined from the standard curve. After that, the copy number of the original purified viral RNA samples was back calculated, accounting for any dilution steps.

2.1.4.1.6 Lentivirus transduction

The target cell lines were cultured in antibiotic-free complete culture media and incubated for 24 h. Culture medium was removed and replaced with medium containing 8 μ g/ml Polybrene to increase the efficiency of infection. Lentiviral particles were added and the cells incubated at 37 °C overnight.

Following that, an identical, second transduction was performed and incubated overnight. The medium was replaced with fresh prewarmed media and incubated overnight. Samples were collected to evaluate the KD efficiency by qPCR as described below.

2.1.4.1.7 qPCR evaluation of GRP-R KD

Cellular total RNA was isolated using the TRIzol™ Plus RNA Purification Kit (Invitrogen, A33254) following the manufacturer's protocol. The cells were lysed and homogenized in TRIzol™ reagent. For adherent cells, the media was removed and 1 ml of reagent per T75 flask was added directly on the cells monolayer then homogenized quickly by pipetting. For suspension cells, the cells were resuspended in 0.75 ml of reagent per 0.25 ml of sample and homogenized by pipetting. The lysate was incubated in Phasemaker™ tube for 5 min at RT for complete dissociation of the nucleoproteins complex. 0.2 ml chloroform per 1 ml TRIzol™ was added then agitated vigorously for 15 seconds and incubated for 3 min at RT before centrifugation for 5 min at 16,000 $\times g$ at 4°C. This separates the two phases (organic and aqueous) and the Phasemaker™ Gel forms a barrier between the upper and lower phases. To isolate the RNA, the aqueous phase (containing the RNA) was transferred into a new tube before adding equal volume of 70% ethanol and vortexing. The sample was then centrifuged at 12,000 $\times g$ for 15 seconds using a spin cartridge with collection tube. The collected liquid was discarded and the cartridge was washed with 500 μL of Wash Buffer II twice using centrifugation at 12,000 $\times g$ for 15 seconds. To elute the RNA, the cartridge was spun at 12,000 $\times g$ for 1 minute to dry it. The RNA was then eluted from the cartridge into a recovery tube by adding RNase-free water and incubated for 1 min then spun at >12,000 $\times g$ for 2 minutes. The quantity and quality of the purified total RNA were determined at 260 nm, 280 nm and 230 nm using Thermo Scientific™ NanoDrop 2000 Spectrophotometer.

The SuperScript™ II Reverse Transcriptase (Invitrogen, 18064022) was used to produce cDNA for PCR. The manufacturer protocol was followed. The first-strand cDNA was synthesized from RNA samples using the SuperScript™ II reverse transcriptase. To prepare the first portion of the RT reaction mix, 2 μg RNA was mixed with oligo-(dT)₁₂₋₁₈ primer (0.5 μg /20 μL reaction), dNTP mix (0.5 mM each/20 μL reaction) and nuclease-free water (up to 12 μL). Following that, the mix was heated for 5 min at 65 °C followed by a quick chill on ice then brief centrifugation. After that, the 5X reaction buffer and DTT (50 mM/20 μL reaction) were added to the RT reaction mix. After that, the mixture mixed gently then incubated at 42 °C for 2 min.

After that, SuperScript™ II RT (200 units/20 µL reaction) was added and mixed gently. The RT reaction mix was incubated at 42 °C for 50 min. following that, the reaction was inactivated by incubating at 70 °C for 15 min.

SYBR® select master mix (Applied Biosystems™, 4472903) was used for performing PCR. The manufacturer protocol was followed. The PCR reaction mix was prepared by mixing the cDNA (80 ng/10 µL PCR reaction) with 2X SYBR® select master mix, forward and reverse primers mix (200 nM) and nuclease-free water. The reaction mixture was mixed gently then centrifuged briefly. After that, the mixture transferred to optical PCR plate and sealed. The PCR reaction was performed on real-time quantitative PCR instrument (7500 Real-Time PCR System, Applied Biosystems™).

2.1.4.1.8 Selection of stable clones

To generate a stable knockdown cell line, the media was replaced with fresh complete medium that contains puromycin for selection of transduced cells. The transfected cells selected using 0.5 µg/mL puromycin over two weeks. Cells were subsequently maintained in 0.2 µg/mL puromycin. The suitable puromycin concentration for each transduced cell line was determined by performing puromycin kill curve. In addition to that, samples of the selected transduced cell line were collected to confirm the knockdown efficiency. This was performed by Western blot or flow cytometry as described in sections 2.1.3.1 and 2.1.3.2 respectively.

2.1.4.2 Overexpression of GRP-R

Cell clones with stable overexpression of GRP-R were prepared as shown in Figure 2.2. Overexpression of GRP-R in A549 cell line was achieved using the HA-tagged GRP-R DNA construct (#GRPR00TN00, cDNA Resource Centre). This construct results in the overexpression of GRP-R with 3x-Hemagglutinin N-terminal tagged human GRP-R. The backbone vector was pcDNA3.1+ (Invitrogen). Briefly, the plasmid was transformed in *E.coli* strain *DH5a* competent cells in the lab. After that, the plasmids were propagated from bacterial stocks then purified. After that, the purified plasmid was transfected into target cells. GRP-R overexpression confirmed by Western blot.

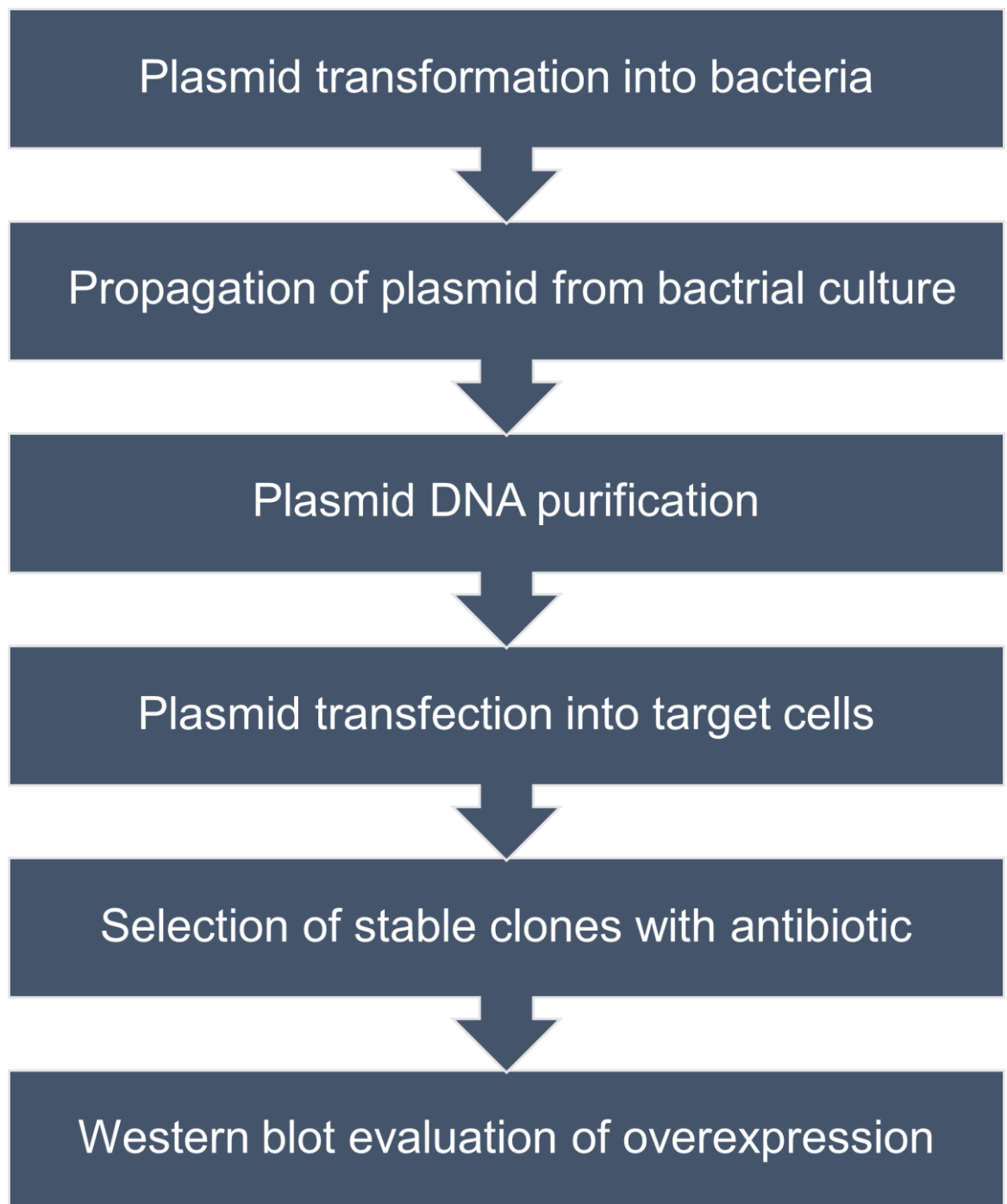


Figure 2.2: Schematic illustration showing the workflow of the generation of the stable overexpression of GRP-R from purified plasmid DNA.

2.1.4.2.1 Bacterial transformation

DH5 α TM cells were thawed on ice and gently mixed. 50 μ l of cells for each transformation were transferred into a cold microcentrifuge tube on ice. 10 ng of DNA was added and mixed gently then left on ice for 30 min. The cells were subjected to heat shock by placing the tube in the water bath at 42 °C for 20 seconds. Following that, the tube was placed on ice for 2 min. 950 μ l of pre-warmed SOC Medium was added. The tube incubated at 37 °C for 1 hour at 225 rpm. After that, 50 μ l of the bacterial suspension was spread into selective plate. The plate was incubated overnight at 37 °C. Single colonies of transformed bacteria were amplified in LB broth and pDNA extracted.

2.1.4.2.2 Plasmid propagation and purification

The propagation of bacterial culture and plasmid purification were performed as described in 2.1.4.1.1 and 2.1.4.1.2 respectively in this chapter.

2.1.4.2.3 Plasmid transfection

The plasmid was transfected into A549 cells using FuGENE[®] transfection reagent as described in section 2.1.4.1.3 of this chapter without introducing viral plasmids. The cells were left with the transfection mix overnight before selection of stable clones with antibiotic as described below.

2.1.4.2.4 Selection of stable clones

After overnight plasmid transfection, the culture media was replaced with fresh complete medium that contains G418 for selection of transfected cells. The transfected cells selected using 750 μ g/mL G418 over three weeks. Cells were subsequently maintained in 100 μ g/mL G418. The suitable G418 concentration for the target transfected cell line was determined by performing G418 kill curve. After selection, samples of the transfected cell line were collected to confirm the GRP-R overexpression efficiency. This was performed by Western blot as described in section 2.1.3.1 of this chapter.

2.1.5 Techniques used to generate and study GRP-R targeted formulations

In the third experimental chapter, the targeted liposomes were synthesised and tested *in vitro*.

2.1.5.1 Synthesis of targeting and control liposomes

To synthesize the targeted liposomes, we started by synthesising the targeting moiety – Cystabn then conjugated the Cystabn with PEG-Lipid.

2.1.5.1.1 Peptide Synthesis

Cystabn (Cys-D-Phe-Gln-Trp-Ala-Val-Gly-His-Sta-Leu-NH₂) was synthesized on the Rink Amide MBHA resin using Fmoc chemistry. After initial deprotection of the resin with 2 x 5 min 5% piperazine in DMF, each coupling step involved addition to 1 eq. of resin, Fmoc-protected amino acid, HCTU, HOBT and DIPEA (4:4:4:8 eq.) in 1.5 mL DMF. The mixture was incubated for 30 min at RT with occasional gentle agitation then washed with DMF (x3). This process was repeated to increase peptide yield. Successful Fmoc removal and coupling of amino acids was confirmed with the Kaiser test. After successful coupling and Fmoc deprotection of the N-terminal amino acid, the resin was washed with DMF (3 x 5 mL, 1 min), then DCM (3 x 5 mL, 5 min) and the resin dried under nitrogen then stored *in vacuo* for 3-5 h. Simultaneous side chain deprotection and peptide cleavage from the resin was achieved using TFA:TIPS:EDT:H₂O (94:2:2:2), performed at RT for 4 h. The peptide was precipitated in diethyl ether overnight at -20 °C. Precipitated peptide was harvested by centrifugation (3000 xg, 10 min, 4 °C). Peptide precipitate was washed (x3 cold diethyl ether) then dissolved in 10% aqueous acetic acid and lyophilised to yield a white powder.

2.1.5.1.2 Characterisation of Peptides

HPLC: Samples were analysed using a gradient elution method using Mobile phase A (H₂O + 0.1% TFA) and B solution (acetonitrile + 0.1% TFA) on a Perkin Elmer HPLC system comprising of binary solvent pump, autosampler, UV/Vis Detector and Peltier Column Oven. Mobile phases were membrane degassed using Millipore Vacuum filtration using 0.2 µm filter. The gradient profile was 0-5 min. 5% B, 5-25 min 5-95% B and 5 min 5% B. Peptide samples (~1 mg/mL in milliQ water) were eluted on a Phenomenex Luna® C18 (2) LC Column (5 µm, 100 Å, 150 x 4.6 mm, Phenomenex, UK). Samples of 10 µl were injected and elution monitored at 280 nm.

MALDI-Tof: Peptide samples (2 mg/mL in 1:1 acetonitrile: milliQ water + 0.1% TFA) were mixed with an equal volume of a saturated solution of α -cyano hydroxycinnamic acid (Sigma) and 1 μ L spotted twice onto the same well of a clean MALDI sample plate. Samples were analysed using linear ion detection mode on a SHIMADZU Axima-CFR MALDI-TOF.

2.1.5.1.3 Peptide-PEG-Lipid Conjugate Synthesis

One equivalent of DSPE-PEG₂₀₀₀-maleimide (6.8 μ mol in 4 mL chloroform) was added to two equivalents of cystabn (13.3 μ mol in 2 mL methanol) and stirred for 24 h at RT under nitrogen gas. To conserve the expensive lipid (DSPE-PEG₂₀₀₀-maleimide) and since this reaction is a mole-to-mole reaction (which means one mole of lipids is needed to react with one mole of peptide to produce the conjugate), we decided to use excess (two equivalents) peptide per each one equivalent lipid used. After confirmation of successful conjugation by MALDI ToF MS analysis the solvent was evaporated and the reaction mixture re-dissolved in milliQ water. Unreacted peptide was removed by dialysis against milliQ water at RT for three days (the water changed every 2 h then left overnight) using 2 kDa MWCO benzoylated dialysis tubing (SpectroPor, Spectrum Labs, New Brunswick, USA). The purified conjugate was lyophilised to a dry white powder.

2.1.5.1.4 Characterisation of Conjugates

HPLC: Samples were analysed as described in section 2.1.5.1.2 of this chapter. Conjugate analysis was performed on a Hypersil™ BDS C8 LC Column (3 μ m, 130Å, 150 x 4.6 m, Thermo Scientific, UK).

MALDI-Tof: Peptide-PEG₂₀₀₀-lipid conjugates were dissolved in chloroform at 2 mg/mL and a 1:1 mixture prepared with saturated methanolic solution of universal MALDI matrix (Sigma Aldrich, UK). The samples were analysed as described in section 2.1.5.1.2 of this chapter.

2.1.5.1.5 Liposomal Formulation

Lipids, for the liposomal formulations used in this work, were selected to serve a specific function and to produce the intended liposomes. One of the primary lipids used in liposomes is phospholipids due to their amphiphilic nature.

Dipalmitoylphosphatidylcholine (DOPC) was chosen to form the bulk of the liposomes because lipids that contain the choline group abundantly found in cell membrane of mammals, amphiphilic, self-assemble into bilayer (Bilayer preferring lipids) and commonly used to form liposomes [129-133]. Cholesterol was added into the formulation because it enhances bilayer stability and reduces aggregation by modulating the bilayer rigidity and increase membrane elasticity [134-137]. The pegylation of the surface of liposomes was achieved by incorporating lipid-PEG₂₀₀₀, which provide longest circulation time in vivo when used in the range of 5-10 mole % because it forms a dense polymer brush at the surface which cause the repulsive steric interaction. In addition to the biological stability, pegylation provides colloidal stability of the system by the steric hindrance effect [138-141]. To add the active targeting capability into the liposomes, a targeting moiety was incorporated as a DSPE-PEG₂₀₀₀-cystabn conjugate. In this way, cystabn will be available unhindered and bind to its receptor on the cancer cell [142-146].

Lipids for each liposomal formulation were dissolved in chloroform and mixed in a round-bottomed flask (see Table 2.4). The concentration of lipid-PEG-peptide conjugate solutions in chloroform were determined by UV spectroscopy using the molar extinction coefficient for the peptide tryptophan residue (5560 AU/mmol/ml). A thin film was produced by slow evaporation of the solvent under vacuum followed by one hour under high vacuum to remove solvent traces. The film was hydrated with PBS to a final lipid concentration of 10 mg/mL then heated to 55 °C and vortexed extensively to produce MLVs. Five cycles of freeze-thawing (dry ice-acetone followed by heating to 55 °C) were performed to produce reduce the lamellarity of the vesicles. Finally, lipid suspensions were extruded (21 x) through polycarbonate membranes of 200 nm, 100 nm and 50 nm pore sizes to produce a narrow size distribution of LUVs.

Table 2.4: Formulation components of liposomes reported in this study

<i>Formulation name</i>	<i>Components</i>
<i>Control-lipo</i>	DOPC: Chol: DOPE-PEG2000 (57: 38: 5 mol. %)
<i>Target-lipo</i>	DOPC: Chol: DOPE-PEG2000: DSPE-PEG2000-Cystabn (57: 38: 4: 1 mol. %)
<i>FL-Control lipo</i>	DOPC: Chol: DOPE-PEG2000: DHPE-Fluorescein (56: 38: 5: 1 mol. %)
<i>FL-Target-lipo</i>	DOPC: Chol: DOPE-PEG2000: DSPE-PEG2000-Cystabn: DHPE-Fluorescein (56: 38: 4: 1: 1 mol. %)

2.1.5.1.6 Characterization of Liposomal Formulations

Liposomes were characterized for size and zeta potential using Zetasizer Nano ZS. For size measurements the liposomal suspension was diluted 1:10 with PBS. For zeta potential measurements, the liposomal suspension was diluted 1:10 with PBS and transferred to a clean folded capillary cell (Malvern, DTS1070).

For colloidal stability, liposomes were diluted 1:10 with PBS or 10% serum then incubated at three different temperatures (4 °C, 25 °C and 37 °C) for 24 h and 72 h then characterized for size as described above.

2.1.5.2 Testing cell association of liposomes using flow cytometry

Cells were washed with warm PBS and blocked for 5 hours in 0.2% BSA in RPMI-1640 medium. The cells were dissociated using Versene and aliquoted at a concentration of 10^6 cells per mL in phenol-red free SFM. The samples were incubated at 37 or 4 °C for 5 min before treating with Control-lipo or Target- Lipo (1 µg/mL total lipids concentration) for 15-80 min. After incubation at 37 °C, cells were transferred onto ice and washed using 500 µL phenol red-free SFM.

Samples were analysed on a Beckman Coulter CytoFlex flow cytometer using exited using 488 nm laser and the emitted wavelength acquired using 585/42 bandpass filter. After doublet exclusion, 10^4 events/sample were acquired in the gated population, and analysed using CytExpert software (v2.3, Beckman Coulter, USA).

Testing uptake of liposomes using flow cytometry Cells were seeded onto 16 mm coverslips and incubated for 24 hrs. Cells were washed (x3) with PBS for 5 min at RT and treated with 1 $\mu\text{g}/\text{mL}$ (total lipid) of fluorescein-labelled control or target liposomes for 5 min at 37 °C. Coverslips were washed (x3) with PBS, fixed with 4% PFA (10 min at RT) and residual PFA quenched by 50 mM NH_4Cl (15 min, RT). The cells washed with PBS (x3) for 5 min, permeabilised with 0.2% Triton X-100 (10 min). Nuclei were stained with Hoechst 33258, 1 $\mu\text{g}/\text{ml}$ in PBST) then mounted on glass slides using Prolong Gold mounting medium (Invitrogen). The cells were viewed under a widefield microscope (Zeiss AxioPlan 2ie) and images taken using Axiovision software and analysed using Fiji software.

2.1.5.3 Live imaging of liposomes-treated cells by Fluorescence microscopy

Cells were cultured in coverslips (18 mm) overnight in complete media. Media was changed to 1 mL/well Opti-MEM for 8 hours before changing media to 200 $\mu\text{L}/\text{well}$ phenol-free media with 0.1% BSA for 1 hour. Treatment was added for the highlighted time before adding the required highlighted marker for further highlighted time in the relevant figures. The cells incubated at 37°C with treatments and markers. They were then washed 3 times before live imaging on coverslip using Zeiss Axiovert widefield microscope.

2.1.5.4 Assessment of colocalization of live cell imaging

EzColocalization plugin in ImageJ was used for measuring colocalization in cells. This EzColocalization plugin was designed by Stauffer et al. [1]. Each live image in this study contains two channels which contains a stack of snaps taken over time (a snap was taken every 10 seconds for every channel over 3.5 min). To colocalize the signal of the two channels over time, one channel was selected. A region of interest (ROI) was drawn around each cell in that channel. The ROIs were then propagated to the other channel and to the rest of the time-series. After that, the EzColocalization plugin was used to measuring colocalization by measuring the Pearson correlation coefficient (PCC). After that, one time point was selected and the average PCC of cells in that slice was plotted.

2.1.6 Statistical analyses

All data were analysed using Prism software (Version 9.0, GraphPad Software, San Diego, CA, USA). The two-way ANOVA test was used to compare test groups unless stated otherwise in the figure legend. Results where $P < 0.05$ were considered statistically significant and are denoted by *. Results represent the mean \pm SEM of 3 or more independent experiments unless stated otherwise in the figure legend.

GRPR EXPRESSION IN HUMAN SCLC CELL MODELS

Chapter 3

3.1 Introduction

SCLC is one of several types of cancer which overexpress the growth factor, GRP and its receptor, GRP-R. This means that SCLC can stimulate its own growth by utilizing this autocrine loop. GRP-R and two other receptors (NMBR and BRS-3) were found to be the mammalian counterparts of a group of related receptors called bombesin family, which is part of GPCR superfamily [44, 147, 148]. There have been several attempts to target GRP-R autocrine signalling in cancer treatment. An antibody was developed against GRP called 2A11 [149], which caused significant reduction in cancer growth due to a blockade of receptor signalling. This means that the tumour, in 1 in 12 of the evaluated patients with previously treated SCLC, shrunk to the extent that it could not be detected radiographically. A similar endpoint was achieved using GRP-R antagonist peptides which caused inhibition of cell proliferation in vitro and in vivo [150-153]. For example, RC-3095 showed a good toxicity profile and antiproliferation effects in preclinical models [38, 154, 155]. In another study, the combination of RC-3095 with gemcitabine treatment significantly shrunk the pancreatic tumour xenograft of CFPAC-1 cell in nude mice, after four weeks of treatment [155]. In another study, ^{99m}Tc-labeled bombesin-like peptide antagonists showed significant uptake by SCLC, prostate cancer and others [156]. GRP antagonists, RC-3095 and RC-3940-II, inhibited tumour growth in SCLC cell line (H-69) [98]. They also inhibited tumour growth in the prostate in vivo [157]. The statine-based antagonist JMV594 also known as RM2 (DPhe-Gln-Trp-Ala-Val-Gly-His-Sta-LeuNH₂) have strong affinity to GRP-R and have been used for cancer imaging and therapy [103, 158, 159]. Many authors showed that JMV594 labelled with different radiolabels can target GRP-R in vivo [103, 160-166]. For example, the use of combination therapy of Trastuzumab antibody and GRP-R antagonist JMV594 in mice with PC-3 prostate cancer xenografts, increased their survival rate [165]. Radiolabelled JMV594 was also shown to inhibit PC-3 cell line proliferation in vitro [166]. This means that, GRP-R over-expression can be exploited to target and enhance delivery of drugs and diagnostics to SCLC. With the aim of developing a GRP-R targeting liposomal formulation for SCLC cells it is key to investigate the relative target expression SCLC target cells and non-target cells.

In this chapter, the expression and functionality of GRP-R was determined in a panel of cell lines using Western Blot, flow cytometry, immunofluorescence, intracellular Ca²⁺ assay and cell growth assays.

3.2 Results

3.2.1 SCLC cell lines characterization

The morphological of H510, H345, H209, H82 and N417 SCLC cell lines were studied using light microscopy. Microscopic imaging of the cell lines revealed that SCLC cells are typically small and grow in clusters suspended in the culture media. The size of the cell clusters varied between cell lines (Figure 3.1).

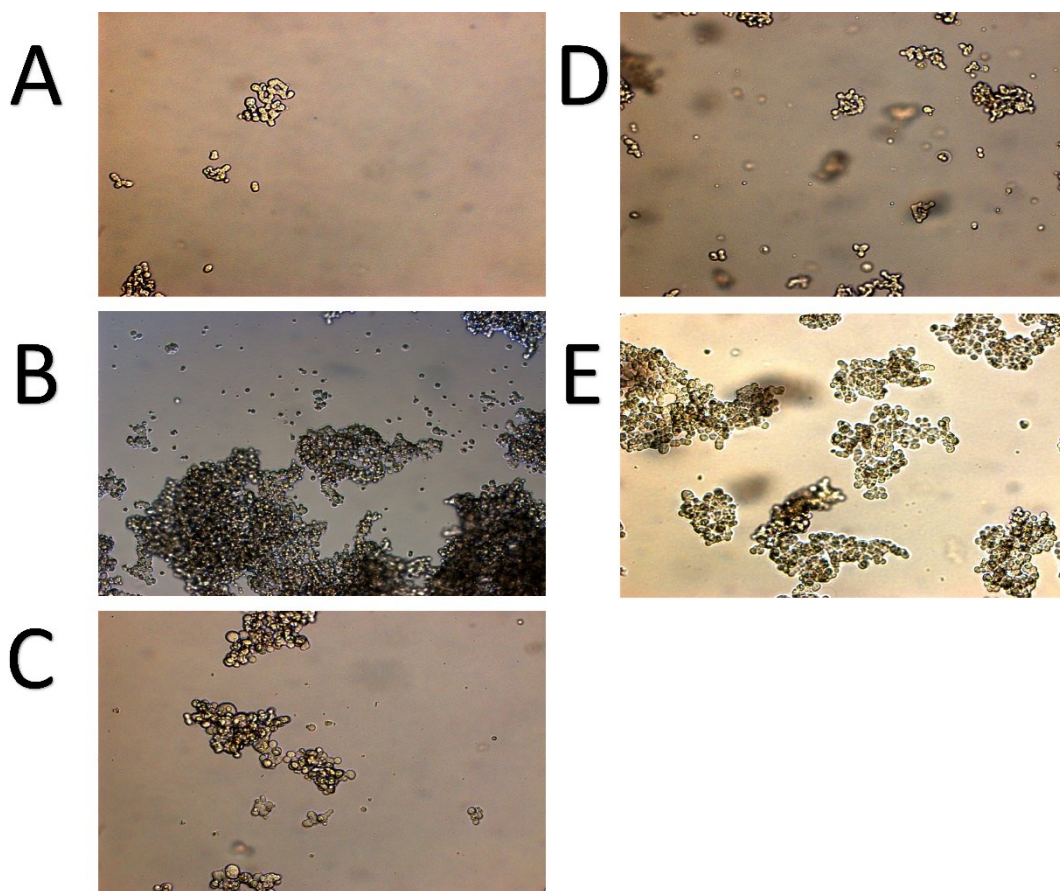


Figure 3.1: SCLC cell lines morphological micrographs. The micrographs were taken by light microscopy using 10x magnification for H510 (A), H345 (B), H209 (C), H82 (D) and N417 (E).

3.2.2 GRP-R expression

The expression of GRP-R was determined by Western Blot in a panel of five cell lines. H345 lysis in the routine lysis buffer (1% Triton X-100) resulted in low protein yields, typically 0.1 $\mu\text{g}/\mu\text{l}$ total protein assay (Table 3.1). A range of different lysis conditions were screened to optimise protein yield (Table 3.1). The highest total protein content resulted by using RIPA buffer and sonication.

To lyse the western blot samples, we used three surfactants with or without sonication to compare between them in terms of total protein yielded from the lysed cells in the tested sample. These surfactants include Triton 1% \pm sonication, high SDS (3% SDS, 60 mM Sucrose in 65 mM TrisHCl pH7.4) + sonication, and RIPA + sonication.

Table 3.1: Optimization of Lysis Conditions.

The table shows the four different lysis conditions compared in their total protein yield using H345 lysate as an example. The total protein in the lysate assayed using BCA total protein assay.

Condition of Lysis	Exemplar (H345)-Protein Concentration ($\mu\text{g}/\mu\text{l}$)
Triton 1%	0.1
Triton 1% + Sonication	2
High SDS + Sonication	0.9
RIPA + Sonication	4.2

Using these lysis conditions, Western blots was performed using three different antibodies (Figure 3.2). The GeneTex antibody (panel A) did not detect the GRP-R protein in the highlighted cell lines and showed non-specific binding. The Santa Cruz antibody detected one or two GRP-R protein bands in a panel of SCLC cell line samples (Figure 3.2). The mature, glycosylated GRP-R bands appeared in the 100 kDa in H510, H345, H209, H82 and N417. H510 showed two bands at 75 kDa and 100 kDa respectively. A third blot was performed using Rabbit polyclonal anti-human GRP-R antibody from Abcam (Figure 3.2).

The Abcam antibody detected only the un-glycosylated GRP-R at 55 kDa with no bands detected in the 65-100 kDa range as seen for the other antibodies. The clarity and sensitivity of the Santa Cruz antibody was judged to be the best of the three tested antibodies for detecting mature GRP-R. The Abcam antibody was appropriate for detecting only immature GRP-R.

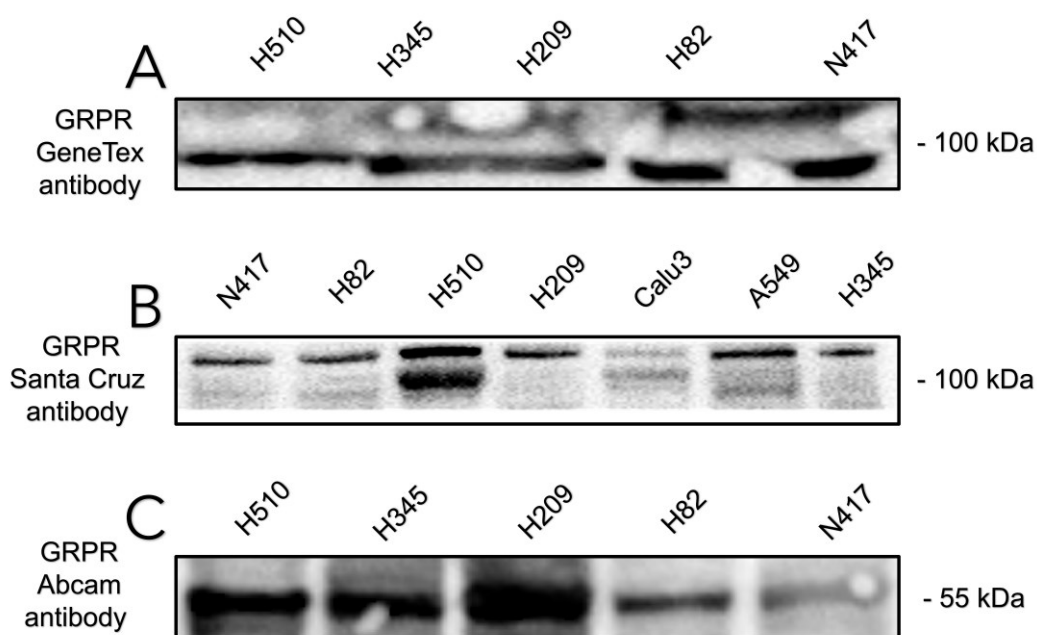
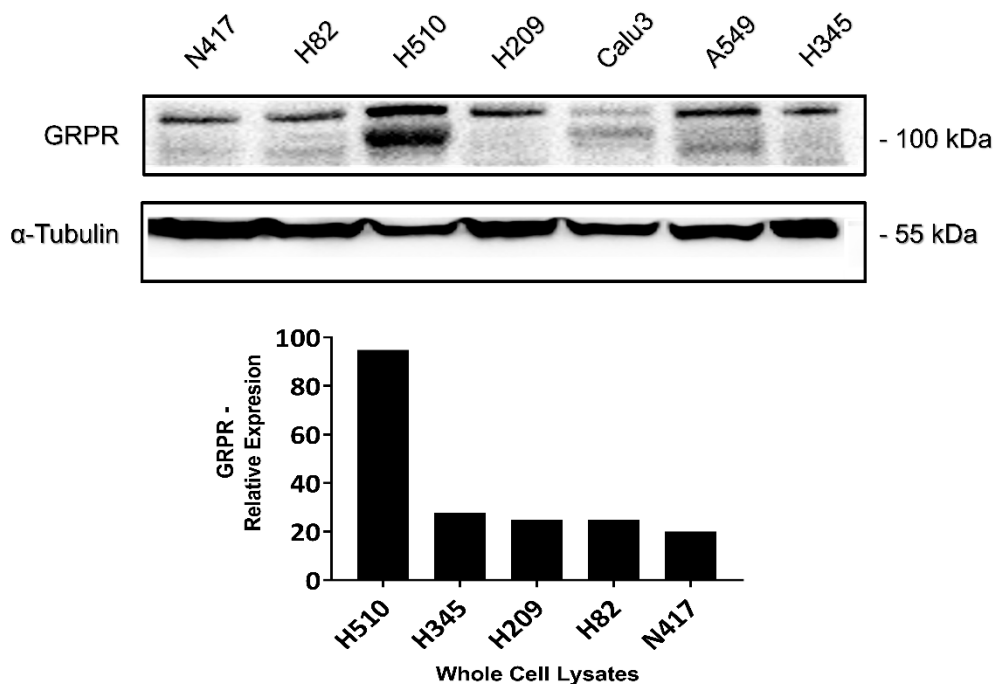


Figure 3.2: GRPR expression comparisons using three different antibodies in a panel of SCLC cell lines. Western blot of 50 μ g total protein loading of a whole cell lysate of 5 cell lines (H510, H345, H209, H82, H82 and N417). The lysates blotted and probed with antibodies against GRP-R. (A) GeneTex, (B) Santa Cruz Biotechnology and (C) Abcam.

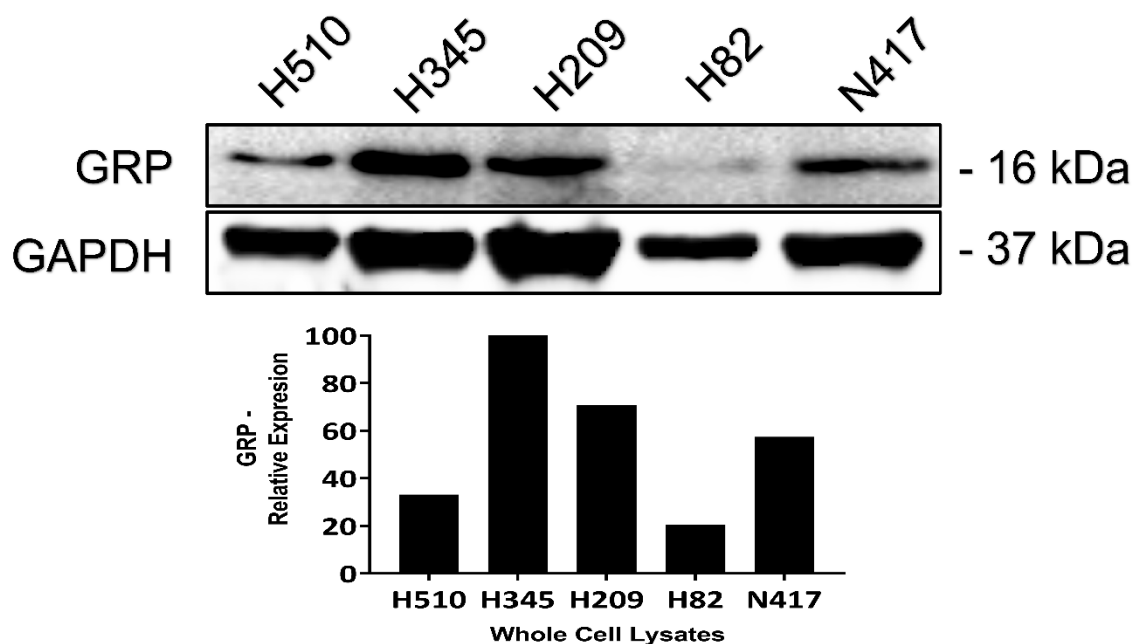
Using the blot performed with the Santa Cruz antibody and a tubulin loading control (Figure 3.3) the relative intensities of mature GRP-R expression were ranked as H510, H345, H82, H209 and N417. The samples relative band intensities are 94.8%, 27.7%, 25% and 20% respectively.



Rank order of GRP-R expression: H510 > H345 > H82 > H209 > N417

Figure 3.3: GRPR Expression in a Panel of SCLC Cell Lines using Santa Cruz Antibody. Western blot of 50 μg total protein loading of a whole cell lysate of 5 cell lines (H510, H345, H209, H82, H82 and N417). The lysates blotted and probed with antibodies against GRP-R and loading control (α -tubulin). The bands were quantified using ImageJ and normalized to the expression of α -tubulin. $N=1$ (one biological replicate therefore no error bars is shown).

I also measured the GRP expression in the samples using a polyclonal anti-human GRP antibody (Figure 3.4). In the blot, the GRP representative bands appeared at 16 kDa in H510, H345, H209, H82 and N417. The H345 showed the highest GRP expression represented by the highest relative band intensity of 100%. The lowest GRP expression detected in H82 with 20.5% relative band intensity. The samples ranked, according to their relative intensities of GRP expression, as the following H345, H209, N417, H510 and H82.



Rank order of GRP expression: H345 > H209 > N417 > H510 > H82

Figure 3.4: GRP Expression in a Panel of SCLC Cell Lines using Abcam Antibody. Western blot of 50 μ g total protein loading of a whole cell lysate of 5 cell lines (H510, H345, H209, H82, H82 and N417). The lysates blotted and probed with antibodies against GRP and loading control (GAPDH). A representative blot is shown in which the top part shows GRP representative bands in the highlighted cell lines and the bottom part shows the loading control (GAPDH) bands. The bands corresponding to GRP and GAPDH were quantified by densitometric analyses using ImageJ. GRP expression were normalized to GAPDH expression. The red dotted triangle highlights the rank order of GRP expression based on relative intensities. N=1 (one biological replicate therefore no error bars is shown).

3.2.3 GRP-R expression by flow cytometry

To examine GRP-R expression levels in intact SCLC cells, an indirect immunolabelling was performed followed by semi-quantitative detection by flow cytometry.

Firstly, the GRP-R antibody labelling conditions were optimised using a dilution range for the Santa Cruz GRP-R antibody with appropriate secondary antibody in PC-3 cells. A matrix of different antibody dilutions for both primary and secondary antibodies was used to identify the optimal conditions for specific cell staining. Figure 3.5, shows a heat map of the MFI on an antibody dilution matrix. The heat map shows a maximal MFI (213212) was produced from 1:30 and 1:100 dilutions of primary (1°) and secondary (2°) antibodies, respectively. The second highest MFI (145908) was produced using of 1° and 2° antibodies, respectively. Primary and secondary dilutions of 1:50 and 1:200 were taken forward for future studies in order to preserve antibody stocks.

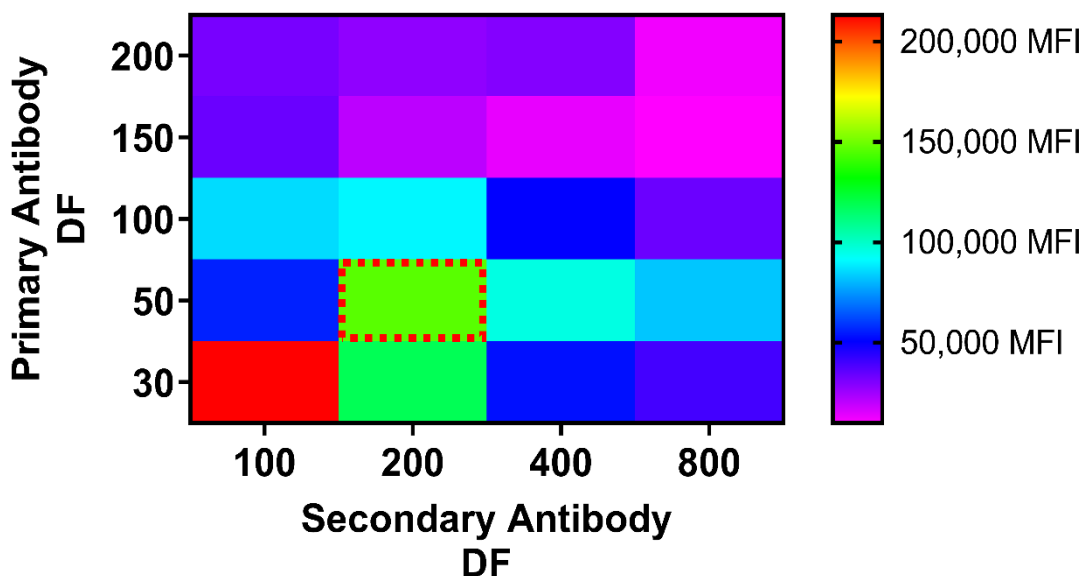


Figure 3.5: Titration matrix of GRP-R antibody in PC-3 cell line. The antibody titration heat map shows the dilution factor (DF) of primary (1°) antibody vs the DF of the secondary (2°) antibody used to produce the FITC median fluorescence intensity (MFI). The PC-3 samples were permeabilized and MFI. The red dotted rectangle highlights the optimal MFI in the matrix produced using the corresponding optimal 1°+2° antibodies DFs. The 1° antibody used was anti-human GRP-R antibody (sc-377316, Santa Cruz Biotechnology). The 2° antibody used was FITC-mouse IgGκ light chain binding protein (sc-516140, Santa Cruz Biotechnology).

A panel of SCLC cell lines was analysed for GRPR expression using the optimized flow cytometry labelling conditions. GRP-R expression is shown in Figure 3.6 as the MFI of permeabilized and non-permeabilized samples of the highlighted cell lines. Permeabilized samples' MFIs represent the samples' total GRP-R expression and the Non-permeabilized samples' MFIs represent the samples' membrane-bound GRP-R expression. In Figure 3.6, the rank order of both the total and membrane-bound GRP-R expression in the tested SCLC cell lines is H510 > H209 > H345 > H82 > N417. Among SCLC cell lines, H510 cell line showed the highest total and cell surface GRP-R expression. The lowest GRP-R expressing cell line is N417 in which the total GRP-R expression. However, the one-way ANOVA statistical analysis revealed no statistical significance among both permeabilized and non-permeabilized samples or between cell lines.

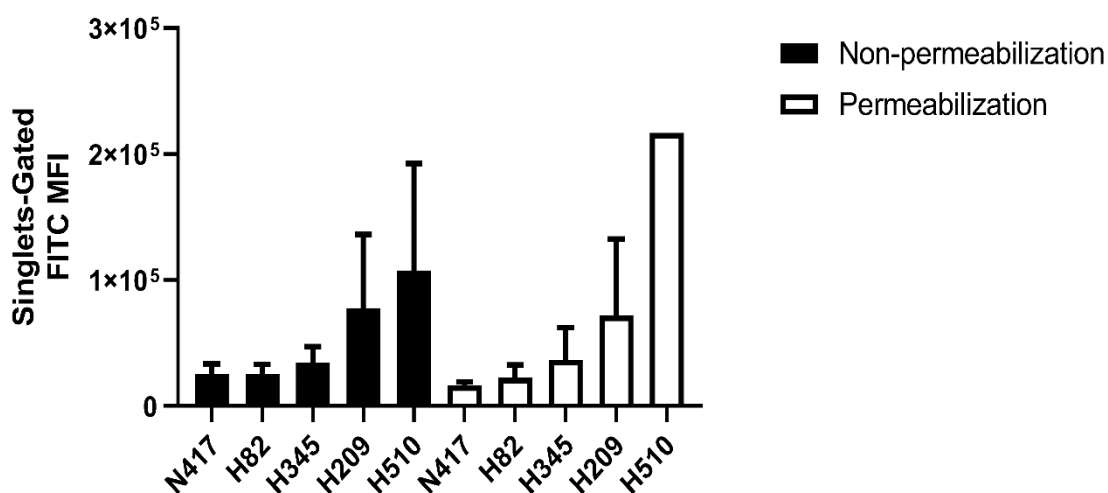


Figure 3.6: GRP-R expression in a panel of SCLC cell lines by flow cytometry. The graph shows the MFIs of non-permeabilized and methanol permeabilized SCLC cell lines. 10000 events acquired per gated sample. Data shown are mean \pm SD. N=3. The permeabilized H510 represents only one biological replicate therefore has no error bar.

3.2.4 GRP-R localization by immunofluorescent imaging

Widefield immunofluorescent imaging was used to show GRP-R localization in the cell. PC-3 cells were used as positive control (Figure 3.7). The punctate staining pattern indicates localization of GRP-R within the cell. In the adherent PC-3 cell line, GRP-R was clearly distributed throughout the cytoplasm and membrane. In contrast to PC3 cells, SCLC cells have a small cytoplasm: nuclear ratio which significantly decreases the cell area available for antibody labelling. As a result, a large proportion of the signal was detected in the central, nuclear region of the cell.

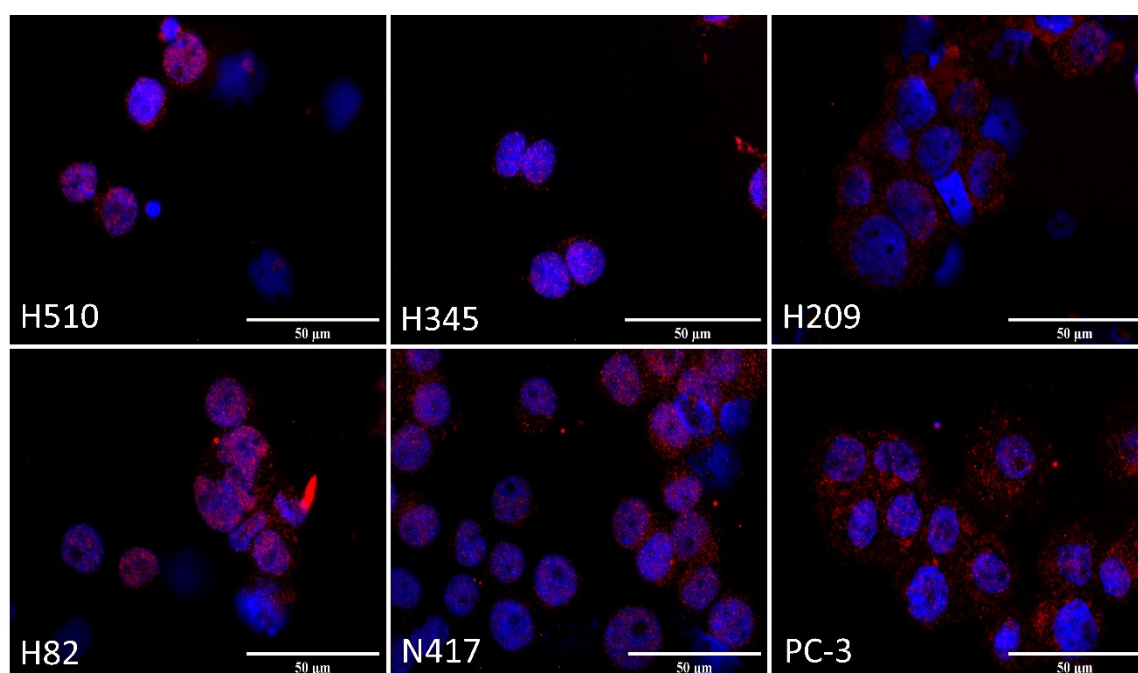


Figure 3.7: GRP-R expression in SCLC cell lines by immunofluorescence. The graph shows the localization of the GRP-R in PC-3, H510, H345, H209, H82 and N417 in higher magnification (x63). The cells were fixed the permeabilized before probing with Santa Cruz anti-GRP-R antibody.

3.2.5 Intracellular Ca^{2+} release assay

To examine for functionality of the GRP-R, intracellular Ca^{2+} release assay was used with the ratiometric calcium indicator fluorescent dye (Fura-2). The GRP-R agonist ligand Tyr⁴-bombesin was used over a 5-fold concentration range to construct a dose-response curve (Figure 3.8). Two SCLC cell lines, H345 and H82, were selected to test the receptor functionality. In spite of the modest expression receptor expression in H345 and H82, these cell lines displayed favourable growth characteristics and were more easily dissociated into single cells than other models. These made them appropriate for further investigation.

In H345 cells, a clear dose-dependent increase in intracellular calcium release was observed for H345 but not the H82. Sigmoidal dose-response curve fitting of the H345 data showed EC_{50} of Tyr⁴-bombesin is 2.4 nM for the GRP-R. Ionomycin is an ionophore which binds calcium and was used as a positive control in this experiment.

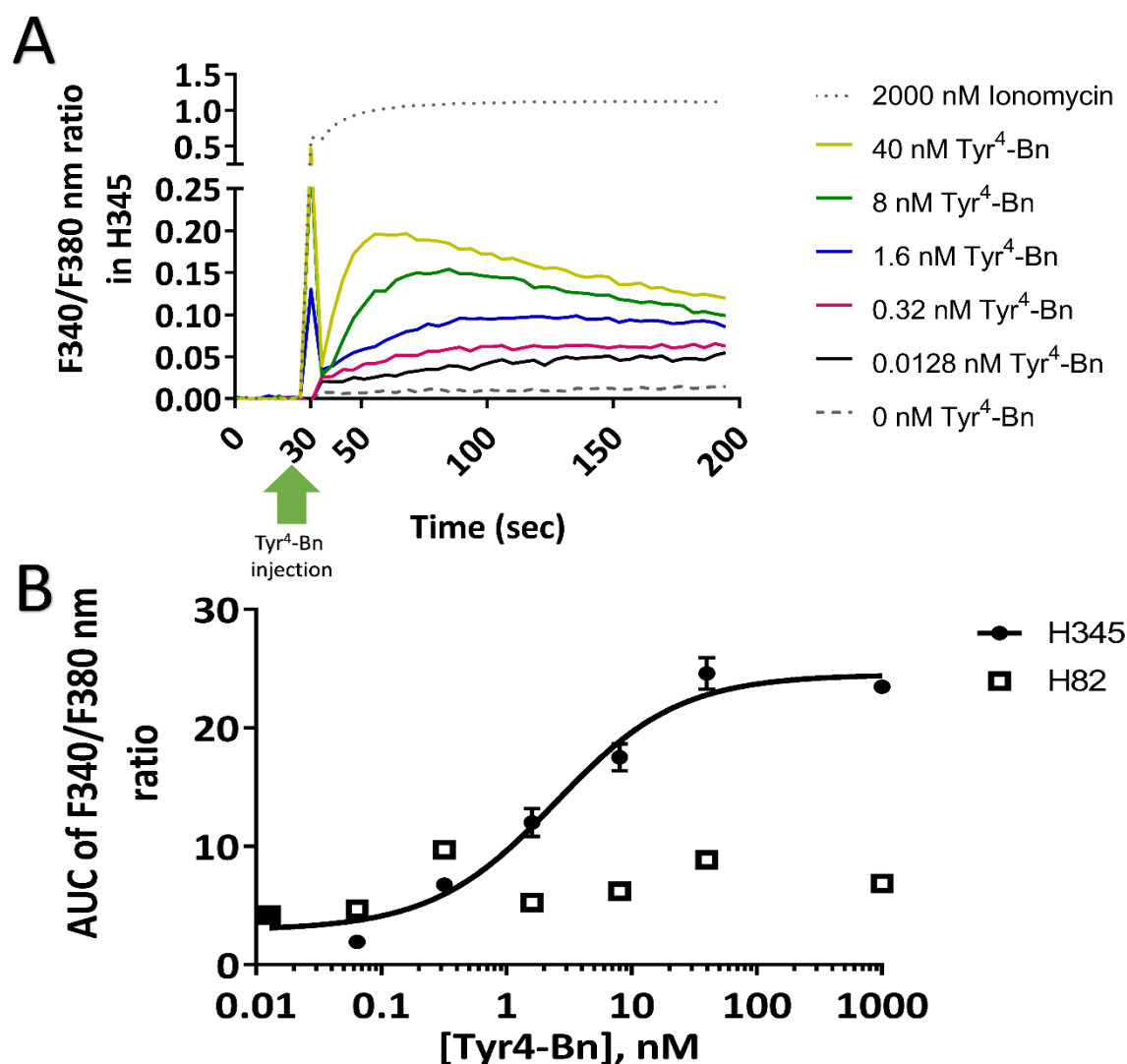


Figure 3.8: Calcium response induced by GRP-R Ligand in SCLC cell line. (A) Exemplar fluorescence trace from H345 cells loaded with Ca²⁺ reporter dye, Fura-2 AM before injection of GRP-R agonist, Tyr⁴-Bn (0-40 nM only). Baseline fluorescence was monitored for 30 s before peptide injection (arrow). (B) Escalating concentrations of Tyr⁴-Bn were injected into H345 or H82 cells and the Fura-2 AM fluorescence emission monitored over 200 s. AUC Fura-2 ratios at 340 nm / 380 nm were plotted against agonist concentration for both cell lines. Data shown are mean \pm SD. N=3.

The response of H345 and H82 cell lines to the BB1 receptor agonist, neuromedin B (NMB), was undertaken for comparison with GRP-R (Figure 3.9). In the H345 cell line, intracellular Ca²⁺ response showed saturable increases in the fluorescence signal with increased agonist concentration. However, the dose-response curve was right-shifted compared to the Tyr⁴-Bn response in the same cell line. Dose-response curve fitting of the H345 data showed EC₅₀ of 52 nM. The H82 cell line showed no notable increase in the fluorescence signal with increasing agonist concentration.

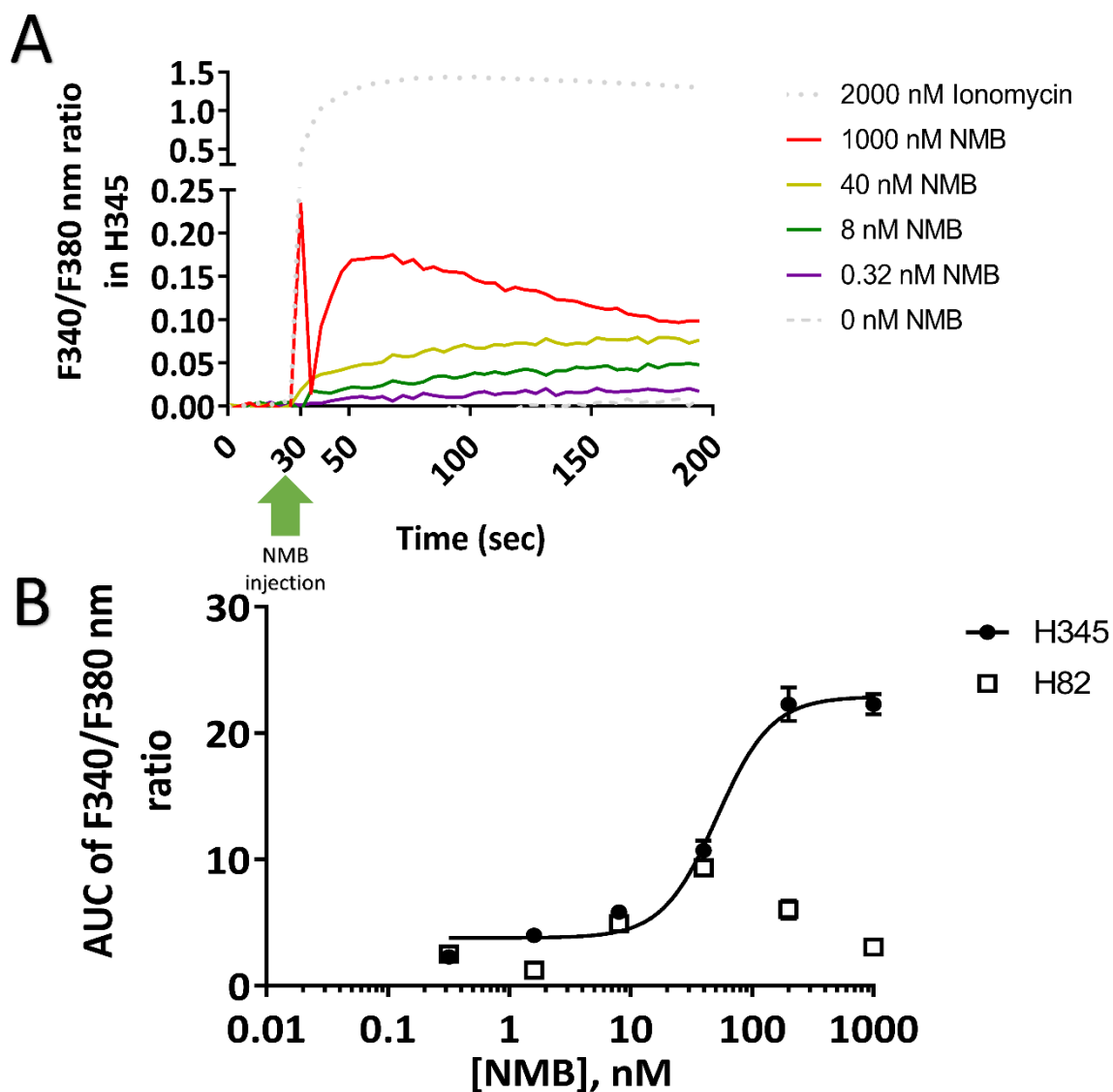


Figure 3.9: Calcium response induced by NMB in SCLC cell line. (A) Exemplar fluorescence trace from H345 cells loaded with Ca^{2+} reporter dye, Fura-2 AM before injection of NMB. Baseline fluorescence was monitored for 30 s before peptide injection (arrow). (B) Escalating concentrations of NMB were injected into H345 or H82 cells and the Fura-2 AM fluorescence emission monitored over 200 s. AUC Fura-2 ratios at 340 nm / 380 nm were plotted against agonist concentration. Data are mean \pm SD. $N=3$.

3.2.6 MTS assay

The MTS assay was performed to assess the mitogenicity or inhibitory effects caused by exposure to Tyr⁴-Bombesin (a GRP-R agonist) or Cystabn (a GRP-R antagonist). H345 and H82 cell lines were treated with 100 nM or 500 nM of agonist/antagonist for 5 days in SIT medium (Figure 3.10). The data are represented as percentage of growth compared to the untreated (control) group. H345 treated with Tyr⁴-Bn caused significant, concentration-dependent growth of the treated cells compared to the untreated group. Treatment with 100 nM Tyr⁴-Bn caused the H345 cells to increase their growth rate by 74% ($P < 0.05$) after 5 days treatment. The treatment also caused a 173% increase ($P < 0.001$) in growth rate after 5 days when the concentration increased to 500 nM.

H345 treated with Cystabn showed significant ($P < 0.002$ to $P < 0.001$) concentration-dependent growth inhibition compared to the untreated group. Cystabn inhibited the H345 cells growth rate ($P < 0.002$) and reduced it to 85% after 5 days treatment with 100 nM concentration. Treatment with 500 nM caused a 2.4-fold decrease ($P < 0.001$) in growth to 42% after 5 days. There were no significant ($P > 0.05$) changes in growth detected in H82 cells after Cystabn treatment.

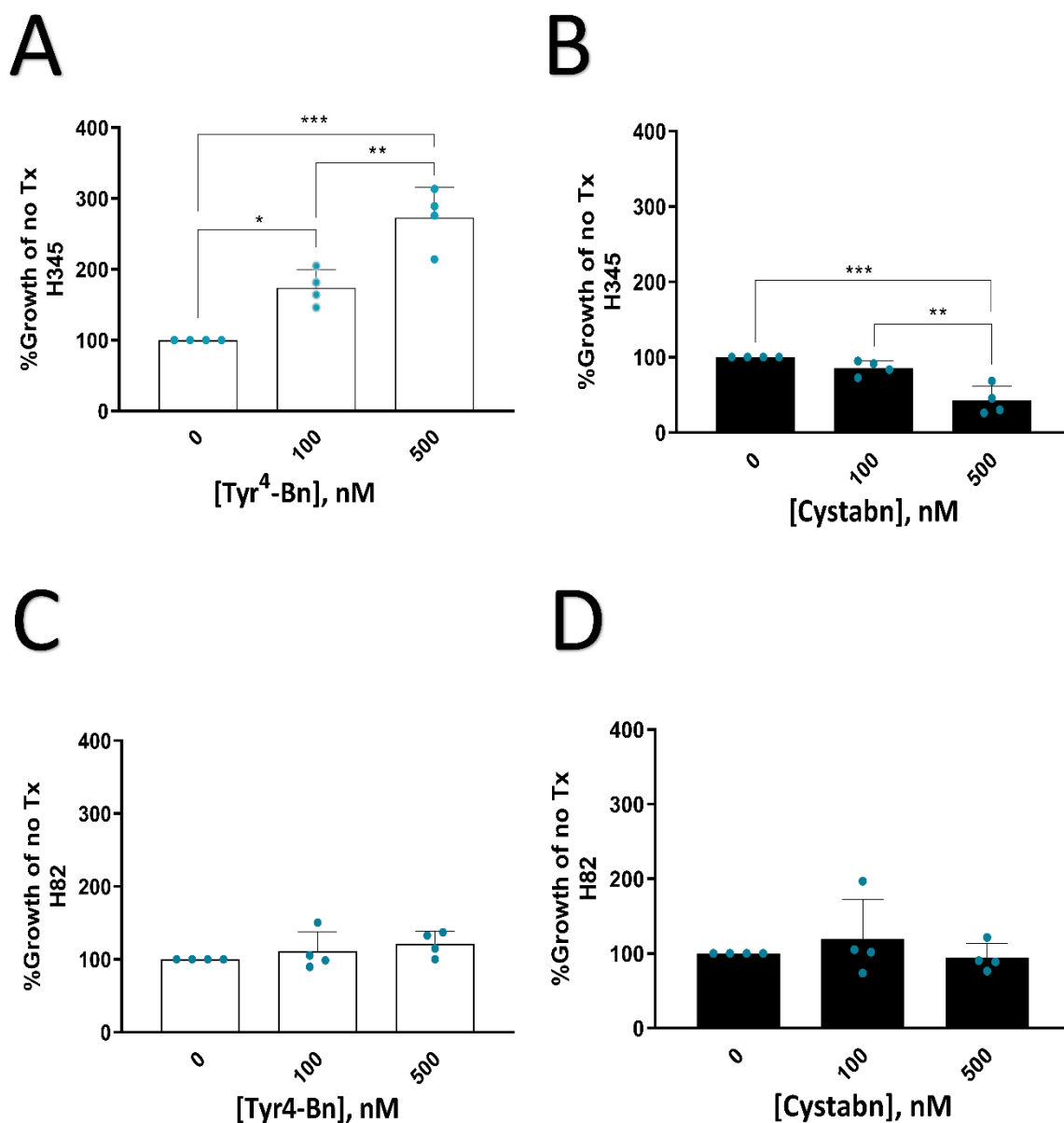


Figure 3.10: SCLC cell lines growth modulation by GRP-R agents. H345 and H82 cells were cultured over 5 days in SIT medium in the presence of escalating concentrations of Tyr⁴-Bn (A) or Cystabn (B) before cell growth quantification by MTS assay. Similarly, (C, D) show MTS growth data for H82 cells in the presence of Tyr⁴-Bn (C) or Cystabn (D). The Y axis represents the percentage of cell growth of treated cells compared to the no treatment (Tx) cells. Errors bars are SD. N=4
*, **, *** < 0.05, 0.002 or 0.001 respectively.

3.2.7 Clonogenic assay

The colony formation assay was also performed on the SCLC cell lines (H345 and H82). The cell lines treated with 10 nM of Tyr⁴-Bn in 2% FBS RPMI. Figure 3.11 show H345 and H82 cell lines treated with 10 nM. After a week, colonies were stained with MTT and counted manually by light microscopy. The data shows that H345 cells increased its colony numbers in response to 10 nM of Tyr⁴-Bn significantly ($P < 0.001$) compared to H82 cell line.

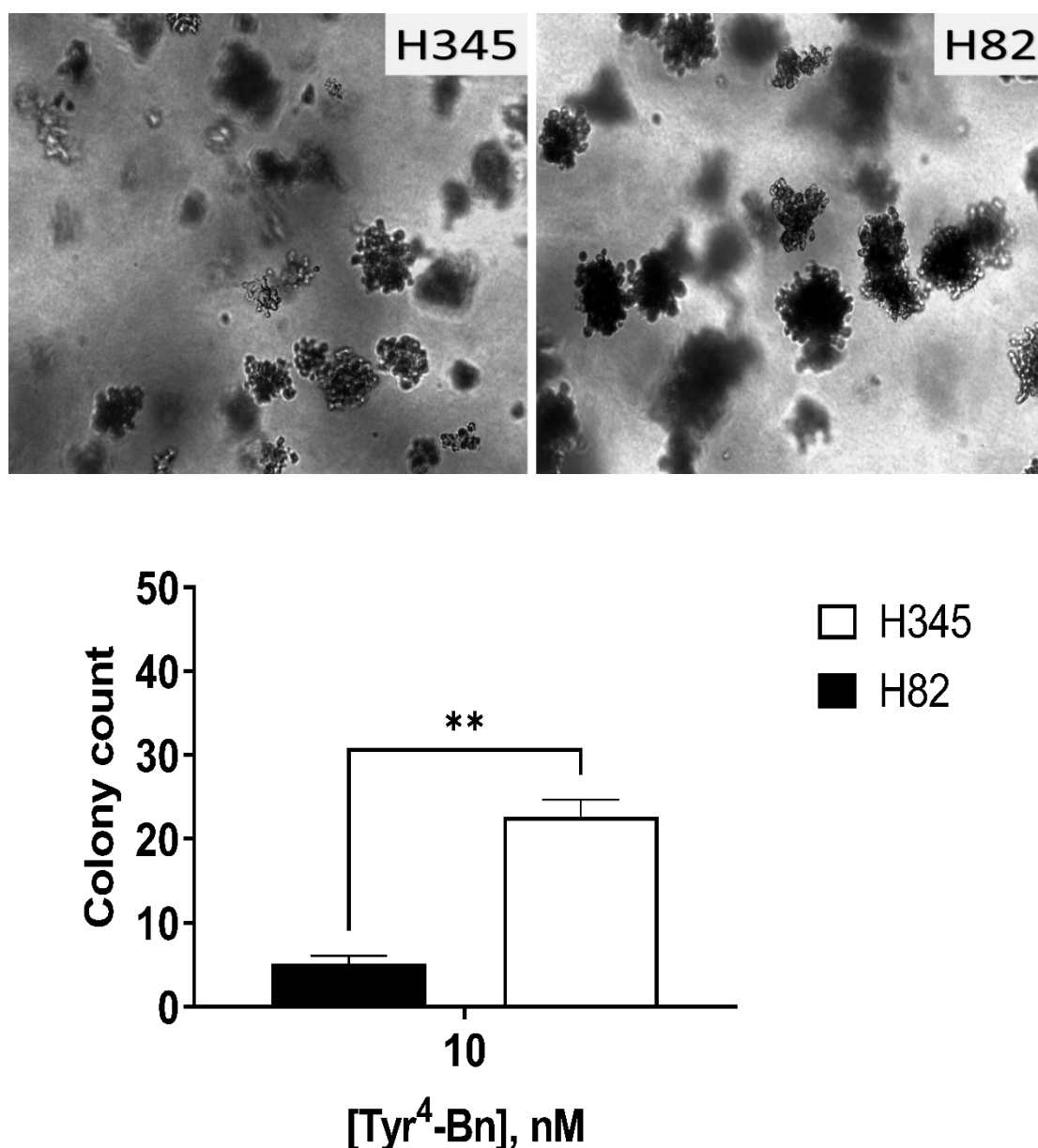


Figure 3.11: Growth modulation by GRP-R ligand using clonogenic assay. H345 and H82 cells were treated with 10 nM Tyr⁴-Bn for 7 days and the number of cell colonies counted microscopically. Errors bars are SD. N=3.

3.3 Discussion

In order to work towards a targeted liposomal formulation for SCLC, it is necessary to identify an appropriate SCLC model for the formulation to be tested on. At this stage of the project, I sought to characterise SCLC cell models in terms of GRP-R expression. The prostate cancer cell line (PC-3) were selected as a positive control in experiments due to its high GRP-R expression compared to lung cancer [38].

Initial experiments involving cell lysis in 1% Triton X100 produced very low protein yields and prompted the optimisation of the cell lysis protocol for SCLC cells. The low ratio of cytoplasmic:nuclear volume of SCLC cells is the most likely factor contributing to low protein yields [167]. The optimized lysis conditions, including lysis in RIPA buffer followed by sonication, was used for Western blot detection of GRP-R protein expression. Three antibodies – from GeneTex, Santa Cruz and Abcam- were compared for their utility in Western analysis. The polyclonal GeneTex antibody was excluded due to poor antigen recognition in all samples. The mouse monoclonal antibody from Santa Cruz detected multiple GRP-R protein bands in some SCLC cells. This monoclonal antibody detected mature, glycosylated GRP-R while the Abcam antibody detected only the immature GRP-R at ca. 55 kDa. Benya et al. showed that mutant GRP-R, in which all extracellular glycosylation sites were removed, migrated with an apparent mass of ca. 52 kDa [44, 168]. This indicates that the Abcam antibody was unable to detect mature GRP-R, while the Santa Cruz detected bands detected between 65-100 kDa represent various glycosylated forms of GRP-R.

As per the literature, it appears that the selected panel of SCLC cell lines include three GRP-R overexpressing lines (H510, H345 and H209) and two GRP-R low/non-expressing SCLC cell lines (H82 and N417). Western blot showed GRP-R is expressed in all SCLC cell lines with variable expression levels. H510 highly expressed the receptor compared to other tested lines, which is in line with the literature as highlighted below. The H345 also expressed the receptor as per the literature. Interestingly, the H82 and N417 cells expressed mature GRP-R. This contradicts published data regarding GRP-R mRNA expression, bombesin immunoreactivity and Ca^{2+} release assay as shown by others [34, 169-178].

I also measured the expression of GRP in SCLC lines using a polyclonal anti-GRP antibody from Abcam. The detected GRP expression pattern in SCLC in general was confirmed in several studies [34, 46, 172, 176, 178-180]. However, the specific expression of GRP in and N417 could not be detected by some studies using PCR and Bombesin-like immunoreactivity [65, 174, 179, 181]. In this study, we detected GRP in all tested SCLC cell lines including in H82 and N417 using different experimental tool (Western blot). However, this does not mean that GRP can act as potent mitogen and drive tumour growth in those two cell lines (H82 and N417). This leads us to investigate the mitogenic functionality of GRP-R in the selected SCLC cell lines.

To support the Western blot findings produced by the Santa Cruz antibody, flow cytometry experiments was performed to confirm the GRP-R expression in the selected cell lines. After optimizing the permeabilization conditions, antibody titration experiment was performed using the Santa Cruz antibody to find the optimal primary and secondary antibodies dilution to improve cell labelling using PC-3 cell line. Analysis of both permeabilized and non-permeabilized samples permits the comparison of “total GRP-R expression” from permeabilised samples and “cell surface expression” of GRP-R. In this study, the receptor surface expression is more relevant rather than the determination of total receptor expression. This is because the targeted nanoparticle can target the membrane-bound receptor.

The flow cytometry data confirmed the GRP-R expression detected by Western. However, the experiment showed no statistically significant differences ($P > 0.05$) in GRP-R expression between cell lines. This led me to investigate the receptor localization in the cells and investigate whether there are any differences in receptor distribution between cell lines. After optimization of the immunofluorescence imaging experiment using three different secondary antibodies to reduce the background fluorescence. From the microscope data, there were no apparent differences between SCLC cell lines in terms of the receptor distribution around the cell. The data also shows that SCLC cell lines have a small dissemination of receptor punctuated signal throughout the cell, including the central nuclear/peri-nuclear region. This could not be resolved in a satisfactory manner without confocal microscopy at this stage of the project.

Since all SCLC cell lines expressed GRP-R in variable amounts, I decided to narrow down the selected cell lines to H345 and H82 to use in the study of receptor functionality. This is because H345 shown to express GRP-R more than H82 by Western blot and flow cytometry. Working with two cell lines only instead of four SCLC lines reduce the time and efforts needed to perform experiments as well as saving resources and use it for more experiments. Furthermore, in the literature, the studies reporting the effect of bombesin-like peptides as mitogens to drive SCLC growth is well reported in H345. For example, H345 was reported to produce GRP and its receptor as well as increase cell proliferation in response to bombesin agonist and decrease cells growth in response to bombesin antagonist [34, 77, 170, 177, 182-186]. The H82 cell line was chosen for its lack of autocrine growth induced by GRP or bombesin. Following that, I moved on to investigate the functionality of the GRP-R receptor in the selected cell lines by intracellular Ca^{2+} release assay with the ratiometric calcium indicator fluorescent dye, Fura-2. A sigmoidal dose-response curve was recorded for H345 cells confirming the extracellular activation of the GRP-R, which leads to intracellular calcium release [187]. H82 cells showed no overall increase in the fluorescence signal with the increase in the agonist concentration which indicates the absence of functional GRP-R. This complements the data obtained from Western blot and flow cytometry. So, the H345 not only expresses GRP-R more than H82 but it also responds to GRP-R agonist which drives its growth, unlike H82. This is in line with Cuttitta et al. report which demonstrated that bombesin-like peptides can function as autocrine growth factor in SCLC *in vitro* and *in vivo* by using bombesin monoclonal antibody to block GRP stimulated growth [34].

In addition to response to GRP-R agonist stimulation, the response to NMB-R agonist was also tested. NMB induced a dose-dependent increase in Fura-2 fluorescence in H345 cells, although the response was weaker in comparison to the response to Tyr⁴-Bn. The weaker response of NMB in H345 cell line confirms that the GRP-R is the dominant highly expressed receptor in the cell. H82 cell line, showed no overall increase in the fluorescence signal with the increase in the NMB concentration which means it does not express significant levels of functional NMB-R.

In the literature, using RT-PCR, SCLC cell line H345 shown to express more than half the levels of GRP-R found in the NSCLC cell line [188]. In another study, intracellular Ca^{2+} mobilization response to 100 nM GRPR agonist (Tyr⁴-bombesin) reported in several SCLC cell lines [189]. The agonist stimulated the mobilization of calcium in H510, H209 and H345 but not in H82 and N417.

After establishing the expression and the signalling functionality of GRP-R, the mitogenicity of the targeting peptide (Cystabn) was tested using MTS assay. The MTS assay uses the MTS reagent to measure cells viability of proliferation by measuring the cells metabolic ability to convert MTS to its formazan dye which can be quantified spectroscopically. Activation of GRP-R leads to activation of phospholipase C (PLC) which increase cellular calcium and activation of the PKC pathway through activation of Gq and G α 12/13 type of G proteins. This also activates ERK/MAPK and PI3K pathways. The stimulation of G α 12/13 leads to activation of Rho family pathway. All of these pathways lead to the survival and growth of the cell [44, 190-192].

In this study we sought to use GRP-R antagonist peptides on the liposomal carriers. This is because the use of an agonist ligand on the nanoparticles could stimulate SCLC growth which is highly undesirable. Cystabn is a GRP-R antagonist which is used in this project to target GRP-R in SCLC cells. We tested the mitogenic effect of this antagonist and compared it to the agonist (Tyr⁴-Bn) using MTS. A panel of SCLC cell lines (H345 and H82) were treated with 100 nM or 500 nM of the treatments for 5 days in SIT medium. Unlike H82, Tyr⁴-Bn stimulated H345 cells growth in a concentration-dependent manner compared to untreated control. This means that, as expected, the Tyr⁴-Bn acted as a mitogen and derived the growth in H345 which indicate that it expresses high levels of functional GRP-R. It also indicates that H82 expresses low levels of functional GRP-R which does not respond to mitogen stimulation. In contrast, Cystabn caused concentration-dependent inhibition of growth in H345 but not H82. This means that Cystabn can effectively inhibit the growth of functional GRP-R expressing cells which make it a good targeting or therapeutic agent. This also indicate that the GRP-R expression is an important driver of growth in SCLC cells and it can be modulated using bombesin-like agents and good therapeutic target.

It was demonstrated that using an antagonistic peptide is preferable to using an agonist. A very good example reported with the use of radiolabelled somatostatin receptor antagonists which showed better biodistribution and high tumour uptake compared to agonists [193]. Similarly, the use of Bombesin antagonist (Demobesin 1) showed preferable biodistribution in vivo in PC-3 xenografts compared to agonists [194]. In addition to that, the use of agonistic GRP-R targeting ligands could stimulate tumour growth if intracellular delivery is inefficient [34]. This favours the use of an antagonist peptide for targeting GRP-R.

We selected a synthetic GRP-R antagonist peptide (d-Phe-Gln-Trp-Ala-Val-Gly-His-Sta-Leu-NH₂) which we termed, Cystabn after bear an N terminal L-cysteine residue, to enables subsequent incorporation to targeted liposomes. The observation of growth inhibition of H345 cells in response to Cystabn treatment validated our choice of targeting ligand.

To further support the MTS assay data, a clonogenic assay was performed using the agonist (Tyr4-Bn). A clonogenic assay also known as colony formation assay. It permits the evaluation of cells survival or proliferation in vitro based on the ability of a single cell to grow into a colony of cells. It can be used after treatment of cells with cytotoxic agent, radiation or mitogen. This assay is one of the standard tools used in cancer research to evaluate the cancer cell's clonogenicity trait to initiate tumours. It also used to compare different agents for their ability to stimulate or inhibits the cell's ability to proliferate. In this study we used this assay to confirm that GRP-R expression level in cells can affect their growth after treatment with Tyr4-Bn. Two cell lines were used, H345 which has higher GRP-R expression levels than H82 cells. The cells treated with 10 nM of Tyr4-Bn. This concentration is sufficient to stimulate clonogenicity in SCLC. As expected, the agonist significantly stimulated colony growth in H345, using 10 nM compared to H82 cell line even after relatively short treatment exposure period (7 days). This further confirms the importance of GRP-R role in SCLC cancer growth and therefore the inhibition of that receptor causes the cancer to slow down SCLC growth. Higher concentrations of Tyr4-Bn were used in the MTS assay compared to the clonogenic assay. This is because of the shorter treatment period (5 days) as well as the serum-free media (SIT) used in the MTS assay. In addition to that, MTS is a colorimetric assay for assessing cell metabolic activity which depends on absorbance for detection of viable cells. This method is generally less sensitive than fluorescent and luminescent methods. It also depends on several factors for detecting viable cells such as cells number per well, cellular metabolic activity and cell type.

3.4 Conclusion

From the experiments conducted I optimised a number of complementary techniques to study bombesin receptor expression and functionality, thereby developing a toolbox that can be used to examine the efficiency of receptor targeting. The H345 cell line was selected as the most appropriate model system to study the targeting of GRP-R in SCLC and will be further studied in Chapter 4. This means that this model can be used to test the targeting capability of the targeted liposomes. It can also test the uptake or internalization of any nanoparticles utilizes the growth loop (GRP/GRP-R) in SCLC which provide an experimental tool for research.

**MANIPULATING BOMBESIN
RECEPTOR EXPRESSION LEVELS
IN SCLC**

Chapter 4

4.1 Introduction

Of the hormones known to be secreted by SCLC cells, GRP, is the most widely studied [38]. GRP was found to be a potent mitogen in malignancies such as SCLC, breast, colon and prostate cancers [46, 195, 196]. GRP receptor is reported to be overexpressed in numerous cancers such as lung, colon, and prostate [38, 44]. SCLC cells express GRP-R and also secrete the cognate ligand, GRP. This receptor-ligand form an autocrine growth loop where the cancer can stimulate its own growth [34, 176, 177]. The role of GRP/-R in cancer survival and growth is crucial and well supported in the literature [38, 197-199]. The use of GRP-R antagonists such as BW2258U89 has been shown to inhibit cancer growth in SCLC cell line H345 and in nude mice [186]. Given the therapeutic potential of GRP-R as a target, we sought to develop a series of cell line models for testing formulations which target GRP-R in lung cancer. We hypothesised that the use of a N-terminal cysteine modified GRP-R antagonistic peptide prevents the growth effect that result from the use of agonistic peptides. Such effect might compromise the active targeting of the cancer cells by causing GRP-R activation and stimulation of cancer growth. Using antagonistic peptide for GRP-R may be preferable in cancer targeting over agonist due to higher tumour uptake and longer tumour washout [194]. GRP-like peptides with antagonist activity at their receptor have been developed. Those antagonists shown to have high affinity binding to GRP-R and stimulates receptor internalisation such as KJGJKG [103, 104, 147].

In this chapter, we sought to modulate GRP-R expression levels in SCLC models. Firstly, we selected two SCLC cell lines with the highest GRP-R expression levels before performing GRP-R knockdown with shRNA technology. We also knocked down and over-expressed GRP-R in A549, an adherent and fast-growing NSCLC cell line.

4.2 Results

4.2.1 GRP-R knockdown efficiency by qRT-PCR

The knockdown of GRP-R expression in the H510 and H345 SCLC cell lines was performed using five shRNA sequences and the lentiviral vectors (LVs). The efficiency of the GRP-R KD was determined using qRT-PCR and Western Blot.

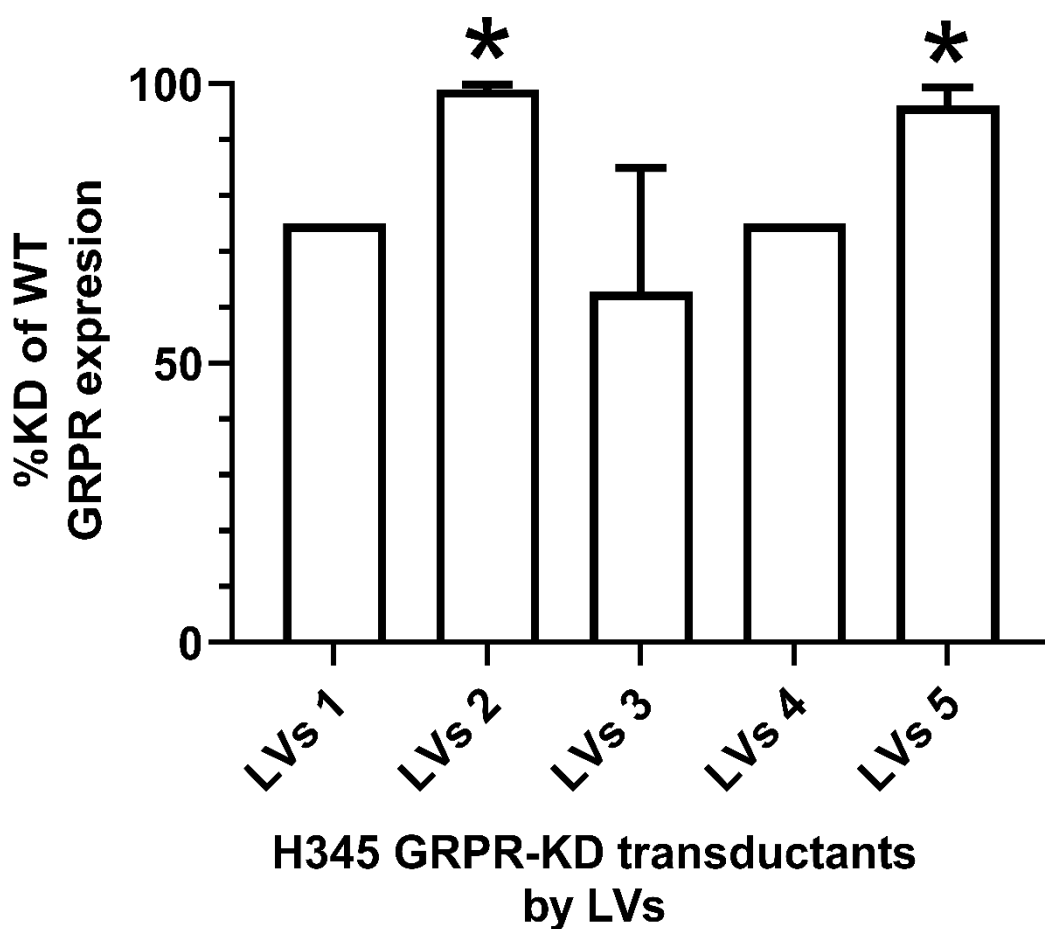


Figure 4.1: GRP-R knockdown efficiency confirmation by qRT-PCR in SCLC. GRP-R mRNA knockdown efficiency detected by RT-qPCR analysis from GRP-R shRNA-treated H345 cells using lentiviral vectors (LVs) of five shRNA sequences at 72 h. The percentages are relative to the WT expression levels \pm SD. N=1 (one biological replicate and error bars represents two technical replicates).

The GRP-R knockdown efficiency compared to WT expression determined by qRT-PCR (Figure 4.1) and revealed a significant ($P < 0.03$) GRP-R knockdown from two lentiviral shRNA vectors (2 and 5). The extent of KD from lentiviral vector 2 and 5 were 99 and 96%, respectively. The extent of KD in other samples were lower with 75%, 63% and 75% by shRNA sequences 1, 3 and 4 respectively. LV2 was selected as the lentiviral construct for antibiotic-selection to produce a stable GRP-R KD H345 cell line. The puromycin selection was done by replacing the media with fresh complete medium that contains 0.5 $\mu\text{g/mL}$ of puromycin for selection of transduced H345. This dose obtained from puromycin kill curve performed on non-transduced H345 (figure A.2).

A stable GRP-R KD H510 cell line was also generated in the same way as described for H345. The highest KD% in GRP-R expression (LV4) was chosen for antibiotic-selection. This was based on the KD efficiency data obtained from qRT-PCR (figure A.1). The cells were subjected to 0.5 $\mu\text{g/mL}$ puromycin selection after identification of the optimum puromycin concentration from a kill curve on H510 (figure A.3).

4.2.2 Confirmation of GRP-R KD after puromycin selection of stable transfectants

Puromycin selection was performed for two weeks in the SCLC cell lines (H510 and H345). Samples from the puromycin-selected cell lines were collected and the GRP-R KD of expression was confirmed by Western blot (Figure 4.2 and Figure 4.3) and flow cytometry (Figure 4.4).

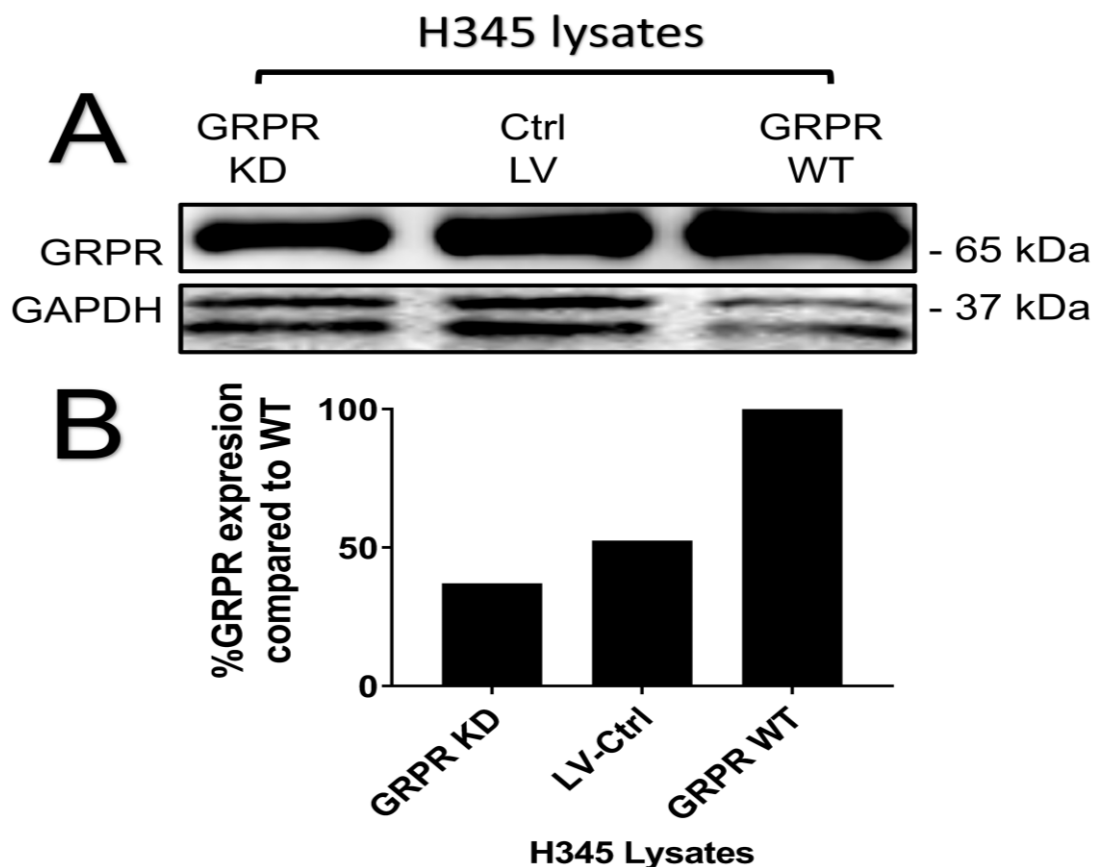


Figure 4.2: GRP-R knockdown efficiency confirmation by Western blot in H345. Western blot of 50 μ g total protein loading of a whole cell lysate of H345 cell line. (A) shows GRP-R representative bands (top) in the highlighted cell line and the bottom part shows the loading control (GAPDH) bands. The bands corresponding to GRP-R and GAPDH were quantified by densitometric analysis and shown in (B). The intensities of the GRP-R bands from blot (A) were normalized to the corresponding bands' intensities of GAPDH and the samples' relative expression was normalized to WT expression. $n=1$ (one biological replicate therefore no error bars is shown).

As shown in Figure 4.2, Western blot analyses of whole cell lysates from WT, empty-LV control and the GRP-R KD H345 cells were performed. GRP-R expression compared to the WT H345 in GRP-R KD sample as well as in LV-ctrl. From Figure 4.2A, the expression of the KD sample was reduced to 70% compared to LV-ctrl relative expression. The LV-ctrl expression was reduced to 59% compared to WT relative expression.

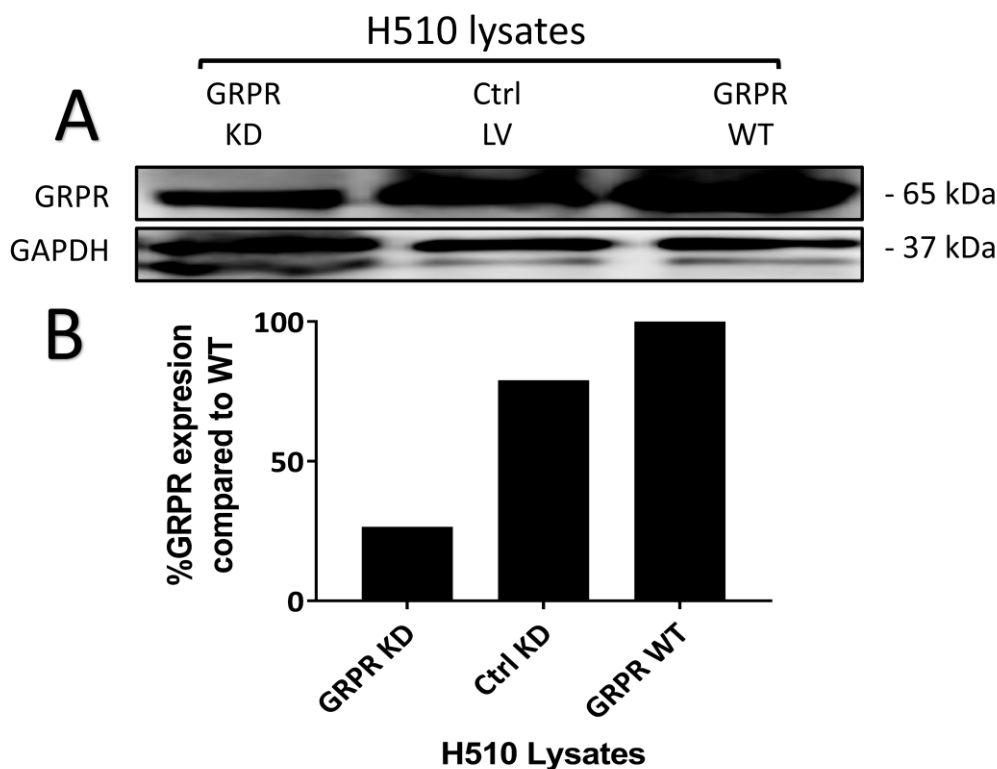


Figure 4.3: GRP-R knockdown efficiency confirmation by Western blot in H510. Western blot of 50 μ g total protein loading of a whole cell lysate of H510 cells. (A) shows GRP-R representative bands (top) in the highlighted cell line and the bottom part shows the loading control (GAPDH) bands. The bands corresponding to GRP-R and GAPDH were quantified by densitometric analysis shown in (B). The intensities of the GRP-R bands were normalized to the corresponding bands' intensities of GAPDH and the samples' relative expression was normalized to WT. $n=1$ (one biological replicate therefore no error bars is shown).

Figure 4.3, shows Western blot analyses of whole cell lysates from WT, empty-LVs control and the GRP-R KD H510 cells were performed. The figure reveals a reduced GRP-R relative expression compared to the WT H510 in GRP-R KD sample as well as in LV-ctrl. From the blot, the expression of the KD sample was reduced to 33% compared to the LV-ctrl relative expression. The LV-ctrl expression was reduced to 81% compared to WT relative expression.

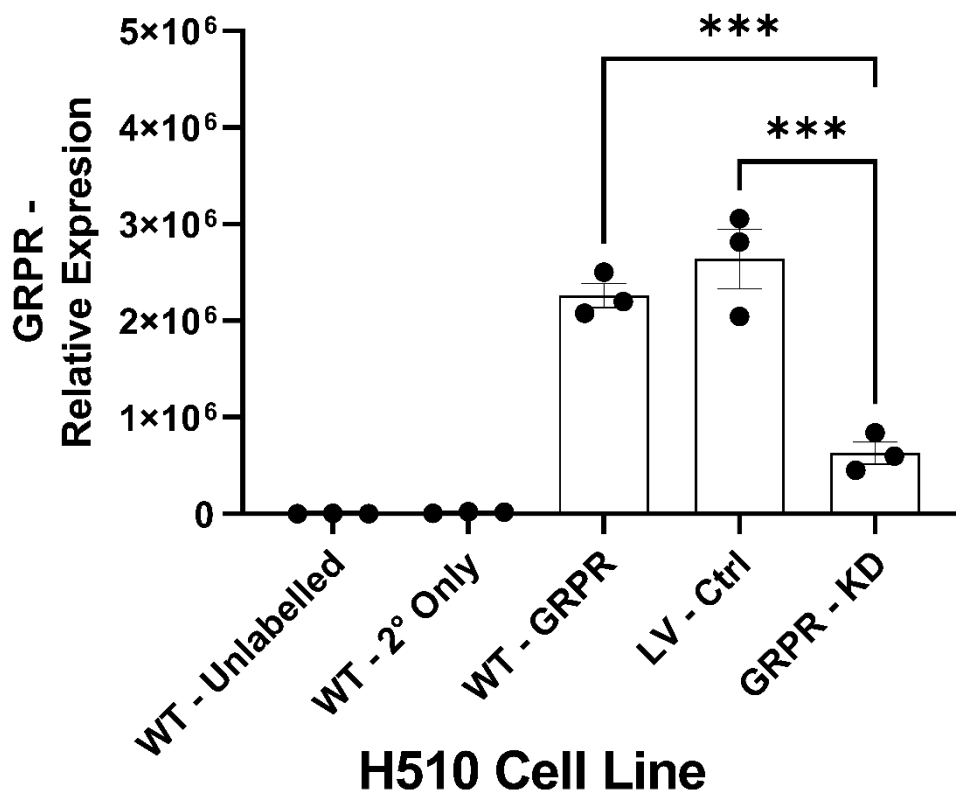


Figure 4.4: GRP-R knockdown efficiency confirmation by FCM in SCLC. The graph shows the permeabilized MFIs in the highlighted samples in H510 cell line. The primary antibody used was Rabbit polyclonal anti-human GRP-R antibody (Abcam). Event numbers 10000 events, Error bars=SEM and N=3.

To further confirm the KD of GRP-R in H510, flow cytometry was used to compare expression in WT, LV-ctrl and GRP-R KD samples. Figure 4.4 shows reduction ($P < 0.001$) in GRP-R expression of the GRP-R KD sample compared to the LV-ctrl expression. The GRP-R expression of the GRP-R KD reduced to 23% compared to the LV-ctrl.

4.2.3 Intracellular calcium response in SCLC after GRP-R KD

To develop a representative GRP-R expression-based cell lines model for targeted formulation testing, we need to demonstrate a loss of functional GRP-R in the KD cell lines. To confirm this, I used the calcium indicator dye – Fura-2.

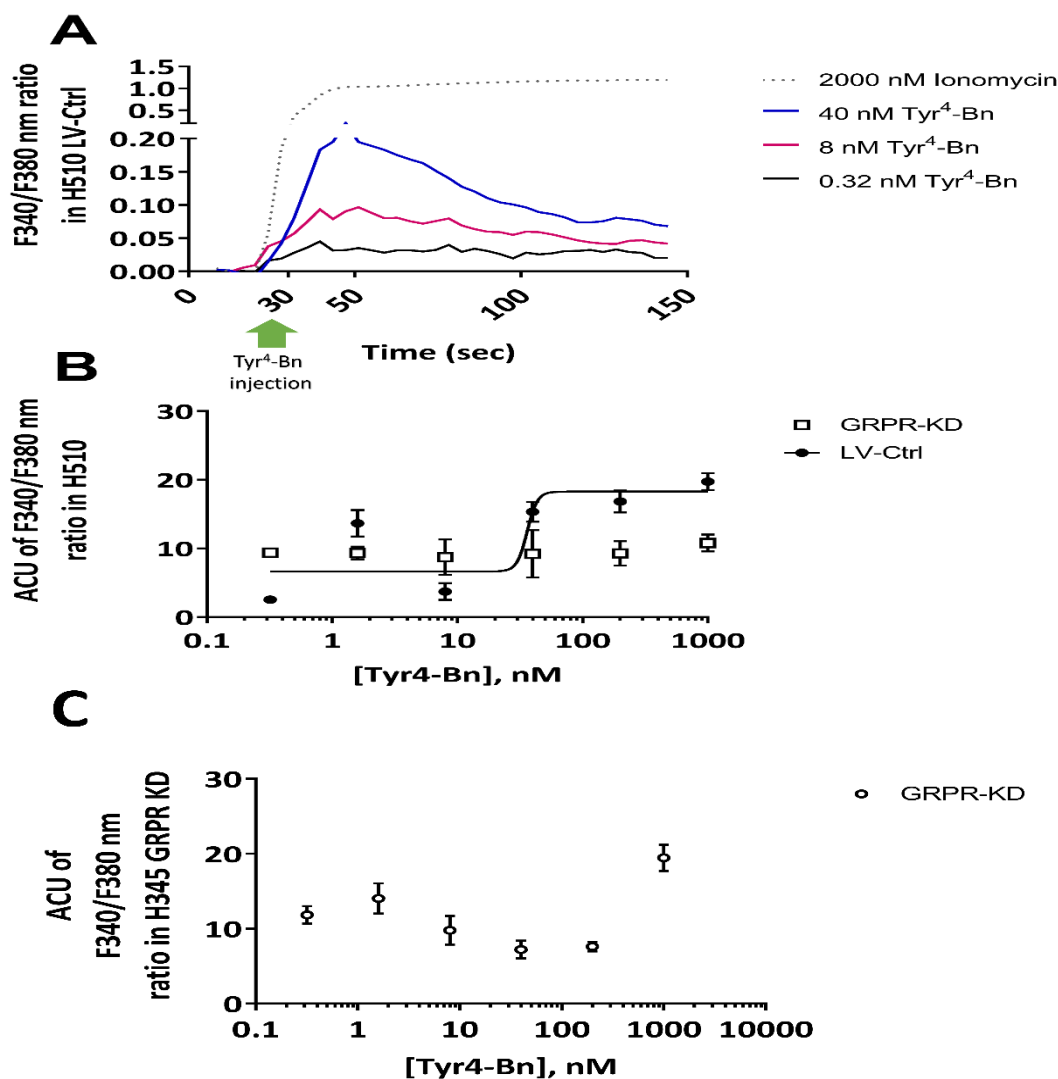


Figure 4.5: Calcium response induced by GRP-R Ligand in GRP-R KD SCLC cell line. (A) Example fluorescence trace from H510 cells loaded with Ca²⁺ reporter dye, Fura-2 AM before injection of GRP-R agonist, Tyr⁴-Bn (0-40 nM only). Baseline fluorescence was monitored for 30 s before peptide injection (arrow). (B) Escalating concentrations of Tyr⁴-Bn were injected into H510 LV-ctrl or H510 GRP-R KD cells. (C) Escalating concentrations of Tyr⁴-Bn were injected into H345 GRP-R KD cells and the Fura-2 AM fluorescence emission monitored over 150 s. AUC Fura-2 ratios at 340 nm / 380 nm were plotted against agonist concentration for both cell lines. Data shown are mean \pm SD. N=1(one biological replicate and error bars represent three technical replicates)..

Intracellular calcium response to GRP-R agonist stimulation by Tyr⁴-Bn was examined in the SCLC lines – H510 and H345. Figure 4.5 shows the intracellular calcium response of H510. Tyr⁴-Bn stimulated a concentration-dependent response in the empty vector control H510 with an EC₅₀ of 36.1 ± 4.5 nM. However, the GRP-R KD H510 (panel B) and GRP-R (panel C) KD H345 did not produce any significant response (P>0.05) to GRP-R agonist stimulation.

4.2.4 Signalling pathway activation in the GRP-R KD SCLC

We next used Western blot to examine the signalling downstream of GRP-R in KD and control SCLC cells by examining the changes in the levels of phosphorylated ERK1/2 (p-44/42) upon GRP-R KD in SCLC cell lines (H510 and H345).

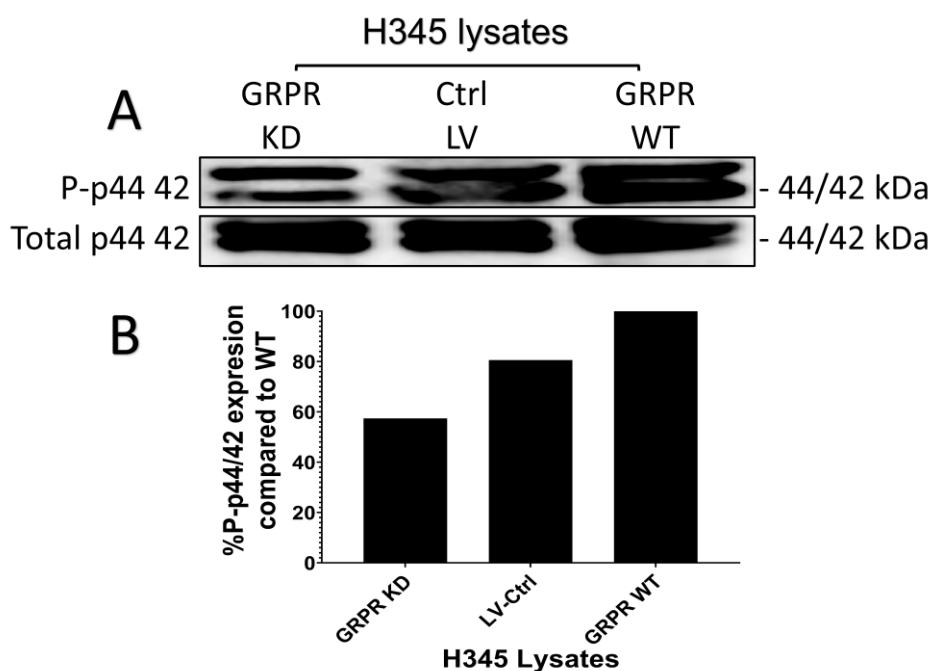


Figure 4.6: effect of GRP-R knockdown on ERK1/2 downstream signalling pathway by Western blot in H345. Western blot of 50 µg total protein loading of a whole cell lysate of H345 cell line. (A) shows phospho-p44/42 (ERK1/2) representative bands (top) in the highlighted cell line and the bottom part shows the total p44/42 bands. The intensities of the P-p44/42 bands were normalized to the WT relative expression in (B).

Figure 4.6 shows the phosphorylated p44/42 levels in the wild type H345, empty vector control H345 and GRP-R KD H345. Compared to the empty vector control, the GRP-R KD had 65% lower levels of phosphorylated p44/42.

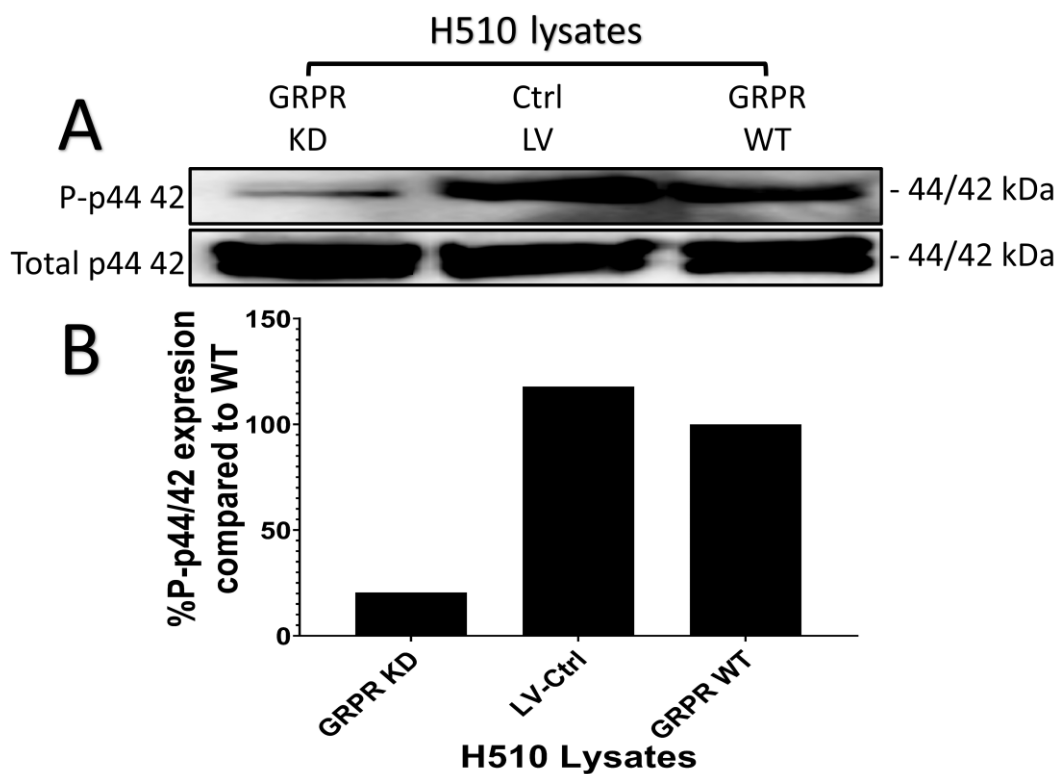


Figure 4.7: effect of GRP-R knockdown on ERK1/2 downstream signalling pathway by Western blot in H510. Western blot of 50 μ g total protein loading of a whole cell lysate of H510 cell line. (A) shows phospho-p44/42 (ERK1/2) representative bands (top) in the highlighted cell line and the bottom part shows the total p44/42 bands. The intensities of the P-p44/42 bands were normalized to the WT relative expression in (B).

From Figure 4.7, the phosphorylated p44/42 levels in H510 WT, empty vector control and GRP-R KD are blotted. Compared to empty vector control, the GRP-R KD produced 29% the levels of the proteins.

4.2.5 GRP-R knockdown efficiency by qRT-PCR in A549

The knockdown of GRP-R expression in the A549 was performed using five shRNA sequences and the lentiviral vectors (LVs) as described before. The efficiency of the GRP-R KD was determined using qRT-PCR (Figure 4.8).

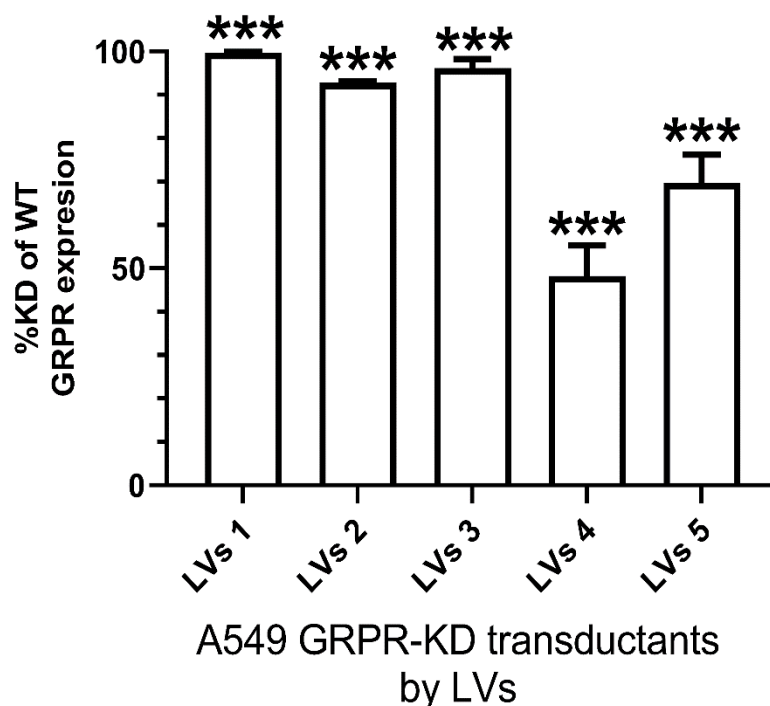


Figure 4.8: GRP-R knockdown efficiency confirmation by qRT-PCR in A549. GRP-R mRNA levels detected by RT-qPCR analysis of A549 cells 72 h after treatment with lentiviral shRNA vectors. The percentages are relative to the WT expression levels \pm SD. Duplicate samples from N=1.

From Figure 4.8, the GRP-R knockdown efficiency analysed using qRT-PCR revealed a significant ($P < 0.001$) KD%, compared to the WT expression, in all A549-transductants samples. Three samples showed KD of expression of GRP-R more than 90% compared to WT. These samples include the samples infected with lentiviral vectors LV1 (KD%=99), LV3 (KD%=96) and LV2 (KD%=92). The rest of the samples had their GRP-R expression knocked down compared to the WT by 48% and 69% by shRNA sequences 4 and 5 respectively (Table 2.3).

We have treated all the A549 samples with puromycin antibiotic for selection of the transduced cells only to produce a stable GRP-R KD A549. The puromycin selection was done by replacing the media with fresh complete medium that contains 1.5 $\mu\text{g/mL}$ of puromycin for selection of transduced A549. This dose was obtained from puromycin kill curve performed on A549 (figure A.4).

4.2.6 GRP-R KD confirmation after puromycin selection by Western blot in A549

The puromycin selection was performed for two weeks in the A549 cell line. Samples from each the puromycin-selected A549 group were collected and the GRP-R KD of expression was confirmed by Western blot as shown in Figure 4.9 below.

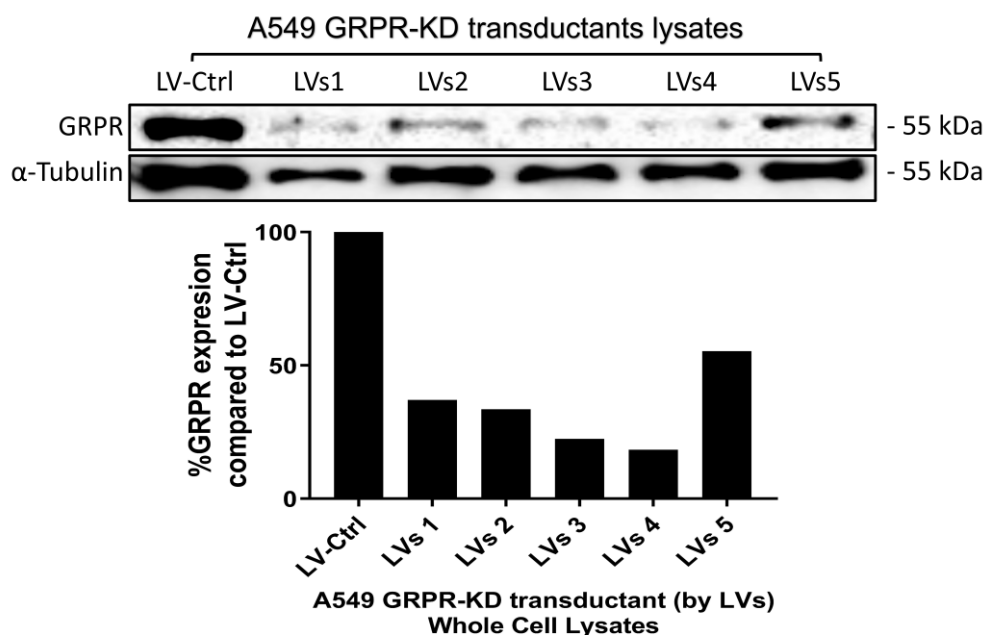


Figure 4.9: GRP-R knockdown efficiency confirmation by Western blot in A549. Western blot of 50 μg total protein loading of a whole cell lysate of A549 cell line treated with GRPR shRNA. The lysates blotted and probed with antibodies against GRP-R and loading control (α -Tubulin).

As shown in Figure 4.9, Western blot analyses of whole cell lysates from empty-LVs control and the GRP-R KD A549 1-5 samples were performed. The figure reveals a reduced GRP-R relative expression compared to the LV-Ctrl A549 in all GRP-R KD samples. From the blot, the expression of the GRP-R KD samples were reduced and represents only 18 % to 55% of LV-ctrl relative expression. The samples were reduced compared to LV-Ctrl to 18%, 22%, 33%, 37% and 55% for LVs 4, 3, 2, 1 and 5 respectively.

4.2.7 GRP-R overexpression in A549

Overexpression of GRP-R in the A549 model was undertaken to complement the knockdown lines generated above. Overexpression was achieved using a pcDNA3.1+ encoding HA-tagged GRP-R and stable transfectants selected with G418 over two weeks. Overexpression of GRP-R was confirmed by Western blot as shown in the Figure 4.10 below.

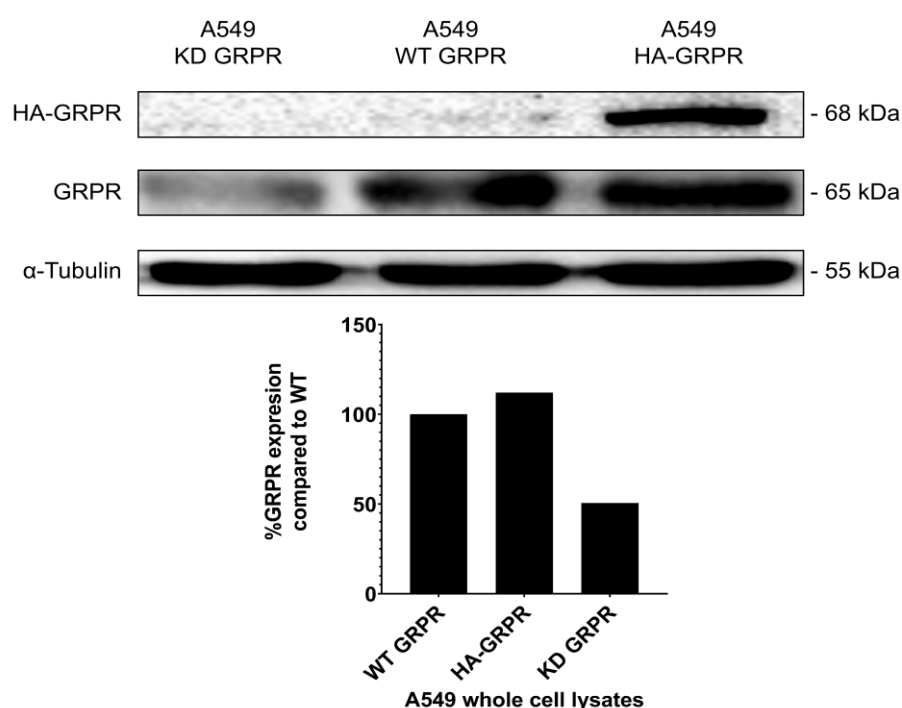


Figure 4.10: Validation of A549 transfection with HA-GRPR pDNA by Western blot. Analysis of 50 μ g total protein loading of a whole cell lysate of A549 cells transfected with HA-GRPR pDNA. The lysates blotted and probed with antibodies against HA tag (top) in the highlighted cell line, GRP-R (middle) and α -tubulin (bottom).

Figure 4.10 Probing with the anti-HA tag antibody detected overexpressed HA-GRPR at 68 kDa in transfected cells only. Probing with a GRP-R antibody showed GRP-R to be overexpressed in the WT GRPR and HA-GRPR transfectants but not in the KD GRP-R.

4.2.8 HA-GRP-R expression by immunofluorescent imaging

Widefield immunofluorescent imaging was used to show HA-GRP-R expression in A549-GRP-R (Figure 4.11). The pattern of fluorescence signal indicates expression of HA-GRP-R in the highlighted cell line. A punctate staining pattern was observed and it appears to be clearly distributed throughout the cell.

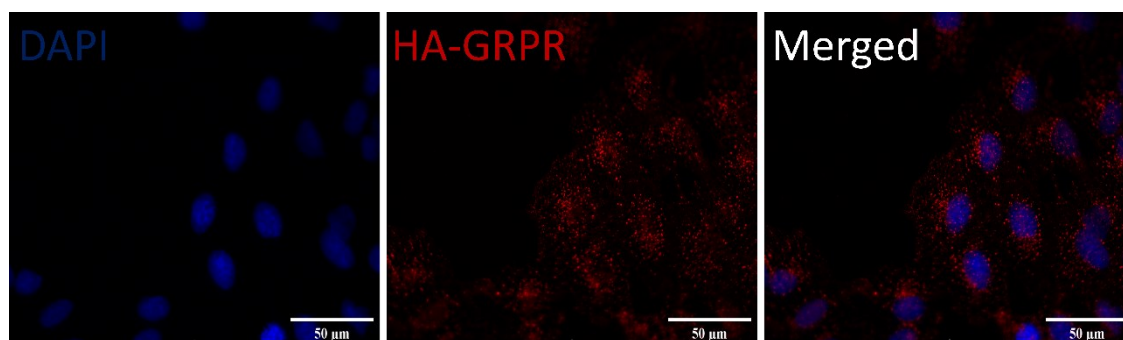


Figure 4.11: HA-GRP-R expression in A549-GRP-R cell line by immunofluorescence. The graph shows the expression of the HA-GRP-R in A549-GRP-R in higher magnification (x40). The cells were fixed and HA-GRP-R labelled with anti-HA-antibody (red) and nuclei labelled with Hoechst (blue).

4.3 Discussion

To validate GRP-R as a target in SCLC we sought to develop a toolbox of cellular models expressing different levels of the receptor. We knocked down GRP-R in two non-adherent SCLC and one control adherent NSCLC line using lentiviral vectors. The adherent NSCLC A549 cell line was also subjected to GRP-R overexpression using a plasmid DNA construct encoding a N terminally HA tagged GRP-R.

We sought to reduce the expression of GRP-R in SCLC cell lines H510 and H345 to investigate the targeting capacity of our targeted liposomes and is it reduced compared to wild type. We chose H510 for KD because it showed high levels of GRP-R expression. In addition, H345 showed high levels of functional GRP-R expression as reported in the previous chapter. We sought to reduce GRP-R expression to see if the targeting capacity would be reduced i.e. the extent of liposome uptake in KD cells would be lower than in WT and increased in the overexpression cells. We screened shRNA sequences for KD efficiency by RT-qPCR and chose one sequence. We then tested whether the GRP-R functionality was reduced in KD cells by measuring intracellular calcium response to the GRP-R agonist Tyr4-Bn- we saw a lack of response in the KD H510 and KD H345. This means the KD of the GRP-R in the mentioned SCLC cell lines was effective. We would expect to see changes in cell growth as reported in the previous chapter with Cystabn. This means we have a model that we can use to test targeting capacity as shown by others.

GRP (10 nM) was shown to act as mitogen and stimulate neuroblastoma growth significantly in multiple cell lines using cell count experiment [200]. GRP-R overexpression was shown to increase growth of human neuroblastoma cells in soft agar whereas GRP-R knockdown with siRNA and shRNA inhibited colony growth in soft agar [201]. In vivo, GRP-R knockdown significantly delayed tumour growth and decreased liver metastases in the neuroblastoma BE(2)-C xenograft mice [201]. Bombesin significantly stimulates growth of the human neuroblastoma SK-N-SH xenografts in mice using 10 µg/kg and 20 µg/kg compared to no treatment control [202].

The Western blot analyses confirmed persistent GRP-R KD in the clones compared to empty vector control. This confirms that the sharp reduction of GRP-R expression in the KD samples was from the silencing of GRP-R expression rather than from the transfection process itself. Surprisingly, empty lentiviral control clones demonstrated a reduction in KD

to 59% and 81% in H345 and H510, respectively in the absence of a targeting shRNA. This is most commonly attributed to off-target effects. The blot in the mentioned figure also showed the glycosylated band for GRP-R in each sample. This is because it has been shown by cross-linking experiments that the GRP-R, in its glycosylated form, has a molecular weight of 60-90 kDa and the deglycosylated form weighs 43 kDa. This blot also showed two bands for GAPDH. This is most likely due to the loading of 50 µg total protein onto the PAGE gel in order to detect the low amounts of GRP-R in SCLC cells with low cytoplasmic volume. This resulted in the appearance of a second closely separated band which represent nonspecific binding of primary antibody [77, 168, 203-207].

To further confirm the KD of GRP-R in H510, flow cytometry was used to compare the expression of GRP-R in the highlighted samples and showed significant ($P < 0.001$) reduction of GRP-R expression compared to empty-vector control. The use of the more sensitive fluorescence-based flow cytometry experiment allowed us to confirm the significant ($P < 0.001$) reduction of GRP-R expression in H510. This is also complementing the data produced by Western blot in SCLC. The antibody detects the membrane-bound and intracellular GRP-R which retains its natural configuration in the flow cytometry whereas it detects the total denatured protein in Western blot. This means that flow cytometry detects the protein in its relevant configuration.

We confirmed the functional loss of GRP-R using a Calcium release assay with the Fura-2 indicator dye. Intracellular calcium release in response to GRP-R agonist treatment with Tyr⁴-Bn was examined in the SCLC lines. Tyr⁴-Bn stimulated a concentration-dependent response in the empty vector control H510 with an EC₅₀ of 36.1 ± 4.5 nM but not in the KD GRP-R H510 and KD GRP-R H345. This means that KD of GRP-R in H510 and H345 successfully diminished the measurable intracellular calcium response to GRP-R agonist stimulation (Tyr⁴-Bn) due to the reduction in cell surface receptor numbers.

The activation of GRP-R results in activation of the MAPK/ERK pathway. The levels of phosphorylated ERK1/2 proteins (P-p44/42) GRP-R KD in SCLC cell lines (H510 and H345) were measured by Western blot. Levels of phosphorylated p44/42 levels in the highlighted H510 and H345 samples were reduced compared to empty vector control as expected because the receptor expression was knocked down which means the receptor activation is reduced. This complements the data reported above and confirms reduced expression of functional GRP-R.

One of the challenges faced when working with SCLC suspension cell lines is that it is more time and labour-intensive than faster growing, adherent cell lines. SCLC models require extra washing or filtration steps due to their anchorage-independent growth. In addition to this, SCLC cell lines have a small cytoplasmic volume which could make it challenging to undertake microscopic evaluation of events such as receptor internalisation and endocytic trafficking of peptides and liposomal formulations, compared to adherent cells with larger cytoplasmic volumes [208]. In addition to that, the suspension cell lines tend to be more sensitive to agitation and tend to naturally form clumps. So, based on all these challenges, we sought that it is reasonable to add the A549 cell line to this study.

To reduce the expression of GRP-R in A549, the same shRNA sequences were screened for KD efficiency by RT-qPCR and chose one sequence. We then tested whether the GRP-R functionality was reduced in KD cells by measuring intracellular calcium response to the GRP-R agonist Tyr4-Bn. A lack of calcium response in the KD A549 confirmed that the GRP-R KD in A549 was effective. This means we have a model that we can use to test targeting capacity.

Further work included the use of a GRP-R overexpression construct in A549 cells. Western blot using the anti-HA antibody confirmed specific receptor overexpression of the tagged receptor in transfected cells but not WT or KD controls. This overexpression construct has been used by other groups to demonstrate both the functionality of agonist and antagonist peptides, mainly in HEK293 cells [194].

In this study we applied an RNA interference technique to develop cell line experimental model in SCLC to study therapeutic formulation. Other studies have developed GRP-R knockout mice [209, 210]. These mice were used to study the physiologic functions of GRP-R in health and disease [44]. GRP-R knockdown A549 cells were used to investigate a peptide-conjugated theranostic nanoparticle targeting lung cancer [211]. GRP-R knockdown PC-3 cells were used to investigate peptide-based targeted polymeric nanoparticles targeting prostate cancer [212]. GRP-R knockdown PC-3 was used to highlight the role of GRP-R in cancer growth [213]. GRP-R silencing in human neuroblastomas cell lines was used to reveal the role of bombesin in angiogenesis and neuroblastoma growth [214].

4.4 Conclusion

In this chapter, GRP-R knockdown cell line models were developed using two SCLC cell lines. In addition, GRP-R knockdown and overexpression models were prepared from the adherent A549 cell line. The original plan for this project would involve this combination of cell models being used to study the uptake, activity and biodistribution of GRP-R targeted formulation *in vitro* and *in vivo*. Regrettably, the emergence of the COVID-19 pandemic forced a change of plan. In the following chapter the uptake and trafficking of GRP-R targeted liposomal formulations in A549 cells was studied only at the *in vitro* level.

Targeted Liposomal Formulation Uptake in a GRP-R overexpressing cell line

Chapter 5

5.1 Introduction

The expression of bombesin-related peptides and the bombesin receptors by SCLC cell lines and primary tumours has been widely studied for the past three decades [175, 184, 189, 215]. GRP and NMB secretion by SCLC is known to cause an autocrine growth loop that drives tumour growth. Therefore, a number of experimental therapeutics or imaging agents targeted at the GRP-GRPR interaction, including anti-GRP antibodies and GRP-R peptide antagonists have been developed. These agents have demonstrated anti-tumour responses in a number of pre-clinical models of pancreatic cancer [216] and imaging of breast [217], prostatic [218] and glioma [219] tumours. The use of GRP-R antagonists is motivated by their inability to cause downstream mitogenic effects by counter-balanced by a greatly reduced rate of receptor internalisation. Nonetheless, a number of reports have illustrated that GRP/BN-based antagonists display superior *in vivo* targeting capacity cf. agonist peptides [194].

Nanomedicines to improve cancer therapy has been widely studied and has resulted in a number of approved therapies such as Doxil® in the 1990s and the recent approval of Onivyde® [220]. In the lung cancer field, cisplatin formulated as a pegylated liposomal formulation (Lipoplatin®) has delivered comparable anti-tumour response against non-small cell lung cancer (NSCLC) tumours with reduced side effects when delivered in combination with paclitaxel compared to when cisplatin and paclitaxel solutions are used in combination [221]. In preclinical studies, improved therapeutic responses have been achieved by adopting an active targeting approach. Typically, this involves the incorporation of a surface bound moiety that selectively binds to a cognate receptor/protein on the tumour cell surface, leading to accumulation of nanocarriers in the tumour. A diversity of targeting ligands has been explored, including antibodies, proteins, peptides and aptamers. Targeted nanoparticles such as HER2-targeted MM-302 [222], transferrin receptor-targeted CALAA-01 [223], and PSMA-targeted BIND-014 [224] have reached clinical trials but detailed information about the clinical advantage of using targeted platforms is still lacking which means more area research is needed in this area .

In this chapter, I generated liposomes decorated with Cystabn and non-targeting (control) liposomes to compare the uptake of the two formulations in lung cancer cells. The original hypothesis involved *in-vivo* testing liposome uptake in SCLC cells after GRP-R knockdown and those overexpressing GRP-R. Due to the COVID-19 pandemic, studies were limited to those using the NSCLC A549 cell line that overexpresses GRP-R *in vitro* only.

5.2 Results

5.2.1 Characterisation of Peptides, Conjugate and Liposomes

The Cystabn was synthesised using Fmoc solid-phase peptide synthesis. The product was characterised using HPLC (Table 5.1) and MALDI-ToF (Table 5.2). The Cystabn-PEG-lipid conjugate was synthesised as described in 2.1.5.1.1 and characterized using HPLC and MALDI-ToF as shown in Figure 5.1. The formulations were prepared using the thin-film technique and characterised using DLS (Table 5.3).

Table 5.1: HPLC data summary for Cystabn

	<i>Peak Rt (min)</i>	<i>Peak Purity (%)</i>
<i>HPLC</i>	<i>14.8</i>	<i>70</i>

Table 5.2: MALDI ToF MS data summary for Cystabn

	<i>[M] (Da)</i>	<i>[M+Na]⁺ (Da)</i>
<i>MALDI ToF MS</i>	<i>1215.4</i>	<i>1238.3</i>

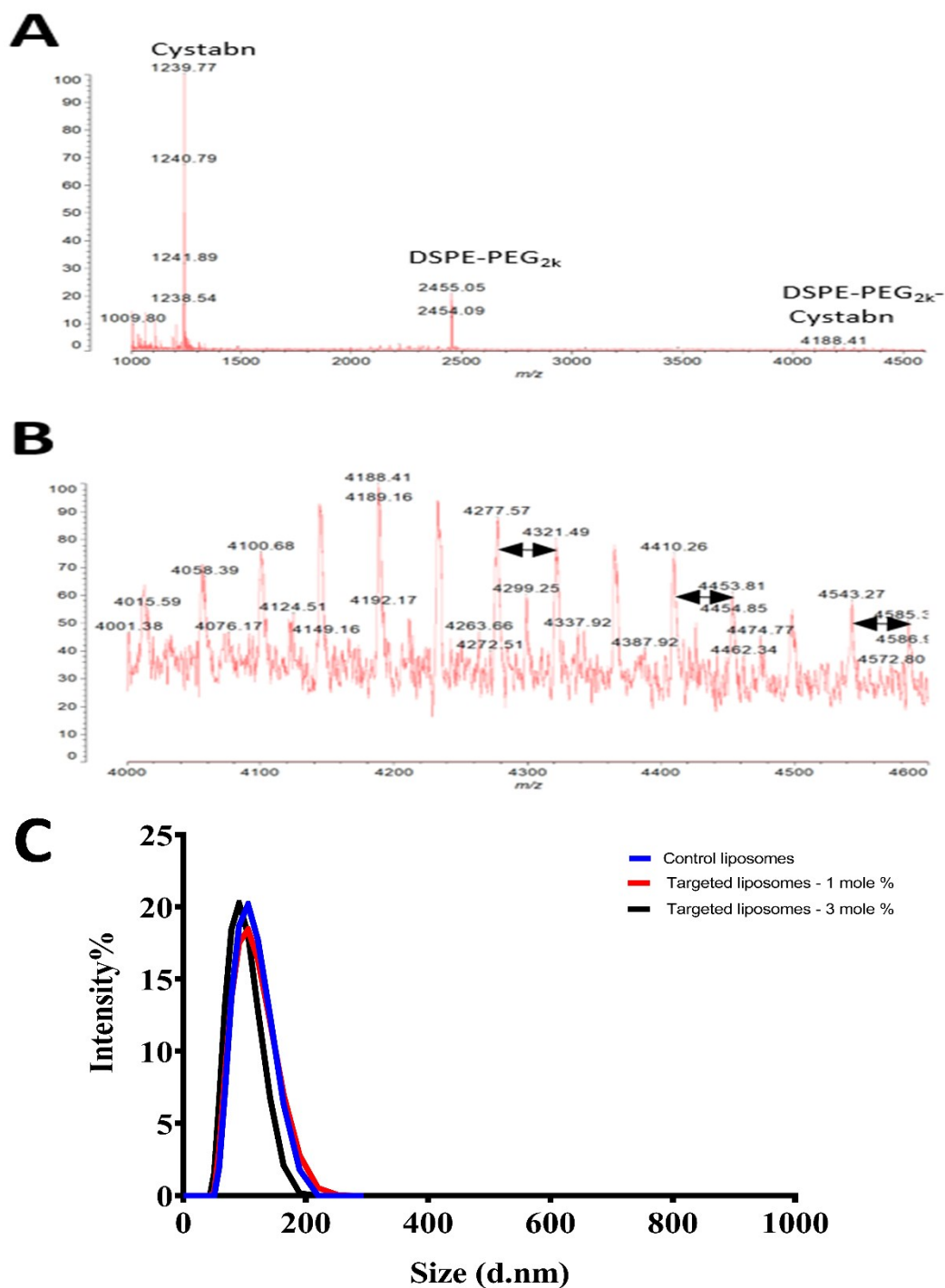


Figure 5.1: Synthesis of targeted and control liposomes. (A,B) MALDI-TOF mass spectra of crude DSPE-PEG₂₀₀₀-cystabn conjugate (A) and purified, post-dialysis, DSPE-PEG₂₀₀₀-cystabn conjugate (B). DLS size distribution curves are shown for control and target liposomes in (C).

The conjugate was analysed with MALDI ToF MS to confirm the molecular mass (Figure 5.1A&B). The exact mass of the DSPE-PEG2000 maleimide was calculated as 4137.41 Da but is unreliable due to the polydisperse nature of the PEG linker. The mass spectrum includes the most abundant ion at 4188 Da. The expected mass difference between ion peaks is 44 Da, which represents ethylene glycol monomers ($C_2H_4O = 44.05$). Figure 5.1B includes, for example, a mass difference from 4277.57 Da to 4321.49 Da, which is equal to one monomer. Two monomer mass differences of ~ 88 Da (4100.68 Da to 4188.41 Da) equivalent to two ethylene glycol monomers were also recorded.

The liposome formulations produced reproducible monodispersed small, unilamellar vesicles - SUVs. The mean diameters for liposomal formulations were 101 ± 2.1 nm, 101 ± 2.3 nm and 91 ± 0.7 nm for control, targeted-1 mole% and targeted-3 mole% liposomes, respectively. The polydispersity index was < 0.1 for all formulations, indicating the preparation of monodispersed population. The zeta potential of formulations were slightly negative i.e. -1.64 ± 2.13 mV, -1.86 ± 1.64 mV and -1.97 ± 0.4 mV for control, targeted-1 mole% and targeted-3 mole% liposomes, respectively. Representative size and zeta potential measurements are summarized in Table 5.3. The values of zeta potential are closer to zero because the formulations contain the zwitterionic phospholipid (DOPC). This means that the formulation is colloidal stable which further tested and shown over time in Figure 5.2 below.

Table 5.3: Colloidal properties of Control and Target-lipo formulations

	<i>Control-lipo</i>	<i>Target-lipo – 1 mole %</i>	<i>Target-lipo – 3 mole %</i>
<i>Z-Ave (d.nm)</i>	101 ± 2.1	100 ± 2.3	91 ± 0.7
<i>PDI</i>	0.058 ± 0.007	0.068 ± 0.019	0.08 ± 0.02
<i>Zeta Potential (mV)</i>	-1.64 ± 2.13	-1.86 ± 1.64	-1.97 ± 0.4

^a Data shown are mean \pm SD, n=3 independent experiments.

Figure 5.1C shows the intensity weighted size distribution with good reproducibility for liposomal formulations (control, targeted-1 mole% and targeted-3 mole% liposomes respectively).

Freshly prepared control and targeted liposomes showed consistent ($p>0.05$) size, zeta potential and polydispersity measurements. A Z-average diameter of 101 nm and a zeta potential of -1.6 mV with a narrow polydispersity index of 0.06 indicating a refined unilamellar formulation for the control formulation. Similarly, the targeted-1 mole% formulation showed size, zeta potential and polydispersity measurement of 100 nm, -1.9 mV and 0.07, respectively. The targeted-3 mole% formulation showed size, zeta potential and polydispersity measurement of 91 nm, -2 mV and 0.08, respectively.

5.2.2 Liposome colloidal stability study

Compared to the respective freshly prepared formulations, there is no significant change ($p>0.05$) in the size and polydispersity for all liposomal formulations upon storage in PBS for the whole storage period at the three different temperatures i.e. 4 °C, 25 °C and 37 °C (Figure 5.2A-C). The largest change recorded for the control formulation from 0.058 ± 0.007 to 0.098 ± 0.07 PDI after incubation at 25 °C for 72 h. In general, the PDI for the targeted-1mole% formulation increased more than that of control and targeted-3mole% liposomes. For example, the PDI rose from 3-fold from 0.068 ± 0.019 to 0.176 ± 0.08 after 72 h incubation at 25 °C. This indicate that the targeted-3mole% liposomes seems to be more stable over time than the targeted-1mole% liposomes, which indicate that the increased percentage of the targeting ligand enhanced colloidal stability of liposomes.

As expected, storage of liposomes in 10% FBS compromised liposomal stability more than storage in PBS (Figure 5.2D-F). There was non-significant change in the parameters of the control and targeted formulations ($p>0.05$) immediately after addition of 10% FBS. For the freshly prepared control formulation, the size slightly decreased from 93.93 ± 1.78 to 89.79 ± 1.52 nm with increase in PDI from 0.083 ± 0.002 to 0.160 ± 0.012 immediately after addition of 10% FBS. For the freshly prepared targeted-1mole% formulation, the size increased slightly from 105.5 ± 3.4 to 113.4 ± 20.5 nm with slight decrease in PDI from 0.055 ± 0.019 to 0.241 ± 0.148 immediately after addition of 10% FBS. For the freshly prepared targeted-3mole% formulation, the size slightly decreased from 91.3 ± 0.65 to 84.77 ± 1.36 nm with slight increase in PDI from 0.08 ± 0.02 to 0.288 ± 0.01 immediately after addition of 10% FBS.

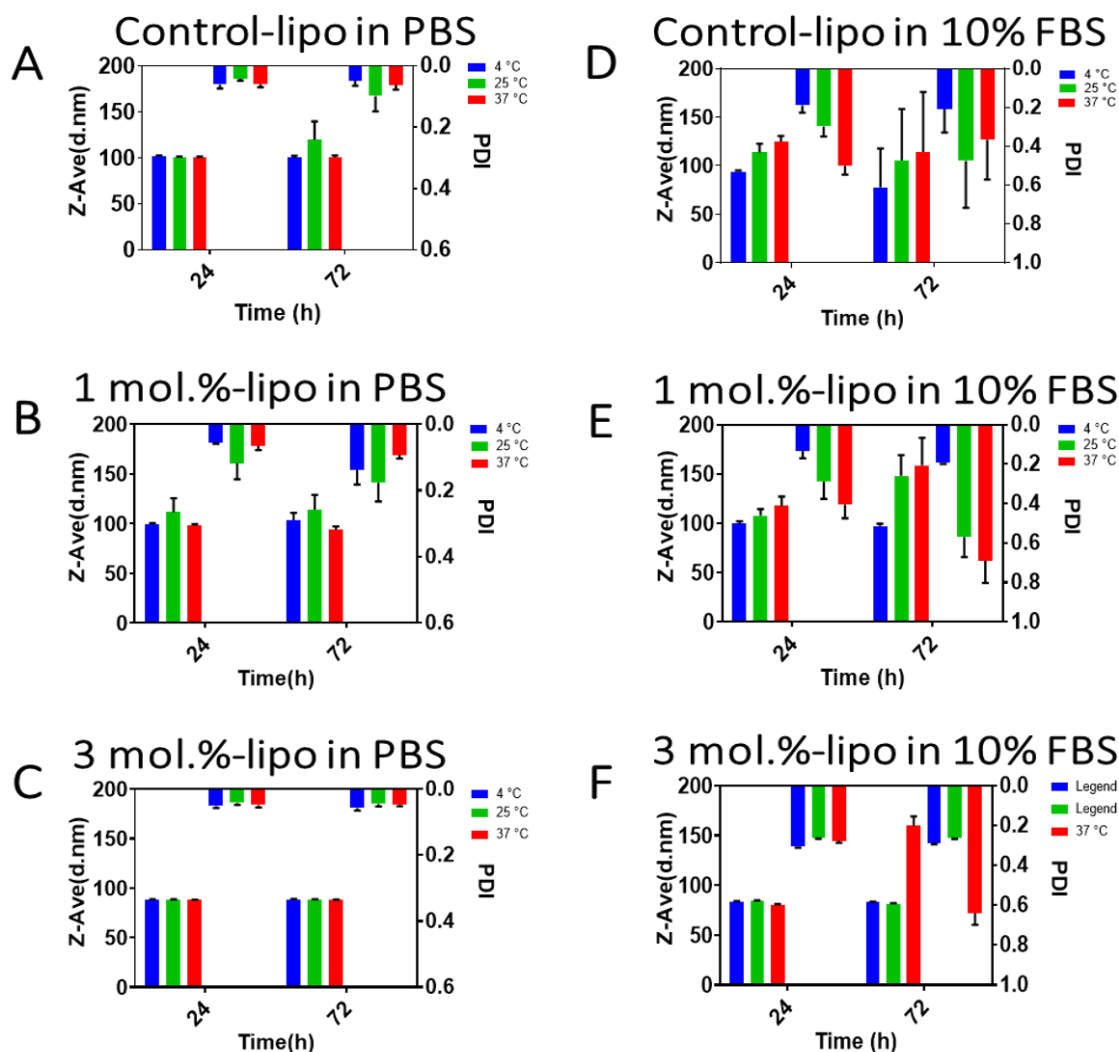


Figure 5.2: Colloidal stability of liposomes. Control and target liposomes were exposed to PBS (A,B&C) or 10% FBS in PBS (D,E&F) at three temperatures for 24 / 72 h then analysed by DLS. Data shown are mean \pm SD, $n=3$.

5.2.3 Cell Uptake of GRP-R-targeted Liposomes by Flow Cytometer

The targeting capacity of cystabn-decorated liposomes was examined by quantification of cell-uptake. This was judged by flow cytometry analysis of adherent A549-GRP-R cells exposed to fluorescently tagged GRP-R-targeted liposomes (FL-target-Lipo) or fluorescently tagged control-liposomes (FL-control-Lipo) formulations. We maintained the total mole % of PEG lipid at 5% and varied the amount of the peptide targeting motif. Preliminary studies using FL-Target-Lipo including 1 mole % targeting lipid showed marginal increases in relative cellular accumulation (Figure 5.3). Fluorescent uptake was quantified by doping the liposomal formulation with 1 mole% DHPE fluorescein.

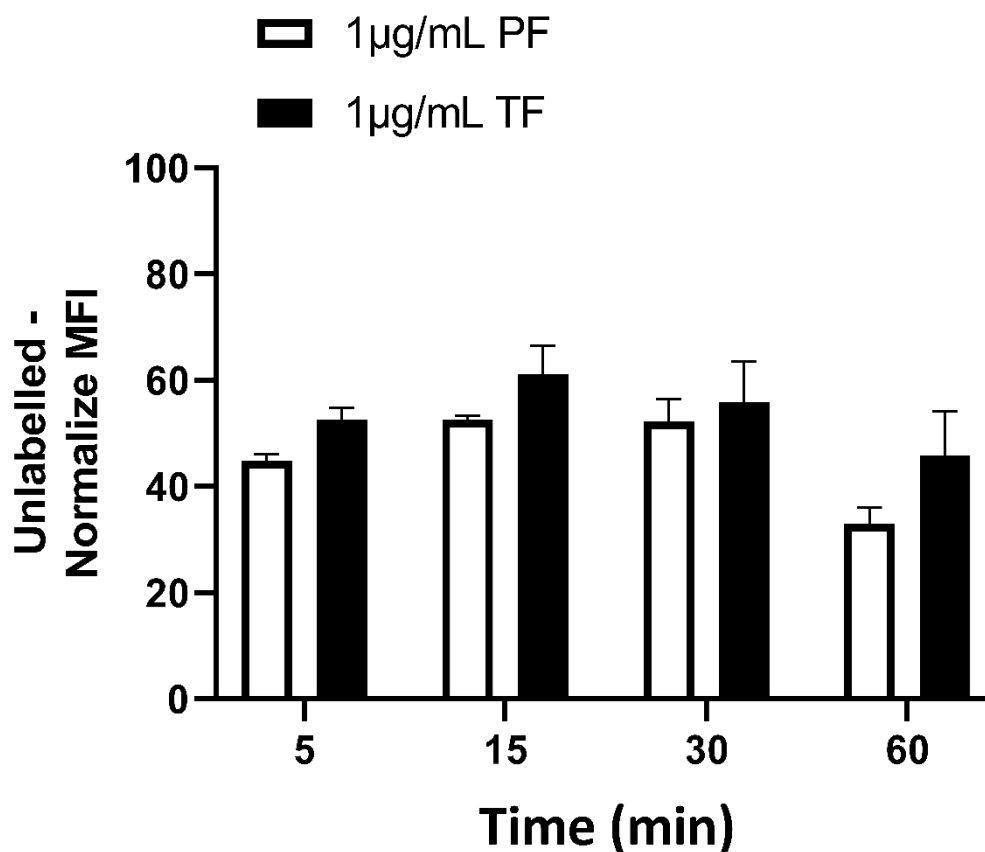


Figure 5.3: Uptake of the targeted liposomal formulation using 1mole% peptide-peg-lipid. A549-GRP-R cells were exposed to 1 µg/mL (of control or target liposomes for 5-60 min before washing and analysis of liposomal DHPE-fluorescein intensity by flow cytometry. Median fluorescence intensity (MFI) was determined by correcting for the background MFI from cells exposed to no formulations. Errors \pm SE. N=2.

To overcome this, the density of targeting peptide-peg-lipid was increased to 3 mole %. To examine for active internalisation and intracellular accumulation of liposomes at the endocytosis permissive temperature of 37 °C, we subtracted the median fluorescence intensity (MFI) attributable to cell-surface adsorption of liposomes at 4 °C, to yield a “4 °C - normalised cell MFI” at each time point and for each formulation.

Firstly, we determined the cellular uptake of 10 µg/mL of plain formulation (PF) and targeted formulation (TF) over 0-30 min. Figure 5.4 shows the increase in MFI overtime but no difference between formulations.

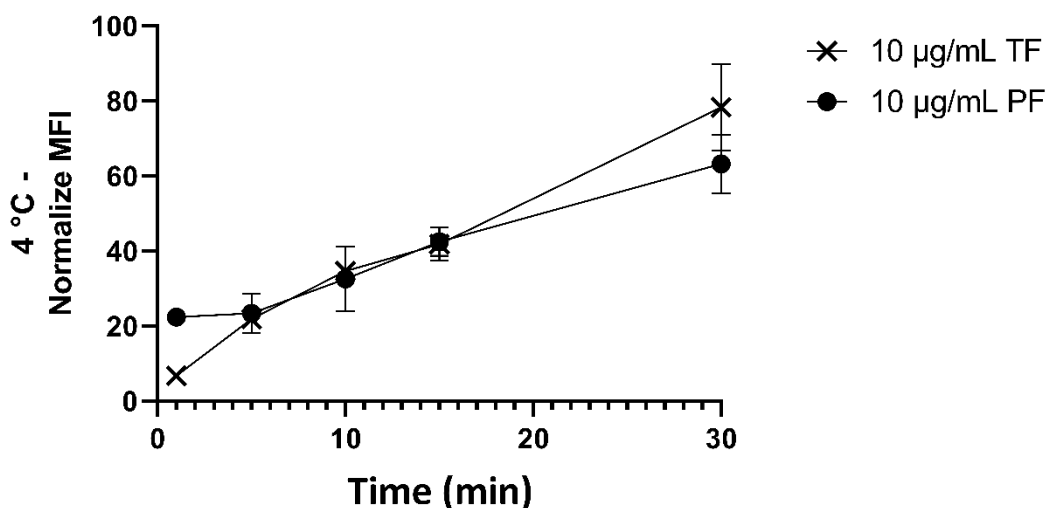


Figure 5.4: Uptake of the targeted liposomal formulation over time. A549-GRP-R cells were exposed to 1 µg/mL of control (PF) or target (TF) liposomes for 0-30 min before washing and analysis of liposomal DHPE-fluorescein intensity by flow cytometry. Median fluorescence intensity (MFI) was determined by correcting for the background MFI from cells exposed for matched time periods on ice. Data shown are mean \pm SEM, $n=3$

The lack of differential accumulation of control and targeted formulations over 30 min prompted the testing of different formulation concentrations over longer timepoints. To examine for the effect of concentration over the cellular accumulation of liposomes (Figure 5.5), we did not subtract the MFI attributable to cell-surface adsorption of liposomes at 4 °C. This allows us to note any increase in the control formulation between concentrations which can indicate the tendency of the formulation to adsorb around the cell. However, no significant difference in MFI between concentrations was noticed.

Figure 5.5, shows increase of MFI over time over the different concentrations. It also shows that MFI increase with the increase in concentration. The increase of the targeted formulation was from 1- to 2-fold over different time points with using 1 µg/mL or 10 µg/mL with no significant difference between time points. For example, the increase in the 2 h MFI is 2.5-fold increase over the 1 h MFI using 1 µg/mL TF. The MFI of the 4 h TF increased 3-fold over the 1 h TF using either the 1 µg/mL or 10 µg/mL. Since the different concentration showed similar fold increase over time, the 1 µg/mL concentration was chosen for further testing over longer timepoints.

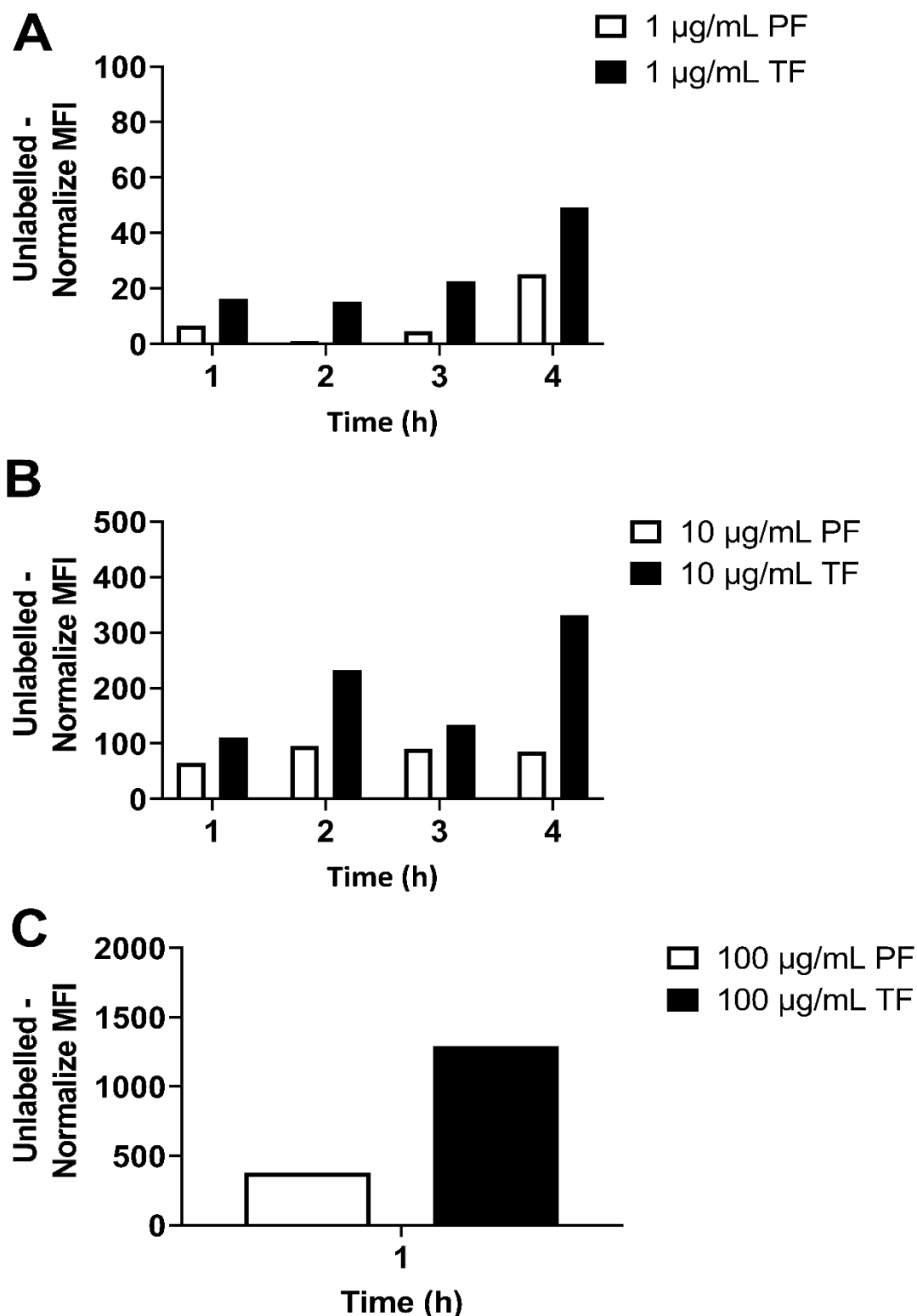


Figure 5.5: Uptake of the targeted liposomal formulation using different concentrations. A549-GRP-R cells were exposed to 1 µg/mL (A), 10 µg/mL (B) & 100 µg/mL (C) of control (PF) or target (TF) liposomes for 1-4 hrs. before washing and analysis of liposomal DHPE-fluorescein intensity by flow cytometry. Median fluorescence intensity (MFI) was determined by correcting for the background MFI from cells exposed to no formulations. $n=1$ (one biological replicate therefore no error bars is shown).

Figure 5.6 shows the targeted formulation showed marginal increase over the control liposomes over from 1 min to 30 min compared to the 4 °C samples. The levels of cell associated fluorescence were largely consistent for the first 30 min for both control and targeted formulations. However, at 60 min and beyond the targeted formulation increased sharply more than the control. The highest increase in targeted formulation uptake recorded over 2 h and 3 h when the fluorescence was more than 3 to 4-fold higher in the targeted group. This indicates that the targeted liposomes internalized into the cells more extensively than the control liposomes which means the ligand decoration of the liposomes enhanced their cell uptake.

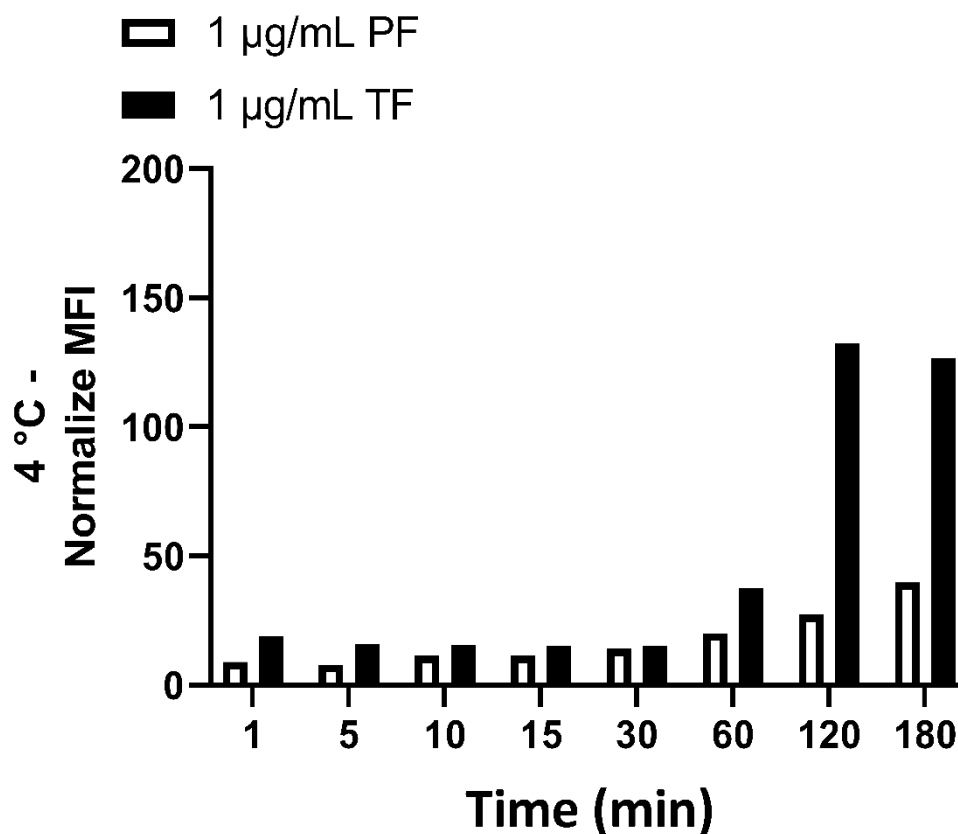


Figure 5.6: Uptake of the targeted liposomal formulation over expanded time period. A549-GRP-R cells were exposed to 1 µg/mL of control (PF) or target (TF) liposomes for 1-4 h. before washing and analysis of liposomal DHPE-fluorescein intensity by flow cytometry. Median fluorescence intensity (MFI) was determined by correcting for the background MFI from cells exposed for matched time periods on ice. $n=1$ (one biological replicate therefore no error bars is shown).

These preliminary findings led to a more detailed examination of the kinetics of liposome uptake. Figure 5.7A showed that there is no significant difference between MFI of the FL-formulations at 4 °C over time. Figure 5.7B showed that the targeted formulation have an increases MFI ($p < 0.05$) compared to the control formulation at 37 °C over time. At 15 min, fluorescence was no greater in cells treated with TF compared to PF. However, at 60 min and beyond cell fluorescence was greater ($p < 0.05$) in cells treated with TF.

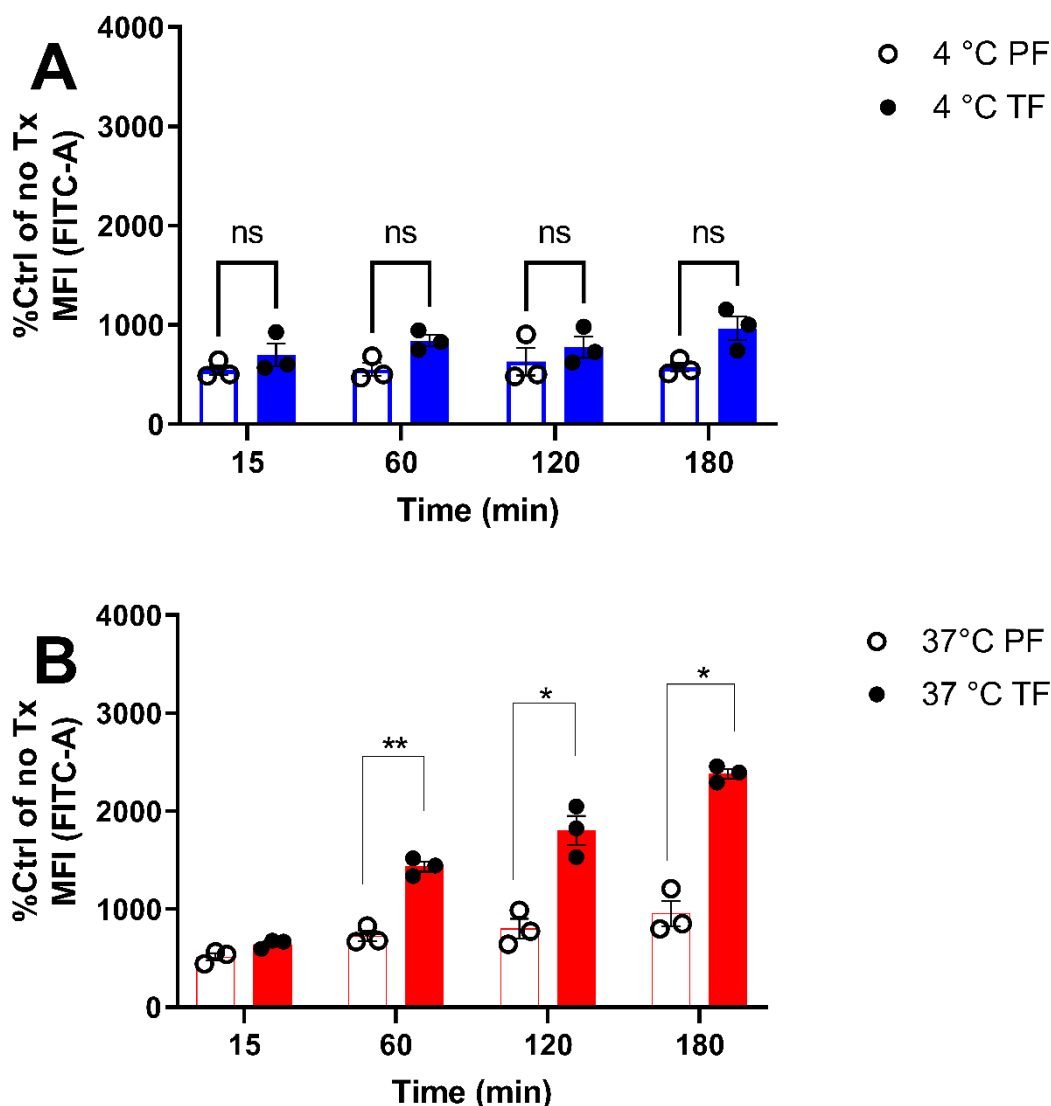


Figure 5.7: Quantification of GRP-R targeting with Cystabn decorated liposomes. A549-GRP-R cells were exposed to 1 $\mu\text{g}/\text{mL}$ of control (PF) or target (TF) liposomes for 15-180 min at 4 °C (A) and 37 °C (B) before washing and analysis of liposomal DHPE-fluorescein intensity by flow cytometry. Median fluorescence intensity (MFI) was determined by correcting for the background MFI from cells exposed to no treatment (Tx). Data shown are mean \pm SEM, $n=3$

5.2.4 Cell Uptake of GRP-R-targeted Liposomes by Fluorescence

Microscopy

We next confirmed the flow cytometric results using fluorescence microscopy. Following 5 min exposure to either target (Figure 5.8 top) or control-liposomes (Figure 5.8 bottom), A549-GRP-R cells displayed greater cellular fluorescence signals in the FL-target-Lipo group. Cells exposed to FL-Control-Lipo displayed a diffuse cell membrane-like staining with few green puncta. Whereas the target-lipo exposed cells displayed many more fluorescent puncta as well as a widespread increase in cellular fluorescence. A549-GRP-R cells displayed fluorescent puncta (red) corresponding to the HA tag of GRP-R expression in the cells in both samples treated with control or targeted formulations.

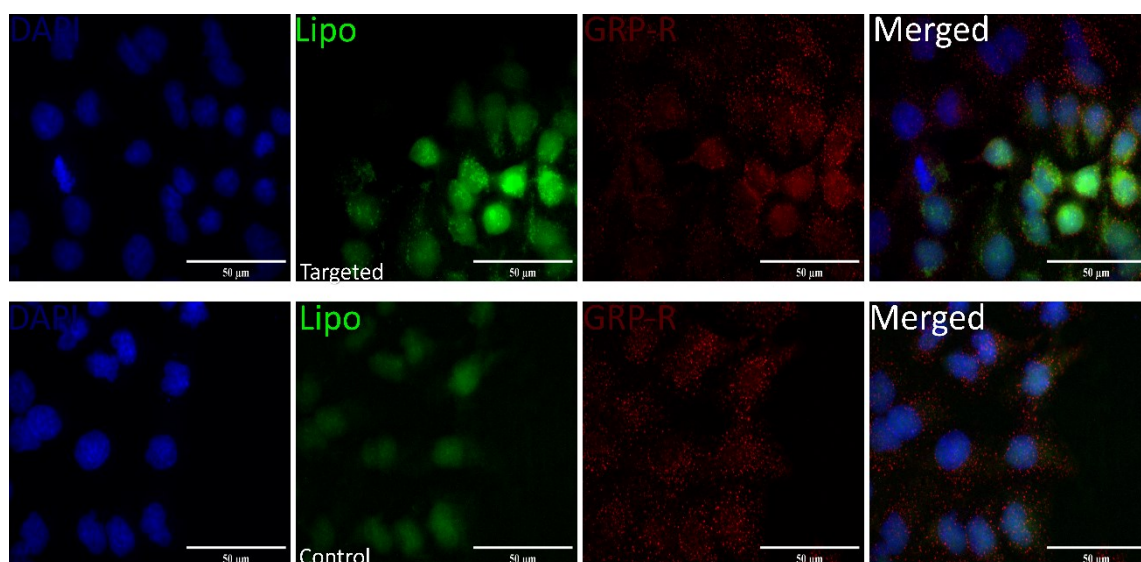


Figure 5.8: GRP-R targeting with Cystabn increases cell accumulation of liposomes. A549-GRP-R cells were exposed to 1 µg/mL of target (top) or control (bottom) liposomes for 5 min, washed, fixed and HA-GRPR labelled with HA-antibody and nuclei labelled with Hoechst.

5.2.5 Insight into the Mechanism of Intracellular Uptake of GRP-R-targeted Liposomes by Live Cell Fluorescence Imaging

We first assessed the colocalization of the targeting peptide (Cystabn) with transferrin (TFn) as well as lysosomal marker (LysoGreen). We compared that with the colocalization of a standard bombesin agonist (Tyr4-Bn) with the same markers.

Figure 5.9 shows punctate staining is noticeable for cells treated with Tyr4-Bn and Cystabn as well as cells treated with Tfn and LysoGreen. This means that endocytosis is activated and some of the peptides went into lysosomal compartments. Figure 5.9A&B shows that there is a partial colocalization of Tyr4-Bn or Cystabn with TFn after 10 min incubation with peptide and 5 min incubation with Tfn. This is visible by the appearance of some yellow fluorescent puncta in the merged micrograph of the TFn panels. This visual observation was confirmed by the Pearson correlation coefficient (PCC) in graph Figure 5.9E. The PCC of Tyr4-Bn or Cystabn colocalization with TFn is 0.55 ± 0.02 and 0.37 ± 0.01 respectively. The Tyr4-Bn PCC is more significant ($p < 0.001$) than the PCC of Cystabn with TFn.

Figure 5.9C&D shows that there is a near complete colocalization of Tyr4-Bn or Cystabn with LysoGreen. This is visually apparent from the appearance of many yellow fluorescent puncta in the merged micrograph of the LysoGreen panels. This visual observation was confirmed by the Pearson correlation coefficient (PCC) in Figure 5.9F. The PCC of Tyr4-Bn or Cystabn colocalization with LysoGreen is 0.83 ± 0.01 and 0.88 ± 0.03 respectively.

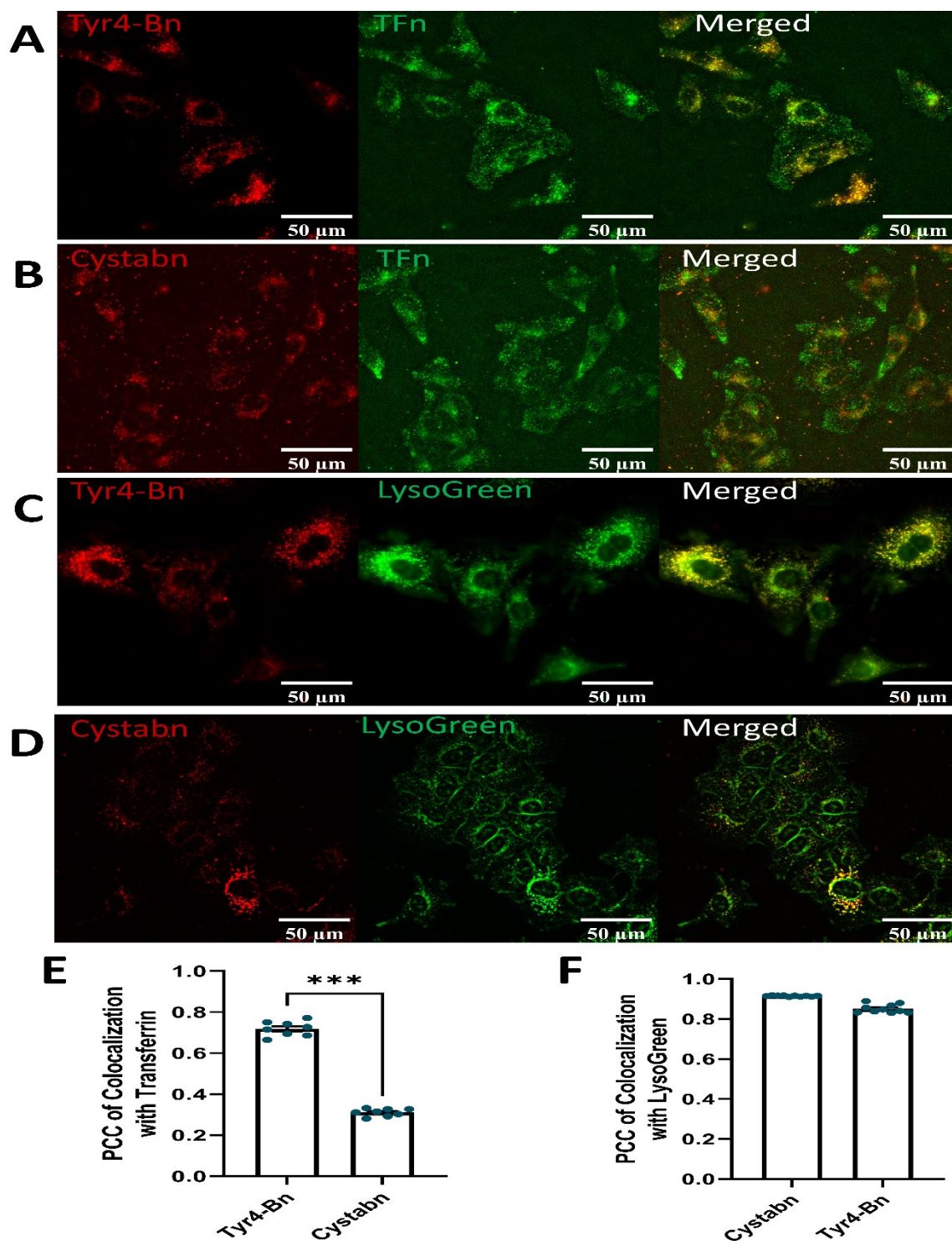


Figure 5.9: Peptides colocalization with transferrin (TFn) and LysoTracker Green. A549 GRP-R cells were exposed to 3 μM of Tyr4-Bn (A) or Cystabn (B) for 5 min before adding 0.313 μM TFn for 5 min. The cells in C & D were exposed to 1 μM LysoTracker Green for 20 min before adding 3 μM of Tyr4-Bn (C) or Cystabn (D) for 10 min. Graph (E) shows the PCC of colocalization of the highlighted peptides with TFn. Graph (F) shows the PCC of colocalization of the highlighted peptides with LysoTracker Green. Data shown are mean \pm SEM, $n \geq 5$ whole images

To confirm the findings from peptide colocalization, we tested the colocalization of the target liposomes with TFn as well as LysoGreen. Figure 5.10A shows that there is a marginal colocalization of control liposomes with TFn. Figure 5.10B shows that there is a partial colocalization of target liposomes with TFn. This is visually visible by the appearance of some yellow fluorescent puncta in the merged micrograph of the TFn panels. This visual observation was confirmed by the Pearson correlation coefficient (PCC) in Figure 5.10E. The PCC of control or target liposomes colocalization with TFn is 0.36 ± 0.002 and 0.07 ± 0.005 respectively. The target liposomes PCC is much more significant ($p < 0.001$) than the PCC of control liposomes with TFn.

Figure 5.10C&D shows that there is an almost complete colocalization of control or target liposomes with LysoGreen. This is visually visible by the appearance of many yellow fluorescent puncta in the merged micrograph of the LysoGreen panels. This visual observation was confirmed by the Pearson correlation coefficient (PCC) in graph Figure 5.10F. The PCC of control or target liposomes colocalization with LysoGreen is 0.67 ± 0.02 and 0.89 ± 0.01 respectively. The targeted liposomes PCC is much greater ($p < 0.001$) than that of control liposomes with LysoGreen. This indicates that the targeted liposomes is internalized mainly by receptor-mediated approach.

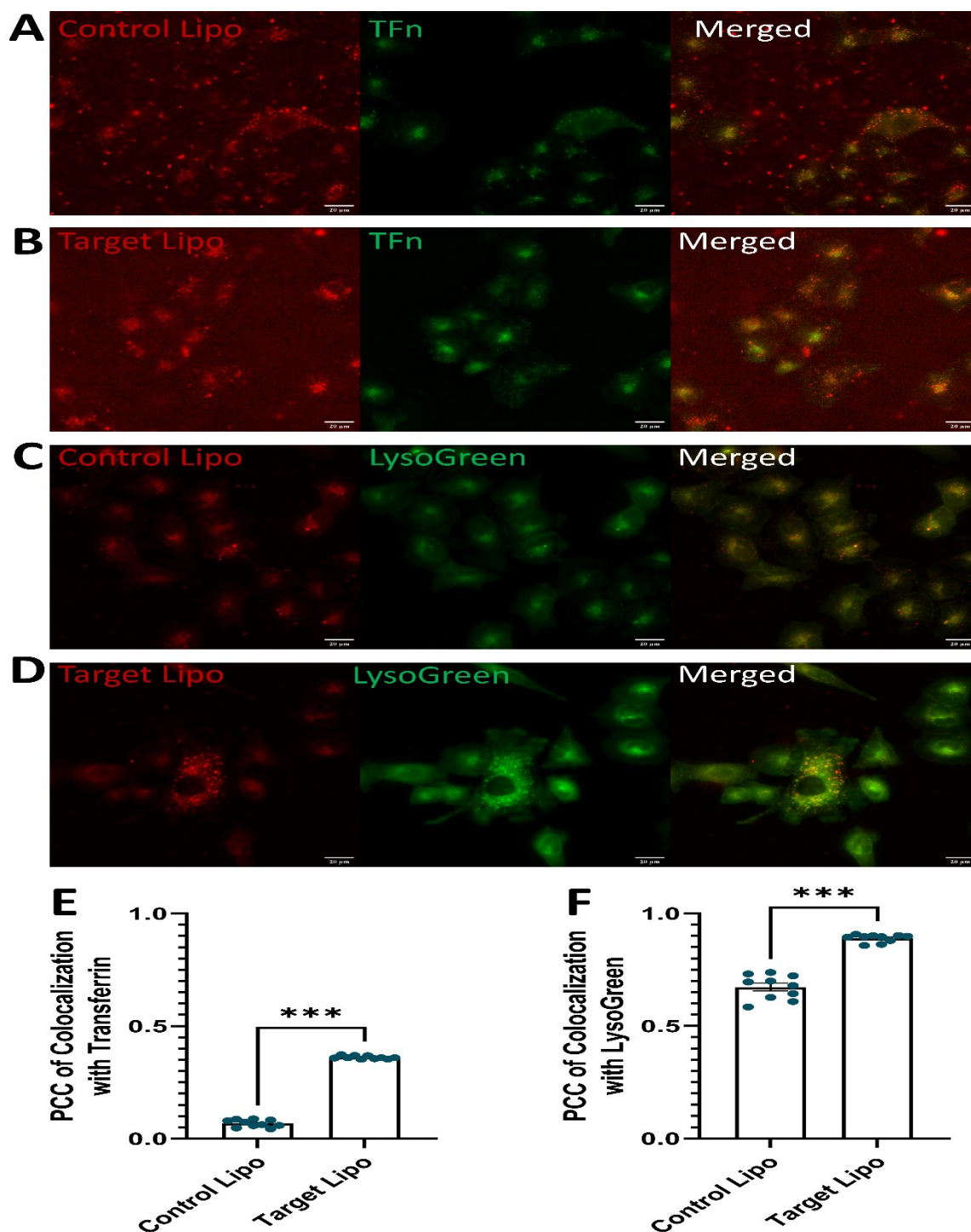


Figure 5.10: Lysosomes colocalization with transferrin (TFN) and LysoGreen. A549 GRP-R cells were exposed to 5 μM of Control Lipo (A) or Targeted Lipo (B) for 5 min before adding 0.313 μM TFN for 5 min. The cells in C & D were exposed to 1 μM LysoGreen for 20 min before adding 5 μM of Control Lipo (C) or Targeted Lipo (D) for 10 min. Graph (E) shows the PCC of colocalization of the highlighted Liposomes with TFN. Graph (F) shows the PCC of colocalization of the highlighted Liposomes with LysoGreen. Data shown are mean \pm SEM, $n \geq 5$ whole images

5.3 Discussion

In this project I aimed to test whether Cystabn can be used in lung cancer for enhanced cytotoxic drug delivery. However, due to time constraints studies were limited to A549-GRPR and the testing of fluorescently labelled liposomes rather than drug loaded liposomes. We used this antagonist peptide to reinforce the concept that the use of GRP-R antagonist peptides was strongly preferable to the use of agonist peptides which have the potential to fuel tumour growth. Based upon preferable *in vitro* and *in vivo* properties reported by others we based our work on the statine-based antagonist peptide (JMV594), d-Phe-Gln-Trp-Ala-Val-Gly-His-Sta-Leu-NH₂.

The JMV594 (also known as RM2) peptide structure was modified to bear an N terminal L-cysteine residue, which enables subsequent attachment to a functionalised lipid carrier. The peptide, which is termed Cystabn in this project, was prepared by Fmoc solid phase peptide synthesis and characterised by HPLC and mass spectrometry. The conjugation of the Cystabn peptide to DSPE-PEG-maleimide was successfully performed to yield a peptide-PEG-lipid conjugate with a mass around 4.5kDa. MALDI-TOF MS was performed as the definitive analytical technique of choice for proving successful peptide-PEG-lipid conjugation. Mass spectra with good resolution were achieved by mixing sample with the matrix in a layer on layer approach. Successful conjugation was concluded when the most abundant mass peak of DSPE-PEG2000-Cystabn (calculated mass: 4137.41 Da, assuming perfect monodispersity of the PEG2000 group) was observed at 4188 Da and was separated from surrounding peaks by 44 Da, which represents the mass of a single ethylene glycol unit. regions of the mass spectrum. For example, a mass difference from 4277.57 Da to 4321.49 Da, which is equal to one monomer.

Liposomal formulations were developed to incorporate DSPE-PEG2000-Cystabn or control DSPE-PEG2000. Liposomes without targeting cystabn peptide (Control-Lipo) contained 5 mol. % DOPE-PEG2000, whereas targeted formulations (Target-Lipo) were loaded with 1 mol. % or 3 mol. % of targeting DSPE-PEG2000-Cystabn conjugate with the total mass of PEG-lipid made up to 5% with DOPE-PEG2000.

This peptide-PEG-lipid conjugate was subsequently used to prepare small and monodisperse vesicles as judged by DLS analysis. The characterization of the liposomes showed a monodisperse liposome suspension with the polydispersity index is < 0.1 for all formulations with slightly negative zeta potential. The value of zeta potential is closer to zero because the formulations contain the zwitterionic phospholipid (DOPC).

The pegylation is important because it provides biological and colloidal stability to the formulation. This is achieved by the steric hindrance effect caused by pegylation. In this project, the pegylation achieved by inclusion of 5 mole % DOPC-PEG₂₀₀₀. This is because of the self-assembly characteristic of phospholipids to form liposomes. This means that the hydrophilic part of the phospholipids (phospholipid head) will orient to the outside the bilayer where it is in contact with water. The hydrophobic tail of phospholipids will orient to the bilayer core where it is in contact with the other phospholipid tail of the other part of the bilayer. In other words, the energetically preferable conformation for this lipid mixture is spherical bilayer shape [107]. The pegylation of the surface of liposomes in the range of 5-10 mole % using PEG₂₀₀₀-lipid found to provide the longest circulation time *in vivo* [225, 226]. At this range, a dense polymer brush formed at the surface and yielding the repulsive steric interaction.

The standard thin-film technique of producing the liposomes in this project was used and produced liposomes in the 100 nm size range for both formulations. This is desired because the optimal size of < 200 nm provide highest tumour retention by utilizing Enhanced Permeability and Retention (EPR) of the tumour in anticancer applications. Most currently approved anticancer nanomedicines have sizes range from 100-200 nm. However, size range of < 20 nm will cause removal of nanoparticles by renal clearance and fenestrated capillaries. In addition to that, as the size increase >150 nm, the accumulation in the spleen, liver and bone marrow enhanced [227]. The mean size of the liposomes were about 100 nm. to actively increase the accumulation of formulation in the tumour, targeting moiety were incorporated as 3 mole % DSPE-PEG₂₀₀₀-maleimid. By using this approach, cystabn will be available unhindered to identify and bind to its receptor on the cancer cell [228, 229].

The colloidal stability of the liposomes was studied and the liposomes (control, 1mole% and 3mole% targeted formulations) were shown to be stable in PBS over 3 days at the highlighted temperatures. As expected, the exposure of liposomes to 10% serum reduced the stability of the liposomes.

Endocytosis has been reported as the mode of cell entry for targeted liposomes [230]. The targeting capacity of cystabn-decorated liposomes was examined by flow cytometry analysis of adherent A549-GRP-R cells exposed to fluorescently tagged target-lipo (FL-target-Lipo) or tagged Control-lipo (FL-Control-Lipo) formulations. A549-GRPR cells were used because of the extent of target overexpression and the adherent nature of the line that permits easy manipulation. Preliminary studies using FL-Target-Lipo including 1 mole % targeting lipid showed marginal increases in relative cellular accumulation. To overcome this, the density of targeting lipid was increased to 3 mole %. To examine for active internalisation and intracellular accumulation of liposomes at the endocytosis permissive temperature of 37 °C, we subtracted the median fluorescence intensity (MFI) attributable to cell-surface adsorption of liposomes at 4 °C, to yield a “4 °C - normalised cell MFI” at each time point and for each formulation. This is because many proteins and enzymes are sensitive to temperature and hence endocytosis is active process, it can be affected by lowered temperatures.

Experiments investigated the optimal incubation time and formulation concentration for uptake studies using flow cytometry. Since we did not notice a preferential accumulation of targeted formulation over 30 min, we extended the incubation time to 1-3 hours. In terms of formulation concentration, we chose to conserve formulation by maintaining a low lipid concentration of 1 µg/mL.

The uptake of the targeted formulation after 30 min is increased in comparison to the control formulation. This is consistent with other studies, for example, Raz et al. reported a rapid increase of radio-labelled liposomes in macrophage cells in the first hour of incubation [231]. In another study, targeted liposomes binding in A549 after 2 hours incubation was significantly higher than nontargeted liposomes [232]. From the literature, it appears that most targeted liposomes are incubated for 1-2 hours to test cellular uptake. This might be due to the diffusion properties of liposomes which means it take relatively long time [233-235].

We demonstrated that after 60 min the targeted formulation internalizes significantly more than the control formulation by flow cytometry. It is important to note that the formulations can bind non-specifically to cell surface proteins which can then hide the true targeting capability of the targeted liposomes. Therefore, the used 4 °C - normalised cell MFI as control to show with more confidence that the signal associated with cells is either from specific receptor binding or internalization.

Drug delivery inside the cells is critical because most drugs work on intracellular targets. There are generally three possible mechanisms of liposome cargo delivery into target cells. Firstly, extracellular release of drugs which create concentration gradient and passive uptake. one of the challenges in the utilization of this mechanism is to ensure selective extracellular drug release. Secondly, passive fusion of liposomes into the cell membrane and intracellular drug release. Thirdly, liposomes can be internalised by receptor-mediated endocytosis followed by intracellular trafficking and drug release. Internalization of liposomes is dependent on many factors, such as liposome size, type of cell and type of target receptor [236-241].

The targeting ligand ability to induce GRP-R internalization was not vital in its choice for targeting GRP-R. the accumulation of the targeted formulation is expected to increase by the increase of the cell membrane bound liposome without the activation of signalling pathways. To examine the efficiency of liposomal internalization and lysosomal trafficking, we used a GRP-R overexpression A549. This model grows faster than SCLC cells and its adherent which allow easier manipulation.

We next confirmed the flow cytometric results using fluorescence microscopy. Following 5 min exposure to either control or target-liposomes, A549-GRP-R cells displayed greater cellular fluorescence signals in the FL-target-Lipo group. Cells exposed to FL-Control-Lipo displayed a diffuse cell membrane-like staining with few green fluorescent puncta. Whereas, the target-lipo exposed cells displayed many more fluorescent puncta as well as a widespread increase in cellular fluorescence. Our observations here indicate that GRP-R targeting with Cystabn peptide increases cell uptake of liposomes, most likely through receptor-mediated uptake. This offers more efficient and superior way of liposomal cargo delivery into the cells.

Taken together the flow cytometry and microscopy data demonstrate that, using a fluorescently labelled model liposomal carrier, the relative increase in cell uptake afforded by cystabn functionalisation is modest but significant. To put our data into context, approximately two-fold enhanced delivery of an oligonucleotide-bombesin (6-14) conjugate was observed by Ming *et al.* [242]. Using a similar approach to ours, Accardo *et al.* studied liposomal delivery of doxorubicin into PC-3 pancreatic cells using a modified bombesin targeting peptide [243]. The authors showed a reduction in mouse PC-3 xenograft size compared to non-targeted doxorubicin liposomes and saline control, consistent with tumour accumulation of the delivery system. In summary, an increase in SCLC cellular accumulation of a liposomal drug cargo would be beneficial for therapy, especially considering the chemotherapeutic resistance profile that is often displayed by clinical SCLC [244].

The colocalization of the Cystabn peptide with Alexa-488 labelled transferrin, a marker for clathrin-coated vesicle endocytosis, was examined in live cells. After treatment for 10 min, there was partial co-localization of the cystabn with transferrin. We then compared that with the colocalization of a standard bombesin agonist (Tyr4-Bn) with the same marker. The data shows that there is a partial colocalization of Tyr4-Bn or Cystabn with TFn. This indicates that the highlighted peptides initially enter cells into early endosomes that is shared by transferrin.

To further pursue the subcellular fate of the highlighted peptides we examined its colocalization with lysosomal marker (LysoGreen). There is an almost complete colocalization of Tyr4-Bn or Cystabn with LysoGreen and a high Pearson correlation coefficient (PCC). The results show that Cystabn and Tyr4-Bn rapidly internalized into endosomes and lysosomes. The colocalization with lysosomes at this short incubation time (30 min) was not expected. However, there is a study which show that Tyr4-Bn rapidly degraded intracellularly by lysosome-dependent mechanism [245]. Another study also shows that GRP of the bombesin family gets degraded rapidly by non-lysosomal mechanisms such as by an ectopeptidase extracellularly. This was shown by measuring radiolabelled GRP in the media by HPLC and correlate the result with binding study at 37 °C and 4 °C [246].

The findings optioned from peptides colocalization was confirmed using the liposomal formulations. The colocalization of the targeted liposomes with Alexa-488 labeled transferrin was examined in live cells. After treatment for 10 min, there was partial colocalization of the targeted liposomes with transferrin and its significantly increased over that of the control liposomes with the same marker. This confirms the finding from the peptide data. It also confirms that target formulation uptake via receptor mediated mechanism.

To further pursue the subcellular fate of the targeted liposomes, we examined there colocalization with lysosomal marker (LysoGreen). There is an almost complete colocalization of both formulations with LysoGreen with the targeted liposomes showed significant increase of this colocalization over the control liposomes.

Future studies on cystabn targeted liposomal carriers will examine the uptake and trafficking of these nanocarriers, particularly with regards to their efficiency of carrying chemotherapeutic agents into the cell. Poor intracellular accumulation of nanocarriers can be improved through targeted and triggered drug release, for example through the incorporation of temperature-sensitive [247] or light-sensitive lipids [248]. These approaches have shown promise in enhancing the cellular/tumoural accumulation of chemotherapeutic agents in various models [116, 249].

In spite of the enhanced cellular delivery shown here, the application of GRP-R targeting nano-sized delivery systems to different cancers should be considered carefully due to variability in GRP-R expression across malignant diseases. Published reports, using techniques such as RT-PCR and immunostaining, have shown that between 63-100% of prostate tumours are GRP-R positive, while SCLC tumours are more heterogeneous, with 29-85% of tumours expressing GRP-R [46]. This demonstrates that GRP-R expression is not a universal marker of SCLC or any other tumour and that future development of GRP-R targeted therapeutics would require patient stratification according to expression status.

5.4 Conclusion

In this chapter it was demonstrated that the functionalisation of liposomes with a GRP-R antagonist peptide is sufficient to promote the accumulation of liposomes within GRP-R expressing cells such as SCLC. Targeted-liposomal formulation offer increased internalization into GRP-R expressing cells. This increased internalisation of GRP-R targeted liposomes in treatment-resistant tumours such as SCLC could offer improved therapeutic outcomes. The target formulation internalises into the cell via receptor mediated approach rapidly and gets sorted into lysosomal vehicle for degradation.

GENERAL DISCUSSION AND CONCLUSION

Chapter 6

6.1 General Discussion

SCLC is a deadly cancer that has neuroendocrine properties with different properties than other types of cancers and therefore different therapeutic management. This type of cancer initially responds to treatment with high recurrence rate and resistance to further treatment. In addition to that, it has high mortality rate [6, 24, 250, 251].

This treatment for SCLC has not changed for 30 years. There have been limited advances made in the treatment and understanding of the pathology of SCLC compared to NSCLC. Currently, there is no targeted therapy approved for treatment of SCLC [6, 252, 253]. In order to approach SCLC, it is imperative to draw efforts on to further our understanding of the pathology as well as diagnosis and development of effective treatment for SCLC. The targeted therapeutic approach can be used in SCLC to target conventional chemotherapeutic treatments to cancer cells to increase the potency and lowers the side effects of therapies. Significant efforts are being drawn to the understanding of SCLC pathology which contributed to the development of targeted therapeutics for SCLC treatment, some of which reached clinical trials [254].

One of the approaches used to deliver targeted therapies to cancer cells is by targeting receptors expressed on the cell membrane by the target cancer type. SCLC is shown to express GRP-R and its ligand which act as autocrine loop and drive the cancer growth [34]. It has been reported that GRP-R expression correlates with tumour growth and behavior in several cancer types such as neuroblastoma and SCLC [65, 180, 201, 255]. This mechanism has been exploited by development of several targeted therapeutics or imaging agents. For example, anti-GRP antibodies and GRP-R peptide antagonists [219] have been developed which showed antitumour responses in several cancer types in vitro [216-218].

Generally, in targeted nanomedicine delivery, small ligands such as peptides are preferred over larger macromolecules like antibodies. This is because small molecules have better pharmacokinetic profile, costs, compliance to therapy, easier to manufacture and to store than macromolecules [256]. Furthermore, it has been shown that using antagonist peptide for targeting therapy in cancer is preferable than using agonist. This is because antagonists do not stimulate the downstream effects, such as growth or angiogenesis, of their receptors.

However, it also shows reduced rate of receptor internalization. Despite that, several studies showed that antagonists, such as agonist GRP-R, displayed preferable in vivo targeting capacity compared to agonists [257].

One of the targeted therapeutic approaches used successfully in cancer therapy is nanoparticles formulations such as Doxil[®] and Onivyde[®] [220]. The pegylated liposomal cisplatin formulation, Lipoplatin[®], was shown to display preferable therapeutic choice in combination with paclitaxel over non-liposomal cisplatin with paclitaxel in lung cancer [221]. Furthermore, the use of active targeting approach using targeting motifs in cancer attracted attentions and worth exploration. This is usually achieved by targeting specific receptors on cancer cells with ligand engrafted on nanoparticles surface. However, no actively targeted liposomal formulation reached the clinic [222, 258, 259]. This means that there is need for more research to be done in this area. Novel actively targeted formulation for SCLC therapy using specific ligand to GRP-R which is overexpressed in SCLC is developed in this work.

In this thesis, we aimed to target the GRP-R/GRP autocrine growth loop in SCLC. To do that we chose an antagonistic peptide to utilize the enhanced targeting capacity of antagonist in targeting SCLC. The antagonist (Cystabn) in this study is derived from JMV594 antagonistic peptide from the work of Mansi et al. who showed that the radiolabelled antagonist peptide has preferable tumour accumulation over agonist peptide [260, 261]. We engrafted Cystabn on the surface of liposomal formulation to utilize the active targeting in the treatment of SCLC. We assumed that the extracellular accumulation of the targeted liposomal formulation can be increased by specific high affinity binding of the antagonistic targeting motif to GRP-R expressed on SCLC cell membrane. Therefore, increase the accumulation of formulation in the target cell without stimulated signalling of cell growth.

In chapter 3 of this thesis, we aimed to establish a SCLC cell lines model for it to be used to test the targeting formulation. We started by selecting a panel of SCLC cell lines that were selected based on the supporting evidence from the literature for their GRP-R expression. As per the literature, it appears that the selected panel of SCLC cell lines include three GRP-R overexpressing lines (H510, H345 and H209) and two GRP-R non-expressing SCLC cell lines (H82 and N417) [34, 172, 175, 176, 178, 179].

However, we showed that all the SCLC cell lines showed variable levels of GRP-R expression by Western blot, flow cytometry and immunofluorescence imaging. We then chose two SCLC cell lines – one with relatively higher GRP-R expression (H345) and the other one with relatively lower GRP-R expression (H82). Functionality of this receptor in the mentioned two cell lines was shown to be functional and responsive to the standard agonist (Tyr4-Bn) in H345 but not H82. Furthermore, the mentioned agonist was shown to be able to drive cell growth by MTS and clonogenic assays. After quantification of GRP-R expression in SCLC cell lines and optimizing a number of techniques to study bombesin expression and functionality, H345 was selected for further studies.

In chapter 4 of this thesis, we sought to develop a toolbox of cellular models expressing different levels of the receptor to validate GRP-R as a target in SCLC. We knocked down GRP-R in two non-adherent SCLC and one control adherent NSCLC line using lentiviral vectors. The adherent NSCLC A549 cell line was also subjected to GRP-R overexpression using a plasmid DNA construct encoding a N terminally HA tagged GRP-R.

We sought to reduce the expression of GRP-R in SCLC cell lines H510 and H345 to investigate the targeting capacity of our targeted liposomes and is it reduced compared to wild type. We chose H345 for KD because it showed high levels of GRP-R expression and receptor functionality as reported in the previous chapter. H510 cell line also showed high GRP-R expression in the previous chapter therefore we expect it to have the same response to GRP-R agonist and antagonist showed with H345. In addition to that, H510 reported to have a functional GRP-R by intracellular calcium assay [262].

We screened shRNA sequences for KD efficiency by RT-qPCR and chose one sequence. We then tested whether the GRP-R functionality was reduced in KD cells by measuring intracellular calcium response to the GRP-R agonist Tyr4-Bn- we saw a lack of response in the KD H510 and KD H345. This means the KD of the GRP-R in the mentioned SCLC cell lines was effective. We would expect to see changes in cell growth as reported in the previous chapter with Cystabn. This means we have a model that we can use to test targeting capacity as shown by others [201].

GRP-R knockdown cell line model were developed using two SCLC cell lines. In addition, GRP-R knockdown and overexpression models were prepared from the adherent A549 cell line. The original plan for this project would involve this combination of cell models being used to study the uptake, activity and biodistribution of GRP-R targeted formulation in vitro and in vivo. Regrettably, the emergence of the COVID-19 pandemic forced a change of plan. In the following chapter the uptake and trafficking of GRP-R targeted liposomal formulations in A549 cells was studied only at the in vitro level.

In chapter 5 of this thesis, we formulated actively targeted liposomal formulation engrafted with Cystabn – the GRP-R antagonist – to test its targeted capacity in A549 overexpressing cells. Cystabn was synthesised and shown to inhibit cell growth in vitro. Cystabn was used to prepare a targeted DSPE-PEG2000 lipid conjugate that was formulated into liposomes. Flow cytometric and microscopic studies showed that fluorescently labelled cystabn-decorated liposomes accumulated more extensively in GRP-R over-expressing cells than matched liposomes that contained no cystabn targeting motif.

The functionalisation of liposomes with a GRP-R antagonist peptide is sufficient to promote the accumulation of liposomes within GRP-R expressing cells such as SCLC. Targeted-liposomal formulation offer increased internalization into GRP-R expressing cells. This increased internalisation of GRP-R targeted liposomes in treatment-resistant tumours such as SCLC could offer improved therapeutic outcomes. The target formulation internalises into the cell via receptor mediated approach rapidly and gets sorted into lysosomal vehicle for degradation.

6.2 General Conclusion

The results shown in this thesis provided an insight into developing in vitro model for testing the targeting capacity of liposomal targeted formulation through manipulation of the targeted receptor expression. we developed the targeting liposomes and demonstrated its targeting ability of GRP-R. The targeting liposomes is colloiddally stable and appears to be preferentially internalised by GRP-R expressing lung cells. The work presented here provides a toolbox for development of in vitro model and targeting cancer. Furthermore, the formulation can be adapted to be used in other types of cancer by modification of targeting moiety.

6.3 Future Work

A major focus for the future studies of this project would be to investigate the uptake and trafficking of drug loaded GRP-R targeted liposomal carriers functionalized with Cystabn. In addition to that, intracellular accumulation of targeted formulation could be improved via the use of stimuli-responsive characteristics, for example through the incorporation of temperature-sensitive [247] or light-sensitive [248] lipids which showed promising results a number of models [116, 249]. Furthermore, the targeting capacity of the Cystabn-functionalized liposomes *in vivo* as well as uptake and biodistribution will be of main focus in future works.

Bibliography

1. Neil Bannister, J.B., *Cancer survival in England: adult, stage at diagnosis and childhood – patients followed up to 2016*, in *Office for National Statistics*. 2017, Office for National Statistics: Office for National Statistics.
2. UK, C.R. *Lung cancer statistics*. 2015 July, 2017]; Available from: <http://www.cancerresearchuk.org/health-professional/cancer-statistics/statistics-by-cancer-type/lung-cancer#heading-Six>.
3. UK, C.R. *Cancer mortality for all cancers combined: Cancer mortality by sex and UK region 2015 July 2017*]; Available from: <http://www.cancerresearchuk.org/health-professional/cancer-statistics/mortality/all-cancers-combined#heading-Zero>.
4. Audit, N.L.C., *National Lung Cancer Audit annual report 2016 (for the audit period 2015)*. 2017, National Lung Cancer Audit.
5. UK, C.R. *Lung Cancer: Survival*. Lung Cancer 2007 July 2016 [cited 2017; Available from: <http://www.cancerresearchuk.org/about-cancer/lung-cancer/survival#collapse-13746-603865254>.
6. Asai, N., et al., *Relapsed small cell lung cancer: treatment options and latest developments*. Therapeutic advances in medical oncology, 2014. **6**(2): p. 69-82.
7. Ou, S.-H.I., A. Ziogas, and J.A. Zell, *Prognostic Factors for Survival in Extensive Stage Small Cell Lung Cancer (ED-SCLC): The Importance of Smoking History, Socioeconomic and Marital Statuses, and Ethnicity*. Journal of Thoracic Oncology, 2009. **4**(1): p. 37-43.
8. Amini, A., et al., *Progress in the management of limited-stage small cell lung cancer*. Cancer, 2014. **120**(6): p. 790-798.
9. William, W.N. and B.S. Glisson, *Novel strategies for the treatment of small-cell lung carcinoma*. Nat Rev Clin Oncol, 2011. **8**(10): p. 611-619.
10. Excellence, N.I.F.H.a.C. *Lung cancer: diagnosis and management*. 2011 July 2017]; Available from: <https://www.nice.org.uk/guidance/cg121/chapter/Patient-centred-care>.
11. Hiddinga, B.I., et al., *Recent developments in the treatment of small cell lung cancer*. European Respiratory Review, 2021. **30**(161): p. 210079.
12. Rudin, C.M., et al., *Small-cell lung cancer*. Nature Reviews Disease Primers, 2021. **7**(1): p. 3.
13. Walia, H.K., et al., *Immunotherapy in Small Cell Lung Cancer Treatment: a Promising Headway for Future Perspective*. Current Treatment Options in Oncology, 2022. **23**(2): p. 268-294.
14. Kahnert, K., D. Kauffmann-Guerrero, and R.M. Huber, *SCLC-State of the Art and What Does the Future Have in Store?* Clin Lung Cancer, 2016. **17**(5): p. 325-333.
15. Owonikoko, T.K., et al., *A phase 1 safety study of veliparib combined with cisplatin and etoposide in extensive stage small cell lung cancer: A trial of the ECOG-ACRIN Cancer Research Group (E2511)*. Lung Cancer, 2015. **89**(1): p. 66-70.
16. Ren, Y., et al., *Multiple paraneoplastic syndromes associated with small cell lung cancer: a unique case of concomitant Lambert-Eaton myasthenic syndrome, paraneoplastic cerebellar degeneration and syndrome of inappropriate secretion of antidiuretic hormone*. INTERNATIONAL JOURNAL OF CLINICAL AND EXPERIMENTAL MEDICINE, 2016. **9**(2): p. 4939-4942.
17. Hobbs, C. and A. Miller, *Review of endocrine syndromes associated with tumours of non-endocrine origin*. Journal of clinical pathology, 1966. **19**(2): p. 119-127.
18. Kanaji, N., et al., *Paraneoplastic syndromes associated with lung cancer*. World Journal of Clinical Oncology, 2014. **5**(3): p. 197-223.
19. Huber, R.M. and A. Tufman, *Update on small cell lung cancer management*. Breathe, 2012. **8**(4): p. 314.
20. Cheung, W.K.C. and D.X. Nguyen, *Lineage factors and differentiation states in lung cancer progression*. Oncogene, 2015. **34**(47): p. 5771-5780.
21. Karachaliou, N., et al., *Cellular and molecular biology of small cell lung cancer: an overview*. Transl Lung Cancer Res, 2016. **5**(1): p. 2-15.

22. Guadamillas, M.C., A. Cerezo, and M.A. del Pozo, *Overcoming anoikis – pathways to anchorage-independent growth in cancer*. *Journal of Cell Science*, 2011. **124**(19): p. 3189-3197.
23. Micke, P., et al., *Staging small cell lung cancer: Veterans Administration Lung Study Group versus International Association for the Study of Lung Cancer—what limits limited disease?* *Lung Cancer*, 2002. **37**(3): p. 271-276.
24. Jackman, D.M. and B.E. Johnson, *Small-cell lung cancer*. *Lancet*, 2005. **366**(9494): p. 1385-96.
25. Saji, H., et al., *Pathological upstaging and treatment strategy of clinical stage I small cell lung cancer following surgery*. *Journal of Thoracic Disease*, 2017. **9**(3): p. E285-E289.
26. Detterbeck, F.C.B., Daniel J Tanoue, Lynn T, *The new lung cancer staging system*. *CHEST Journal*, 2009. **136**(1): p. 260-271.
27. Mirsadraee, S., et al., *The 7th lung cancer TNM classification and staging system: Review of the changes and implications*. *World Journal of Radiology*, 2012. **4**(4): p. 128-134.
28. Alvarado-Luna, G. and D. Morales-Espinosa, *Treatment for small cell lung cancer, where are we now?—a review*. *Translational Lung Cancer Research*, 2016. **5**(1): p. 26-38.
29. Fruh, M., et al., *Small-cell lung cancer (SCLC): ESMO Clinical Practice Guidelines for diagnosis, treatment and follow-up*. *Ann Oncol*, 2013. **24 Suppl 6**: p. vi99-105.
30. Sørensen, J., et al., *Performance status assessment in cancer patients. An inter-observer variability study*. *British journal of cancer*, 1993. **67**(4): p. 773.
31. Kurup, A. and N.H. Hanna, *Treatment of small cell lung cancer*. *Critical reviews in oncology/hematology*, 2004. **52**(2): p. 117-126.
32. Morabito, A., et al., *Treatment of small cell lung cancer*. *Critical reviews in oncology/hematology*, 2014. **91**(3): p. 257-270.
33. Veronesi, G., et al., *When is surgery indicated for small-cell lung cancer?* *Lung Cancer*, 2015. **90**(3): p. 582-9.
34. Cuttitta, F., et al., *Bombesin-like peptides can function as autocrine growth factors in human small-cell lung cancer*. *Nature*, 1985. **316**(6031): p. 823-6.
35. Bologna, M., et al., *Bombesin stimulates growth of human prostatic cancer cells in vitro*. *Cancer*, 1989. **63**(9): p. 1714-1720.
36. Corjay, M.H., et al., *Two distinct bombesin receptor subtypes are expressed and functional in human lung carcinoma cells*. *J Biol Chem*, 1991. **266**(28): p. 18771-9.
37. Lui, V.W.Y., et al., *Mitogenic effects of gastrin-releasing peptide in head and neck squamous cancer cells are mediated by activation of the epidermal growth factor receptor*. *Oncogene*, 2003. **22**(40): p. 6183-6193.
38. Cornelio, D.B., R. Roesler, and G. Schwartzmann, *Gastrin-releasing peptide receptor as a molecular target in experimental anticancer therapy*. *Ann Oncol*, 2007. **18**(9): p. 1457-66.
39. Moody, T.W., I. Ramos-Alvarez, and R.T. Jensen, *Neuropeptide G Protein-Coupled Receptors as Oncotargets*. *Frontiers in Endocrinology*, 2018. **9**.
40. Slice, L.W., H.F. Yee, Jr., and J.H. Walsh, *Visualization of internalization and recycling of the gastrin releasing peptide receptor-green fluorescent protein chimera expressed in epithelial cells*. *Recept Channels*, 1998. **6**(3): p. 201-12.
41. Calebiro, D. and A. Godbole, *Internalization of G-protein-coupled receptors: Implication in receptor function, physiology and diseases*. *Best Pract Res Clin Endocrinol Metab*, 2018. **32**(2): p. 83-91.
42. McDonald, T., et al., *Characterization of a gastrin releasing peptide from porcine non-antral gastric tissue*. *Biochemical and biophysical research communications*, 1979. **90**(1): p. 227-233.
43. Anastasi, A., V. Erspamer, and M. Bucci, *Isolation and amino acid sequences of alytesin and bombesin, two analogous active tetradecapeptides from the skin of European discoglossid frogs*. *Arch Biochem Biophys*, 1972. **148**(2): p. 443-6.
44. Jensen, R.T., et al., *International Union of Pharmacology. LXVIII. Mammalian bombesin receptors: nomenclature, distribution, pharmacology, signaling, and functions in normal and disease states*. *Pharmacol Rev*, 2008. **60**(1): p. 1-42.

45. Minamino, N., K. Kangawa, and H. Matsuo, *Neuromedin B: a novel bombesin-like peptide identified in porcine spinal cord*. Biochemical and biophysical research communications, 1983. **114**(2): p. 541-548.
46. Patel, O., A. Shulkes, and G.S. Baldwin, *Gastrin-releasing peptide and cancer*. Biochim Biophys Acta, 2006. **1766**(1): p. 23-41.
47. Xiao, D., et al., *The human gastrin-releasing peptide receptor gene structure, its tissue expression and promoter*. Gene, 2001. **264**(1): p. 95-103.
48. Ferris, H.A., et al., *Location and Characterization of the Human GRP Receptor Expressed by Gastrointestinal Epithelial Cells*. Peptides, 1997. **18**(5): p. 663-672.
49. Bartholdi, M.F., et al., *In situ hybridization for gastrin-releasing peptide receptor (GRP receptor) expression in prostatic carcinoma*. International journal of cancer, 1998. **79**(1): p. 82-90.
50. Fleischmann, A., et al., *Gastrin-releasing peptide receptors in normal and neoplastic human uterus: involvement of multiple tissue compartments*. J Clin Endocrinol Metab, 2005. **90**(8): p. 4722-9.
51. Flores, D.G., et al., *Gastrin-releasing peptide receptor content in human glioma and normal brain*. Brain Research Bulletin, 2010. **82**(1): p. 95-98.
52. Emanuel, R.L., et al., *Bombesin-like peptides and receptors in normal fetal baboon lung: roles in lung growth and maturation*. American Journal of Physiology-Lung Cellular and Molecular Physiology, 1999. **277**(5): p. L1003-L1017.
53. Sunday, M.E., et al., *Anti-bombesin monoclonal antibodies modulate fetal mouse lung growth and maturation in utero and in organ cultures*. The Anatomical Record, 1993. **236**(1): p. 25-34.
54. Joshi, S. and S. Kotecha, *Lung growth and development*. Early Human Development, 2007. **83**(12): p. 789-794.
55. Moody, T., T. O'donohue, and D. Jacobowitz, *Biochemical localization and characterization of bombesin-like peptides in discrete regions of rat brain*. Peptides, 1981. **2**(1): p. 75-79.
56. Tsutsumi, Y., et al., *Simultaneous immunohistochemical localization of gastrin releasing peptide (GRP) and calcitonin (CT) in human bronchial endocrine-type cells*. Virchows Archiv, 1983. **400**(2): p. 163-171.
57. Whitley, J., A.S. Giraud, and A. Shulkes, *Expression of gastrin-releasing peptide (GRP) and GRP receptors in the pregnant human uterus at term*. The Journal of Clinical Endocrinology & Metabolism, 1996. **81**(11): p. 3944-3950.
58. di Sant'Agnese, P., *Calcitoninlike immunoreactive and bombesinlike immunoreactive endocrine-paracrine cells of the human prostate*. Archives of pathology & laboratory medicine, 1986. **110**(5): p. 412-415.
59. Ghatei, M., et al., *Bombesin-like immunoreactivity in the pancreas of man and other mammalian species*. Cellular and Molecular Life Sciences, 1984. **40**(8): p. 884-886.
60. Piantelli, M., et al., *Neuropeptide-immunoreactive cells in human thymus*. Brain, behavior, and immunity, 1990. **4**(3): p. 189-197.
61. Wharton, J., et al., *Neuron-specific enolase as an immunocytochemical marker for the diffuse neuroendocrine system in human fetal lung*. Journal of Histochemistry & Cytochemistry, 1981. **29**(12): p. 1359-1364.
62. Siegfried, J.M., et al., *Expression of mRNA for gastrin-releasing peptide receptor by human bronchial epithelial cells. Association with prolonged tobacco exposure and responsiveness to bombesin-like peptides*. Am J Respir Crit Care Med, 1997. **156**(2 Pt 1): p. 358-66.
63. Wang, D., H. Yeger, and E. Cutz, *Expression of gastrin-releasing peptide receptor gene in developing lung*. American journal of respiratory cell and molecular biology, 1996. **14**(5): p. 409-416.
64. DeMichele, M., et al., *Expression of mRNA for three bombesin receptor subtypes in human bronchial epithelial cells*. American journal of respiratory cell and molecular biology, 1994. **11**(1): p. 66-74.
65. Toi-Scott, M., C.L. Jones, and M.A. Kane, *Clinical correlates of bombesin-like peptide receptor subtype expression in human lung cancer cells*. Lung Cancer, 1996. **15**(3): p. 341-54.
66. Yang, D., et al., *Intertumoral Heterogeneity in SCLC Is Influenced by the Cell Type of Origin*. Cancer Discovery, 2018. **8**(10): p. 1316.

67. Uchida, K., et al., *Expression of progastrin-releasing peptide and gastrin-releasing peptide receptor mRNA transcripts in tumor cells of patients with small cell lung cancer*. J Cancer Res Clin Oncol, 2002. **128**(12): p. 633-40.
68. Hohla, F., et al., *Growth inhibition of non-small-cell lung carcinoma by BN/GRP antagonist is linked with suppression of K-Ras, COX-2, and pAkt*. Proceedings of the National Academy of Sciences, 2007. **104**(47): p. 18671-18676.
69. Burns, D., et al., *Breast cancer cell-associated endopeptidase EC 24.11 modulates proliferative response to bombesin*. British journal of cancer, 1999. **79**(2): p. 214.
70. Narayan, S., et al., *Specific binding and growth effects of bombesin-related peptides on mouse colon cancer cells in vitro*. Cancer research, 1990. **50**(21): p. 6772-6778.
71. Moody, T.W., et al., *Neuromedin B binds with high affinity, elevates cytosolic calcium and stimulates the growth of small-cell lung cancer cell lines*. Journal of Pharmacology and Experimental Therapeutics, 1992. **263**(1): p. 311-317.
72. Wasilenko, W.J., et al., *Calcium signaling in prostate cancer cells: evidence for multiple receptors and enhanced sensitivity to bombesin/GRP*. Prostate, 1997. **30**(3): p. 167-73.
73. Mikoshiba, K., *The InsP3 receptor and intracellular Ca²⁺ signaling*. Current Opinion in Neurobiology, 1997. **7**(3): p. 339-345.
74. Rozengurt, E., *Signal transduction pathways in the mitogenic response to G protein-coupled neuropeptide receptor agonists*. Journal of Cellular Physiology, 1998. **177**(4): p. 507-517.
75. Dorsam, R.T. and J.S. Gutkind, *G-protein-coupled receptors and cancer*. Nature Reviews Cancer, 2007. **7**(2): p. 79-94.
76. Calebiro, D., et al., *Signaling by internalized G-protein-coupled receptors*. Trends in Pharmacological Sciences, 2010. **31**(5): p. 221-228.
77. Kane, M.A., et al., *Isolation of a gastrin releasing peptide receptor from normal rat pancreas*. Peptides, 1991. **12**(2): p. 207-213.
78. Maeda, H., et al., *Tumor vascular permeability and the EPR effect in macromolecular therapeutics: a review*. J Control Release, 2000. **65**(1-2): p. 271-84.
79. Shi, Y., et al., *The EPR effect and beyond: Strategies to improve tumor targeting and cancer nanomedicine treatment efficacy*. Theranostics, 2020. **10**(17): p. 7921-7924.
80. Huynh, E. and G. Zheng, *Cancer nanomedicine: addressing the dark side of the enhanced permeability and retention effect*. Nanomedicine, 2015. **10**(13): p. 1993-1995.
81. Park, J., et al. *Alliance with EPR Effect: Combined Strategies to Improve the EPR Effect in the Tumor Microenvironment*. Theranostics, 2019. **9**, 8073-8090 DOI: 10.7150/thno.37198.
82. *New Insights into "Permeability" as in the Enhanced Permeability and Retention Effect of Cancer Nanotherapeutics*. ACS Nano, 2017. **11**(10): p. 9567-9569.
83. Gabizon, A., et al., *In vivo fate of folate-targeted polyethylene-glycol liposomes in tumor-bearing mice*. Clinical cancer research, 2003. **9**(17): p. 6551-6559.
84. Song, S., et al., *Novel peptide ligand directs liposomes toward EGF-R high-expressing cancer cells in vitro and in vivo*. The FASEB Journal, 2009. **23**(5): p. 1396-1404.
85. Amreddy, N., et al., *Tumor-targeted and pH-controlled delivery of doxorubicin using gold nanorods for lung cancer therapy*. Int J Nanomedicine, 2015. **10**: p. 6773-88.
86. Sanna, V. and M. Sechi, *Therapeutic Potential of Targeted Nanoparticles and Perspective on Nanotherapies*. ACS Medicinal Chemistry Letters, 2020. **11**(6): p. 1069-1073.
87. Raha, S., T. Paunesku, and G. Woloschak, *Peptide-mediated cancer targeting of nanoconjugates*. Wiley Interdiscip Rev Nanomed Nanobiotechnol, 2011. **3**(3): p. 269-81.
88. Yeh, C.-Y., et al., *Peptide-conjugated nanoparticles for targeted imaging and therapy of prostate cancer*. Biomaterials, 2016. **99**: p. 1-15.
89. Kalimuthu, K., et al., *Gold nanoparticles stabilize peptide-drug-conjugates for sustained targeted drug delivery to cancer cells*. Journal of Nanobiotechnology, 2018. **16**(1): p. 34.

90. Yao, Y., et al., *Nanoparticle-Based Drug Delivery in Cancer Therapy and Its Role in Overcoming Drug Resistance*. Frontiers in Molecular Biosciences, 2020. **7**.
91. Lembo, D. and R. Cavalli, *Nanoparticulate delivery systems for antiviral drugs*. Antiviral Chemistry and Chemotherapy, 2010. **21**(2): p. 53-70.
92. Allen, T.M., *Ligand-targeted therapeutics in anticancer therapy*. Nature Reviews Cancer, 2002. **2**(10): p. 750-763.
93. *Antitumor activity of an anti-gastrin releasing peptide (GRP) murine monoclonal antibody (2A11). Phase II trial and in vitro correlation with peptide and receptor expression*. Lung Cancer, 1994. **11**: p. 4.
94. Beck, A., et al., *Strategies and challenges for the next generation of therapeutic antibodies*. Nat Rev Immunol, 2010. **10**(5): p. 345-52.
95. Jin, S., et al., *Emerging new therapeutic antibody derivatives for cancer treatment*. Signal Transduction and Targeted Therapy, 2022. **7**(1): p. 39.
96. Zahavi, D. and L. Weiner, *Monoclonal antibodies in cancer therapy*. Antibodies, 2020. **9**(3): p. 34.
97. Modjtahedi, H., S. Ali, and S. Essapen, *Therapeutic application of monoclonal antibodies in cancer: advances and challenges*. British Medical Bulletin, 2012. **104**(1): p. 41-59.
98. Koppán, M., et al., *Bombesin/gastrin-releasing peptide antagonists RC-3095 and RC-3940-II inhibit tumor growth and decrease the levels and mRNA expression of epidermal growth factor receptors in H-69 small cell lung carcinoma*. Cancer, 1998. **83**(7): p. 1335-43.
99. Kiaris, H., et al., *Targeted cytotoxic analogue of bombesin/gastrin-releasing peptide inhibits the growth of H-69 human small-cell lung carcinoma in nude mice*. British journal of cancer, 1999. **81**(6): p. 966.
100. Taylor, J.E., et al., *In vitro and in vivo inhibition of human small cell lung carcinoma (NCI-H69) growth by a somatostatin analogue*. Biochem Biophys Res Commun, 1988. **153**(1): p. 81-6.
101. Thomas, F., et al., *Antitumoral activity of bombesin analogues on small cell lung cancer xenografts: relationship with bombesin receptor expression*. Cancer research, 1992. **52**(18): p. 4872-4877.
102. Mahmoud, S., et al., *[Psi13, 14] bombesin analogues inhibit growth of small cell lung cancer in vitro and in vivo*. Cancer research, 1991. **51**(7): p. 1798-1802.
103. Llinares, M., et al., *Syntheses and biological activities of potent bombesin receptor antagonists*. J Pept Res, 1999. **53**(3): p. 275-83.
104. Tokita, K., et al., *Molecular basis for selectivity of high affinity peptide antagonists for the gastrin-releasing peptide receptor*. J Biol Chem, 2001. **276**(39): p. 36652-63.
105. Marsouvanidis, P.J., et al., *Gastrin releasing peptide receptor-directed radioligands based on a bombesin antagonist: synthesis, ¹¹¹In-labeling, and preclinical profile*. Journal of medicinal chemistry, 2013. **56**(6): p. 2374-2384.
106. Bangham, A.D. and R. Horne, *Negative staining of phospholipids and their structural modification by surface-active agents as observed in the electron microscope*. Journal of molecular biology, 1964. **8**(5): p. 660IN2-668IN10.
107. Sessa, G. and G. Weissmann, *Phospholipid spherules (liposomes) as a model for biological membranes*. Journal of lipid research, 1968. **9**(3): p. 310-318.
108. Daoud, S.S., L.R. Hume, and R.L. Juliano, *Liposomes in cancer therapy*. Advanced Drug Delivery Reviews, 1989. **3**(3): p. 405-418.
109. Meybeck, A., *Past, present and future of liposome cosmetics*, in *Liposome Dermatics*. 1992, Springer. p. 341-345.
110. Kim, H.-H.Y. and I.C. Baianu, *Novel liposome microencapsulation techniques for food applications*. Trends in Food Science & Technology, 1991. **2**: p. 55-61.
111. Gregoriadis, G., P. Leathwood, and B.E. Ryman, *Enzyme entrapment in liposomes*. FEBS letters, 1971. **14**(2): p. 95-99.

112. Michel, S. *Predicting the fate of liposomes*. 2014 January 2014 [cited 2016 september 2016]; Available from: <http://www.materials-talks.com/blog/2014/01/20/predicting-the-fate-of-liposomes/>.
113. Maruyama, K., *Intracellular targeting delivery of liposomal drugs to solid tumors based on EPR effects*. *Adv Drug Deliv Rev*, 2011. **63**(3): p. 161-9.
114. Koshkaryev, A., et al., *Immunoconjugates and long circulating systems: origins, current state of the art and future directions*. *Advanced drug delivery reviews*, 2013. **65**(1): p. 24-35.
115. Akbarzadeh, A., et al., *Liposome: classification, preparation, and applications*. *Nanoscale Research Letters*, 2013. **8**(1): p. 1-9.
116. Allen, T.M. and P.R. Cullis, *Liposomal drug delivery systems: From concept to clinical applications*. *Advanced Drug Delivery Reviews*, 2013. **65**(1): p. 36-48.
117. Torchilin, V.P., *Recent advances with liposomes as pharmaceutical carriers*. *Nat Rev Drug Discov*, 2005. **4**(2): p. 145-160.
118. Vaage, J., et al., *Tissue distribution and therapeutic effect of intravenous free or encapsulated liposomal doxorubicin on human prostate carcinoma xenografts*. *Cancer*, 1994. **73**(5): p. 1478-1484.
119. Gabizon, A., et al. *Prolonged circulation time and enhanced accumulation in malignant exudates of doxorubicin encapsulated in polyethylene-glycol coated liposomes*. *Cancer Res* 1994 June 2015 [cited 54 4]; 1994/02/15:[987-92]. Available from: <https://www.doxil.com/hcp/mechanism-of-action>.
120. Krishna, R., et al., *Liposomal and nonliposomal drug pharmacokinetics after administration of liposome-encapsulated vincristine and their contribution to drug tissue distribution properties*. *J Pharmacol Exp Ther*, 2001. **298**(3): p. 1206-12.
121. Gabizon, A., H. Shmeeda, and Y. Barenholz, *Pharmacokinetics of Pegylated Liposomal Doxorubicin*. *Clinical Pharmacokinetics*, 2003. **42**(5): p. 419-436.
122. Philippot, J., S. Mutaftschiev, and J. Liautard, *A very mild method allowing the encapsulation of very high amounts of macromolecules into very large (1000 nm) unilamellar liposomes*. *Biochimica et Biophysica Acta (BBA)-Biomembranes*, 1983. **734**(2): p. 137-143.
123. Sercombe, L., et al., *Advances and challenges of liposome assisted drug delivery*. *Frontiers in pharmacology*, 2015. **6**.
124. Gautam, A. and N. Koshkina, *Paclitaxel (taxol) and taxoid derivatives for lung cancer treatment: potential for aerosol delivery*. *Curr Cancer Drug Targets*, 2003. **3**(4): p. 287-96.
125. Torrico Guzmán, E.A., Q. Sun, and S.A. Meenach, *Development and Evaluation of Paclitaxel-Loaded Aerosol Nanocomposite Microparticles and Their Efficacy Against Air-Grown Lung Cancer Tumor Spheroids*. *ACS Biomaterials Science & Engineering*, 2019. **5**(12): p. 6570-6580.
126. Mangal, S., et al., *Pulmonary delivery of nanoparticle chemotherapy for the treatment of lung cancers: challenges and opportunities*. *Acta Pharmacologica Sinica*, 2017. **38**(6): p. 782-797.
127. Stathopoulos, G.P., et al., *Comparison of liposomal cisplatin versus cisplatin in non-squamous cell non-small-cell lung cancer*. *Cancer Chemother Pharmacol*, 2011. **68**(4): p. 945-50.
128. Stathopoulos, G.P., *Liposomal cisplatin: a new cisplatin formulation*. *Anticancer Drugs*, 2010. **21**(8): p. 732-6.
129. Antonietti, M. and S. Förster, *Vesicles and liposomes: a self-assembly principle beyond lipids*. *Advanced Materials*, 2003. **15**(16): p. 1323-1333.
130. Salunkhe, S. and N. Bhatia, *Benchmark in the era of drug carriers for semisolid based topical delivery system*. *Am. J. PharmTech Res.*, 2013. **3**: p. 493-510.
131. Li, J., et al., *A review on phospholipids and their main applications in drug delivery systems*. *Asian Journal of Pharmaceutical Sciences*, 2015. **10**(2): p. 81-98.
132. Sessa, G. and G. Weissmann, *Phospholipid spherules (liposomes) as a model for biological membranes*. *J Lipid Res*, 1968. **9**(3): p. 310-8.
133. Bozzuto, G. and A. Molinari, *Liposomes as nanomedical devices*. *International journal of nanomedicine*, 2015. **10**: p. 975.

134. Nakhaei, P., et al., *Liposomes: Structure, Biomedical Applications, and Stability Parameters With Emphasis on Cholesterol*. Frontiers in Bioengineering and Biotechnology, 2021. **9**.
135. Briuglia, M.L., et al., *Influence of cholesterol on liposome stability and on in vitro drug release*. Drug Deliv Transl Res, 2015. **5**(3): p. 231-42.
136. Kaddah, S., et al., *Cholesterol modulates the liposome membrane fluidity and permeability for a hydrophilic molecule*. Food and Chemical Toxicology, 2018. **113**: p. 40-48.
137. Wu, H., et al., *Cholesterol-tuned liposomal membrane rigidity directs tumor penetration and anti-tumor effect*. Acta Pharmaceutica Sinica B, 2019. **9**(4): p. 858-870.
138. Milla, P., F. Dosio, and L. Cattel, *PEGylation of proteins and liposomes: a powerful and flexible strategy to improve the drug delivery*. Curr Drug Metab, 2012. **13**(1): p. 105-19.
139. Nosova, A., et al., *Diversity of PEGylation methods of liposomes and their influence on RNA delivery*. MedChemComm, 2019. **10**(3): p. 369-377.
140. Shen, Z., et al., *1 - PEGylated "stealth" nanoparticles and liposomes*, in *Engineering of Biomaterials for Drug Delivery Systems*, A. Parambath, Editor. 2018, Woodhead Publishing. p. 1-26.
141. Immordino, M.L., F. Dosio, and L. Cattel, *Stealth liposomes: review of the basic science, rationale, and clinical applications, existing and potential*. International journal of nanomedicine, 2006. **1**(3): p. 297-315.
142. Deshpande, P.P., S. Biswas, and V.P. Torchilin, *Current trends in the use of liposomes for tumor targeting*. Nanomedicine (London, England), 2013. **8**(9): p. 1509-1528.
143. Riaz, M.K., et al., *Surface Functionalization and Targeting Strategies of Liposomes in Solid Tumor Therapy: A Review*. International journal of molecular sciences, 2018. **19**(1): p. 195.
144. Nogueira, E., et al., *Design of liposomal formulations for cell targeting*. Colloids and surfaces B: Biointerfaces, 2015. **136**: p. 514-526.
145. Noble, G.T., et al., *Ligand-targeted liposome design: challenges and fundamental considerations*. Trends Biotechnol, 2014. **32**(1): p. 32-45.
146. Forssen, E. and M. Willis, *Ligand-targeted liposomes*. Advanced Drug Delivery Reviews, 1998. **29**(3): p. 249-271.
147. Gonzalez, N., et al., *Bombesin-related peptides and their receptors: recent advances in their role in physiology and disease states*. Curr Opin Endocrinol Diabetes Obes, 2008. **15**(1): p. 58-64.
148. Sano, H., et al., *Characterization of the bombesin-like peptide receptor family in primates*. Genomics, 2004. **84**(1): p. 139-46.
149. Kelley, M.J., et al., *Antitumor activity of a monoclonal antibody directed against gastrin-releasing peptide in patients with small cell lung cancer*. Chest, 1997. **112**(1): p. 256-61.
150. Roesler, R. and G. Schwartzmann, *GRPR antagonists for prostate cancer--prospects and caveats*. Nat Rev Urol, 2013. **10**(7): p. 424.
151. Yang, M., et al., *F-Labeled GRPR Agonists and Antagonists: A Comparative Study in Prostate Cancer Imaging*. Theranostics, 2011. **1**: p. 220-9.
152. Pereira, D.V., et al., *Effects of an antagonist of the gastrin-releasing peptide receptor in an animal model of uveitis*. Invest Ophthalmol Vis Sci, 2009. **50**(11): p. 5300-3.
153. Abouzayed, A., et al., *Preclinical Evaluation of the GRPR-Targeting Antagonist RM26 Conjugated to the Albumin-Binding Domain for GRPR-Targeting Therapy of Cancer*. Pharmaceutics, 2020. **12**(10).
154. Schwartzmann, G., et al., *A phase I trial of the bombesin/gastrin-releasing peptide (BN/GRP) antagonist RC3095 in patients with advanced solid malignancies*. Invest New Drugs, 2006. **24**(5): p. 403-12.
155. Hong, S.-K., et al., *RC-3095, a Gastrin-Releasing Peptide Receptor Antagonist, Synergizes With Gemcitabine to Inhibit the Growth of Human Pancreatic Cancer CFPAC-1 In Vitro and In Vivo*. Pancreas, 2014. **43**(1).
156. Varvarigou, A., et al., *Gastrin-releasing peptide (GRP) analogues for cancer imaging*. Cancer Biother Radiopharm, 2004. **19**(2): p. 219-29.

157. Jungwirth, A., et al., *Luteinizing hormone-releasing hormone antagonist Cetrorelix (SB-75) and bombesin antagonist RC-3940-II inhibit the growth of androgen-independent PC-3 prostate cancer in nude mice*. *The Prostate*, 1997. **32**(3): p. 164-172.
158. Abiraj, K., et al., *Bombesin antagonist-based radioligands for translational nuclear imaging of gastrin-releasing peptide receptor-positive tumors*. *J Nucl Med*, 2011. **52**(12): p. 1970-8.
159. Mansi, R., et al., *Development of a potent DOTA-conjugated bombesin antagonist for targeting GRPR-positive tumours*. *Eur J Nucl Med Mol Imaging*, 2011. **38**(1): p. 97-107.
160. Varasteh, Z., et al., *Synthesis and characterization of a high-affinity NOTA-conjugated bombesin antagonist for GRPR-targeted tumor imaging*. *Bioconjug Chem*, 2013. **24**(7): p. 1144-53.
161. Varasteh, Z., et al., *The effect of mini-PEG-based spacer length on binding and pharmacokinetic properties of a ⁶⁸Ga-labeled NOTA-conjugated antagonistic analog of bombesin*. *Molecules*, 2014. **19**(7): p. 10455-72.
162. Varasteh, Z., et al., *The effect of macrocyclic chelators on the targeting properties of the ⁶⁸Ga-labeled gastrin releasing peptide receptor antagonist PEG2-RM26*. *Nucl Med Biol*, 2015. **42**(5): p. 446-454.
163. Varasteh, Z., et al., *In Vitro and In Vivo Evaluation of a ¹⁸F-Labeled High Affinity NOTA Conjugated Bombesin Antagonist as a PET Ligand for GRPR-Targeted Tumor Imaging*. *PLOS ONE*, 2013. **8**(12): p. e81932.
164. Mitran, B., et al., *High Contrast PET Imaging of GRPR Expression in Prostate Cancer Using Cobalt-Labeled Bombesin Antagonist RM26*. *Contrast Media & Molecular Imaging*, 2017. **2017**: p. 6873684.
165. Mitran, B., et al., *Trastuzumab cotreatment improves survival of mice with PC-3 prostate cancer xenografts treated with the GRPR antagonist (177) Lu-DOTAGA-PEG(2) -RM26*. *Int J Cancer*, 2019. **145**(12): p. 3347-3358.
166. Hofstetter, M., et al., *Effect of the versatile bifunctional chelator AAZTA(5) on the radiometal labelling properties and the in vitro performance of a gastrin releasing peptide receptor antagonist*. *EJNMMI Radiopharm Chem*, 2020. **5**(1): p. 29.
167. Vollmer, R.T., *The effect of cell size on the pathologic diagnosis of small and large cell carcinomas of the lung*. *Cancer*, 1982. **50**(7): p. 1380-1383.
168. Benya, R.V., et al., *Glycosylation of the Gastrin-Releasing Peptide Receptor and Its Effect on Expression, G Protein Coupling, and Receptor Modulatory Processes*. *Molecular Pharmacology*, 2000. **58**(6): p. 1490.
169. Kaighn, M., et al., *Establishment and characterization of a human prostatic carcinoma cell line (PC-3)*. *Investigative urology*, 1979. **17**(1): p. 16-23.
170. Moody, T.W., et al., *High levels of intracellular bombesin characterize human small-cell lung carcinoma*. *Science*, 1981. **214**(4526): p. 1246-8.
171. Erisman, M.D., et al., *Human lung small-cell carcinoma contains bombesin*. *Proc Natl Acad Sci U S A*, 1982. **79**(7): p. 2379-83.
172. Moody, T.W., V. Bertness, and D.N. Carney, *Bombesin-like peptides and receptors in human tumor cell lines*. *Peptides*, 1983. **4**(5): p. 683-6.
173. Zachary, I. and E. Rozengurt, *Modulation of the epidermal growth factor receptor by mitogenic ligands: effects of bombesin and role of protein kinase C*. *Cancer surveys*, 1984. **4**(4): p. 729-765.
174. Carney, D.N., et al., *Establishment and identification of small cell lung cancer cell lines having classic and variant features*. *Cancer Res*, 1985. **45**(6): p. 2913-23.
175. Moody, T.W., et al., *High affinity receptors for bombesin/GRP-like peptides on human small cell lung cancer*. *Life Sci*, 1985. **37**(2): p. 105-13.
176. Weber, S., et al., *Gastrin releasing peptide is a selective mitogen for small cell lung carcinoma in vitro*. *J Clin Invest*, 1985. **75**(1): p. 306-9.
177. Moody, T.W., et al., *BN/GRP-like peptides and receptors in small cell lung cancer*. *Int J Neurosci*, 1988. **40**(1-2): p. 141-8.

178. Maruno, K., et al., *Immunoreactive gastrin-releasing peptide as a specific tumor marker in patients with small cell lung carcinoma*. *Cancer Res*, 1989. **49**(3): p. 629-32.
179. Carney, D.N., et al., *Selective stimulation of small cell lung cancer clonal growth by bombesin and gastrin-releasing peptide*. *Cancer Res*, 1987. **47**(3): p. 821-5.
180. Moody, T.W. and F. Cuttitta, *Growth factor and peptide receptors in small cell lung cancer*. *Life Sci*, 1993. **52**(14): p. 1161-73.
181. Cardona, C., et al., *Production of Neuromedin B and Neuromedin B Gene Expression in Human Lung Tumor Cell Lines*. *Cancer Research*, 1991. **51**(19): p. 5205.
182. Trepel, J.B., et al., *A novel bombesin receptor antagonist inhibits autocrine signals in a small cell lung carcinoma cell line*. *Biochemical and Biophysical Research Communications*, 1988. **156**(3): p. 1383-1389.
183. Gazdar, A.F., et al., *Establishment of continuous, clonable cultures of small-cell carcinoma of lung which have amine precursor uptake and decarboxylation cell properties*. *Cancer Res*, 1980. **40**(10): p. 3502-7.
184. Moody, T.W. and L.Y. Korman, *The release of bombesin-like peptides from small cell lung cancer cells*. *Ann N Y Acad Sci*, 1988. **547**: p. 351-9.
185. Trepel, J.B., et al., *Modulation of bombesin-induced phosphatidylinositol hydrolysis in a small-cell lung-cancer cell line*. *Biochem J*, 1988. **255**(2): p. 403-10.
186. Moody, T.W., et al., *BW2258U89: a GRP receptor antagonist which inhibits small cell lung cancer growth*. *Life Sci*, 1995. **56**(7): p. 521-9.
187. Ramos-Álvarez, I., et al., *Insights into bombesin receptors and ligands: Highlighting recent advances*. *Peptides*, 2015. **72**: p. 128-44.
188. Oejo-Garcia, M., et al., *Use of RT-PCR to detect co-expression of neuropeptides and their receptors in lung cancer*. *Lung Cancer*, 2001. **33**(1): p. 1-9.
189. Moody, T.W., et al., *Bombesin-like peptides elevate cytosolic calcium in small cell lung cancer cells*. *Biochem Biophys Res Commun*, 1987. **147**(1): p. 189-95.
190. Laukkanen, M.O. and M.D. Castellone, *Gastrin-Releasing Peptide Receptor Targeting in Cancer Treatment: Emerging Signaling Networks and Therapeutic Applications*. *Curr Drug Targets*, 2016. **17**(5): p. 508-14.
191. New, D.C. and Y.H. Wong, *Molecular mechanisms mediating the G protein-coupled receptor regulation of cell cycle progression*. *J Mol Signal*, 2007. **2**: p. 2.
192. Roesler, R., et al., *Gastrin-releasing peptide receptor signaling in the integration of stress and memory*. *Neurobiology of Learning and Memory*, 2014. **112**: p. 44-52.
193. Ginj, M., et al., *Radiolabeled somatostatin receptor antagonists are preferable to agonists for in vivo peptide receptor targeting of tumors*. *Proc Natl Acad Sci U S A*, 2006. **103**(44): p. 16436-41.
194. Cescato, R., et al., *Bombesin receptor antagonists may be preferable to agonists for tumor targeting*. *J Nucl Med*, 2008. **49**(2): p. 318-26.
195. Carroll, R.E., et al., *Gastrin-releasing peptide is a mitogen and a morphogen in murine colon cancer*. *Cell Growth Differ*, 2000. **11**(7): p. 385-93.
196. Weber, S., et al., *Gastrin releasing peptide is a selective mitogen for small cell lung carcinoma in vitro*. *The Journal of Clinical Investigation*, 1985. **75**(1): p. 306-309.
197. Rivera, C.A., et al., *Expression of GRP and its receptor is associated with improved survival in patients with colon cancer*. *Clin Exp Metastasis*, 2009. **26**(7): p. 663-71.
198. Morgat, C., et al., *Expression of Gastrin-Releasing Peptide Receptor in Breast Cancer and Its Association with Pathologic, Biologic, and Clinical Parameters: A Study of 1,432 Primary Tumors*. *J Nucl Med*, 2017. **58**(9): p. 1401-1407.
199. Baratto, L., et al., *Imaging the Distribution of Gastrin-Releasing Peptide Receptors in Cancer*. *Journal of Nuclear Medicine*, 2020. **61**(6): p. 792.
200. Kim, S., et al., *Gastrin-releasing peptide is a growth factor for human neuroblastomas*. *Ann Surg*, 2002. **235**(5): p. 621-9; discussion 629-30.

201. Qiao, J., et al., *Gastrin-releasing peptide receptor silencing suppresses the tumorigenesis and metastatic potential of neuroblastoma*. Proceedings of the National Academy of Sciences, 2008. **105**(35): p. 12891.
202. Kang, J., et al., *Bombesin induces angiogenesis and neuroblastoma growth*. Cancer Lett, 2007. **253**(2): p. 273-81.
203. Jensen, R.T., *Gastrin-Releasing Peptide*, in *Encyclopedia of Gastroenterology*, L.R. Johnson, Editor. 2004, Elsevier: New York. p. 179-185.
204. Spindel, E.R., et al., *Cloning and functional characterization of a complementary DNA encoding the murine fibroblast bombesin/gastrin-releasing peptide receptor*. Mol Endocrinol, 1990. **4**(12): p. 1956-63.
205. Benya, R.V., et al., *Gastrin-releasing peptide receptor-induced internalization, down-regulation, desensitization, and growth: possible role for cyclic AMP*. Molecular Pharmacology, 1994. **46**(2): p. 235.
206. Fanger, B.O., A.C. Wade, and A.D. Cardin, *Characterization of the murine pancreatic receptor for gastrin releasing peptide and bombesin*. Regulatory Peptides, 1991. **32**(3): p. 241-251.
207. Kroog, G.S., et al., *The Gastrin-releasing Peptide Receptor Is Rapidly Phosphorylated by a Kinase Other Than Protein Kinase C After Exposure to Agonist (*)*. Journal of Biological Chemistry, 1995. **270**(14): p. 8217-8224.
208. Travis, W.D., *Update on small cell carcinoma and its differentiation from squamous cell carcinoma and other non-small cell carcinomas*. Modern Pathology, 2012. **25**: p. S18-S30.
209. Wada, E., et al., *Generation and Characterization of Mice Lacking Gastrin-Releasing Peptide Receptor*. Biochemical and Biophysical Research Communications, 1997. **239**(1): p. 28-33.
210. Hampton, L.L., et al., *Loss of bombesin-induced feeding suppression in gastrin-releasing peptide receptor-deficient mice*. Proceedings of the National Academy of Sciences, 1998. **95**(6): p. 3188-3192.
211. Wang, W., et al., *Peptide-Conjugated Long-Lived Theranostic Imaging for Targeting GRPr in Cancer and Immune Cells*. Angewandte Chemie International Edition, 2020. **59**(41): p. 17897-17902.
212. Hussein, W.M., et al., *Peptide-based targeted polymeric nanoparticles for siRNA delivery*. Nanotechnology, 2019. **30**(41): p. 415604.
213. Cheng, C.-Y., et al., *Membrane metalloendopeptidase suppresses prostate carcinogenesis by attenuating effects of gastrin-releasing peptide on stem/progenitor cells*. Oncogenesis, 2020. **9**(3): p. 38.
214. Kang, J., et al., *Bombesin induces angiogenesis and neuroblastoma growth*. Cancer Letters, 2007. **253**(2): p. 273-281.
215. Bepler, G., et al., *Substance P analogues function as bombesin receptor antagonists and inhibit small cell lung cancer clonal growth*. Peptides, 1988. **9**(6): p. 1367-72.
216. Chanda, N., et al., *Bombesin functionalized gold nanoparticles show in vitro and in vivo cancer receptor specificity*. Proc Natl Acad Sci U S A, 2010. **107**(19): p. 8760-5.
217. Santos-Cuevas, C.L., et al., *Targeted imaging of gastrin-releasing peptide receptors with ^{99m}Tc-EDDA/HYNIC-[Lys³]-bombesin: biokinetics and dosimetry in women*. Nucl Med Commun, 2008. **29**(8): p. 741-7.
218. Mansi, R., et al., *Bombesin-Targeted PET of Prostate Cancer*. J Nucl Med, 2016. **57**(Suppl 3): p. 67s-72s.
219. Zhang, J., et al., *⁶⁸Ga-NOTA-Aca-BBN(7-14) PET/CT in Healthy Volunteers and Glioma Patients*. J Nucl Med, 2016. **57**(1): p. 9-14.
220. Shi, J., et al., *Cancer nanomedicine: progress, challenges and opportunities*. Nature Reviews Cancer, 2017. **17**(1): p. 20-37.
221. Stathopoulos, G.P., et al., *Liposomal cisplatin combined with paclitaxel versus cisplatin and paclitaxel in non-small-cell lung cancer: a randomized phase III multicenter trial*. Annals of Oncology, 2010. **21**(11): p. 2227-2232.

222. Miller, K., et al., *HERMIONE: a randomized Phase 2 trial of MM-302 plus trastuzumab versus chemotherapy of physician's choice plus trastuzumab in patients with previously treated, anthracycline-naïve, HER2-positive, locally advanced/metastatic breast cancer*. BMC Cancer, 2016. **16**: p. 352.
223. Zuckerman, J.E., et al., *Correlating animal and human phase Ia/Ib clinical data with CALAA-01, a targeted, polymer-based nanoparticle containing siRNA*. Proceedings of the National Academy of Sciences, 2014. **111**(31): p. 11449-11454.
224. *A Phase 2 Study to Determine the Safety and Efficacy of BIND-014 (Docetaxel Nanoparticles for Injectable Suspension) as Second-line Therapy to Patients With Non-Small Cell Lung Cancer*. 2013.
225. Allen, C., et al., *Controlling the physical behavior and biological performance of liposome formulations through use of surface grafted poly(ethylene glycol)*. Biosci Rep, 2002. **22**(2): p. 225-50.
226. Kenworthy, A.K., et al., *Range and magnitude of the steric pressure between bilayers containing phospholipids with covalently attached poly(ethylene glycol)*. Biophysical Journal, 1995. **68**(5): p. 1921-1936.
227. Tang, L., et al., *Investigating the optimal size of anticancer nanomedicine*. Proceedings of the National Academy of Sciences, 2014. **111**(43): p. 15344-15349.
228. Deshpande, P.P., S. Biswas, and V.P. Torchilin, *Current trends in the use of liposomes for tumor targeting*. Nanomedicine (Lond), 2013. **8**(9): p. 1509-28.
229. Noble, G.T., et al., *Ligand-targeted liposome design: challenges and fundamental considerations*. Trends in biotechnology, 2014. **32**(1): p. 32-45.
230. Federman, N. and C.T. Denny, *Targeting Liposomes Toward Novel Pediatric Anticancer Therapeutics*. Pediatric Research, 2010. **67**(5): p. 514-519.
231. Raz, A., et al., *Biochemical, morphological, and ultrastructural studies on the uptake of liposomes by murine macrophages*. Cancer Res, 1981. **41**(2): p. 487-94.
232. Wong, B.C., et al., *Carbonic anhydrase IX-directed immunoliposomes for targeted drug delivery to human lung cancer cells in vitro*. Drug Des Devel Ther, 2014. **8**: p. 993-1001.
233. Cheng, L., et al., *GE11-modified liposomes for non-small cell lung cancer targeting: preparation, ex vitro and in vivo evaluation*. International journal of nanomedicine, 2014. **9**: p. 921.
234. Xu, S., et al., *Targeting receptor-mediated endocytotic pathways with nanoparticles: rationale and advances*. Advanced drug delivery reviews, 2013. **65**(1): p. 121-138.
235. Santos, A.O., et al., *Design of peptide-targeted liposomes containing nucleic acids*. Biochimica et Biophysica Acta (BBA) - Biomembranes, 2010. **1798**(3): p. 433-441.
236. Montizaan, D., et al., *Comparison of the uptake mechanisms of zwitterionic and negatively charged liposomes by HeLa cells*. Nanomedicine: Nanotechnology, Biology and Medicine, 2020. **30**: p. 102300.
237. Daleke, D.L., K. Hong, and D. Papahadjopoulos, *Endocytosis of liposomes by macrophages: binding, acidification and leakage of liposomes monitored by a new fluorescence assay*. Biochim Biophys Acta, 1990. **1024**(2): p. 352-66.
238. Ishii, Y., et al., *Preparation of EGF labeled liposomes and their uptake by hepatocytes*. Biochemical and Biophysical Research Communications, 1989. **160**(2): p. 732-736.
239. Lundberg, B., K. Hong, and D. Papahadjopoulos, *Conjugation of apolipoprotein B with liposomes and targeting to cells in culture*. Biochim Biophys Acta, 1993. **1149**(2): p. 305-12.
240. Matthey, K.K., et al., *Role of ligand in antibody-directed endocytosis of liposomes by human T-leukemia cells*. Cancer Res, 1989. **49**(17): p. 4879-86.
241. Straubinger, R.M., et al., *Endocytosis of liposomes and intracellular fate of encapsulated molecules: encounter with a low pH compartment after internalization in coated vesicles*. Cell, 1983. **32**(4): p. 1069-79.
242. Ming, X., et al., *Intracellular delivery of an antisense oligonucleotide via endocytosis of a G protein-coupled receptor*. Nucleic Acids Research, 2010. **38**(19): p. 6567-6576.
243. Accardo, A., et al., *Bombesin peptide antagonist for target-selective delivery of liposomal doxorubicin on cancer cells*. J Drug Target, 2013. **21**(3): p. 240-249.

244. Sabari, J.K., et al., *Unravelling the biology of SCLC: implications for therapy*. *Nat Rev Clin Oncol*, 2017. **14**(9): p. 549-561.
245. Williams, B.Y., S.B. Dion, and A. Schonbrunn, *Role of receptor and protein kinase C activation in the internalization of the gastrin-releasing peptide receptor*. *Mol Pharmacol*, 1998. **54**(5): p. 889-98.
246. Zachary, I. and E. Rozengurt, *Internalization and degradation of peptides of the bombesin family in Swiss 3T3 cells occurs without ligand-induced receptor down-regulation*. *Embo j*, 1987. **6**(8): p. 2233-9.
247. Dou, Y., K. Hynynen, and C. Allen, *To heat or not to heat: Challenges with clinical translation of thermosensitive liposomes*. *Journal of Controlled Release*, 2017. **249**: p. 63-73.
248. Lou, J., X. Zhang, and M.D. Best, *Lipid Switches: Stimuli-Responsive Liposomes through Conformational Isomerism Driven by Molecular Recognition*. *Chemistry—A European Journal*, 2019. **25**(1): p. 20-25.
249. Weinstein, J., et al., *Liposomes and local hyperthermia: selective delivery of methotrexate to heated tumors*. *Science*, 1979. **204**(4389): p. 188-191.
250. Rudin, C.M. and J.T. Poirier, *Small-cell lung cancer in 2016: Shining light on novel targets and therapies*. *Nat Rev Clin Oncol*, 2017. **14**(2): p. 75-76.
251. Fruh, M., et al., *Small-cell lung cancer (SCLC): ESMO Clinical Practice Guidelines for diagnosis, treatment and follow-up*. *Ann Oncol*, 2013. **24 Suppl 6**: p. vi99-105.
252. Saltos, A., M. Shafique, and A. Chiappori, *Update on the Biology, Management, and Treatment of Small Cell Lung Cancer (SCLC)*. *Frontiers in Oncology*, 2020. **10**(1074).
253. Taniguchi, H., T. Sen, and C.M. Rudin, *Targeted Therapies and Biomarkers in Small Cell Lung Cancer*. *Front Oncol*, 2020. **10**: p. 741.
254. Yang, S., Z. Zhang, and Q. Wang, *Emerging therapies for small cell lung cancer*. *Journal of Hematology & Oncology*, 2019. **12**(1): p. 47.
255. Yang, H.K., et al., *Correlation of expression of bombesin-like peptides and receptors with growth inhibition by an anti-bombesin antibody in small-cell lung cancer cell lines*. *Lung Cancer*, 1998. **21**(3): p. 165-75.
256. Zhong, L., et al., *Small molecules in targeted cancer therapy: advances, challenges, and future perspectives*. *Signal Transduction and Targeted Therapy*, 2021. **6**(1): p. 201.
257. Cescato, R., et al., *Bombesin Receptor Antagonists May Be Preferable to Agonists for Tumor Targeting*. *Journal of Nuclear Medicine*, 2008. **49**(2): p. 318.
258. Yao, Y., et al., *Nanoparticle-Based Drug Delivery in Cancer Therapy and Its Role in Overcoming Drug Resistance*. *Frontiers in Molecular Biosciences*, 2020. **7**(193).
259. Hrkach, J., et al., *Preclinical development and clinical translation of a PSMA-targeted docetaxel nanoparticle with a differentiated pharmacological profile*. *Sci Transl Med*, 2012. **4**(128): p. 128ra39.
260. Mansi, R., et al., *Evaluation of a 1,4,7,10-Tetraazacyclododecane-1,4,7,10-Tetraacetic Acid-Conjugated Bombesin-Based Radioantagonist for the Labeling with Single-Photon Emission Computed Tomography, Positron Emission Tomography, and Therapeutic Radionuclides*. *Clinical Cancer Research*, 2009. **15**(16): p. 5240.
261. Mansi, R., et al., *Evaluation of Three Different Families of Bombesin Receptor Radioantagonists for Targeted Imaging and Therapy of Gastrin Releasing Peptide Receptor (GRP-R) Positive Tumors*. *Journal of Medicinal Chemistry*, 2015. **58**(2): p. 682-691.
262. Heikkila, R., et al., *Bombesin-related peptides induce calcium mobilization in a subset of human small cell lung cancer cell lines*. *J Biol Chem*, 1987. **262**(34): p. 16456-60.

APPENDIX

Chapter A

A.1 GRP-R knockdown efficiency by qRT-PCR

A stable GRP-R KD H510 cell line was also generated in the same way as described for H345 in section 4.2.1 and the KD efficiency data obtained from qRT-PCR is shown in figure A.1.

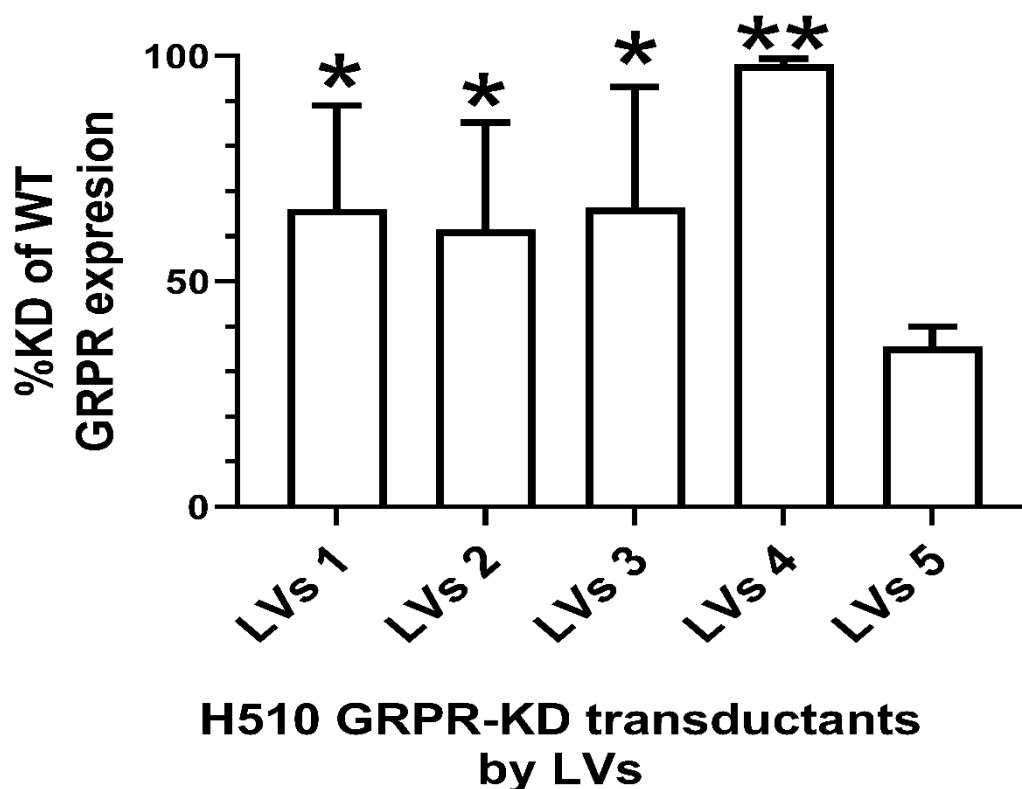


Figure A.1: GRP-R knockdown efficiency confirmation by qRT-PCR in SCLC. GRP-R mRNA knockdown efficiency detected by RT-qPCR analysis from GRP-R shRNA-treated H510 cells using lentiviral vectors (LVs) of five shRNA sequences at 72 h. The percentages are relative to the WT expression levels \pm SD. N=1 (one biological replicate and error bars represents two technical replicates).

A.2 Puromycin kill curve

The optimal puromycin concentration needed to eliminate non-transduced cells was determined using a kill curve experiment where the cells are subjected to increasing amounts of puromycin to determine the minimum antibiotic concentration needed to kill 50% of the cells over the course of 4 days. To make sure all non-transduced cells were eliminated, the cells were treated with the chosen concentration of puromycin for at least two weeks.

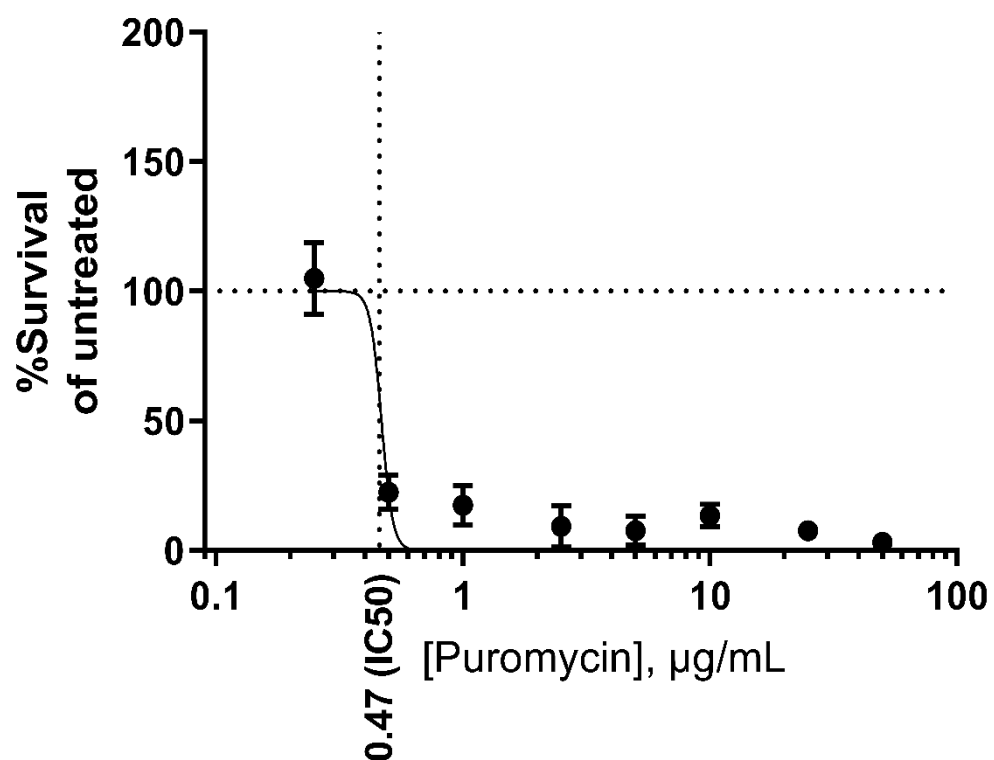


Figure A.2: Puromycin kill curve in H345. H345 cells were cultured over 4 days in the presence of escalating concentrations of puromycin before cell growth quantification by MTS assay. The Y axis represents the percentage of cell growth of treated cells compared to the no treatment cells. Errors bars are SD of three technical replicates. N=1.

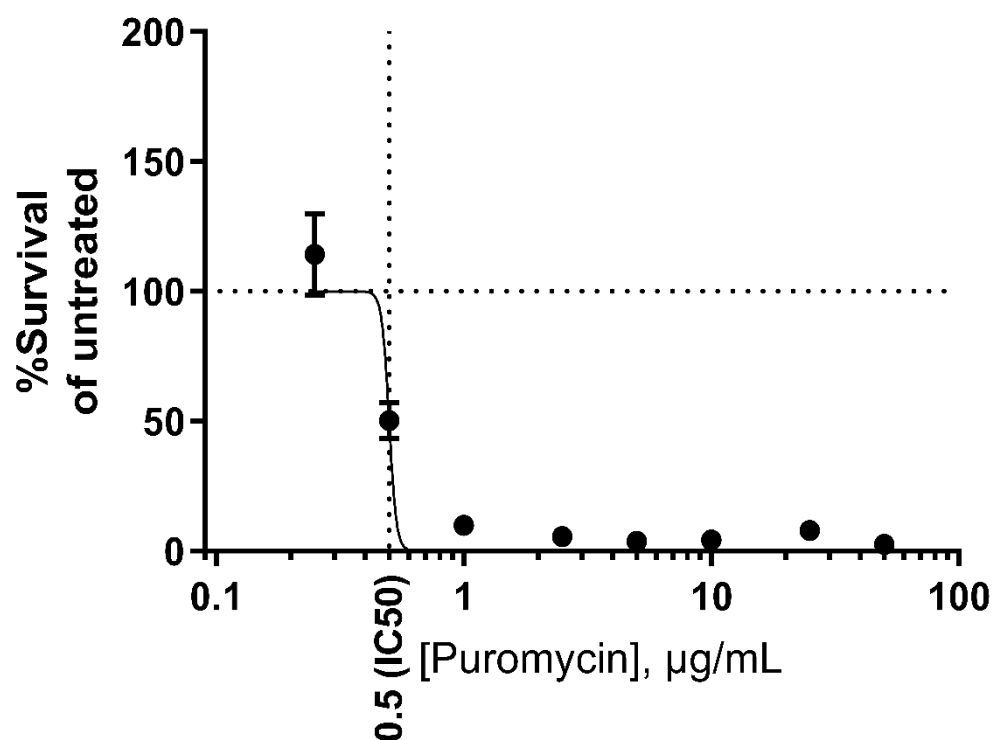


Figure A.3: Puromycin kill curve in H510. H510 cells were cultured over 4 days in the presence of escalating concentrations of puromycin before cell growth quantification by MTS assay. The Y axis represents the percentage of cell growth of treated cells compared to the no treatment cells. Errors bars are SD of three technical replicates. N=1.

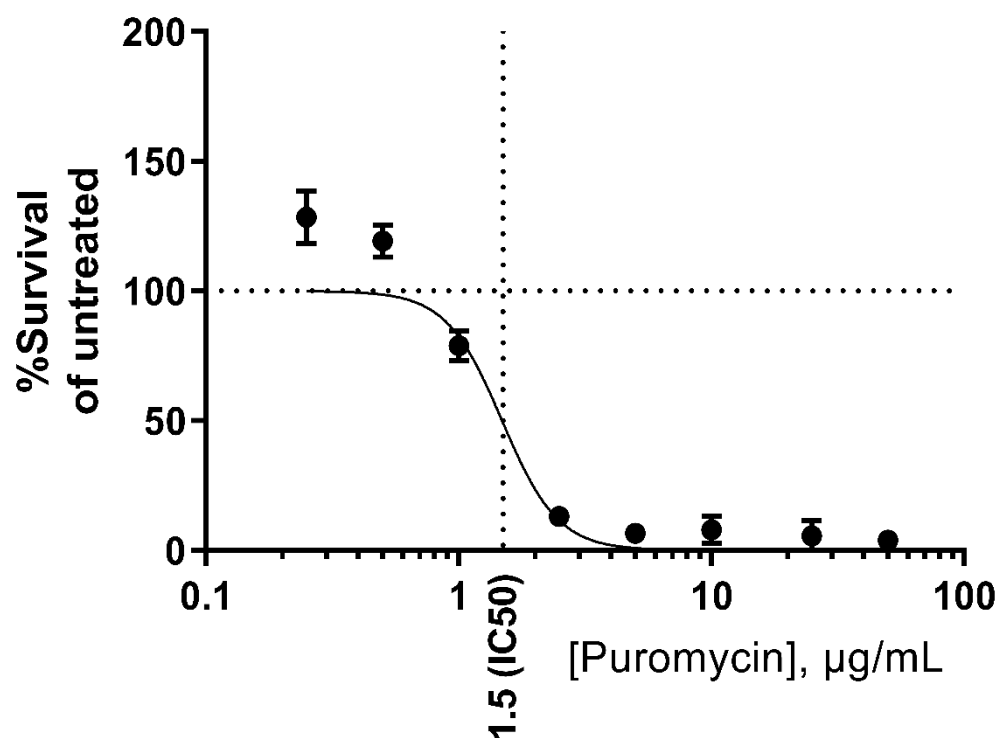


Figure A.4: Puromycin kill curve in A549. A549 cells were cultured over 4 days in the presence of escalating concentrations of puromycin before cell growth quantification by MTS assay. The Y axis represents the percentage of cell growth of treated cells compared to the no treatment cells. Errors bars are SD of three technical replicates. N=1.